NUREG/CR-6564

Analysis of Source Spectra, Attenuation, and Site Effects From Central and Eastern United States Earthquakes

Manuscript Completed: August 1997
Date Published: February 1998

Prepared by
G. Lindley

Institute for Crustal Studies
University of California
Santa Barbara, CA 93106-1100

E. Zurflueh, NRC Project Manager

Prepared for
Division of Engineering Technology
Office of Nuclear Regulatory Research
U.S. Nuclear Regulatory Commission
Washington, DC 20555-0001
NRC Job Code W6380

DISCLAIMER

ABSTRACT

This report describes the results from three studies of source spectra, attenuation, and site effects of central and eastern United States earthquakes. In the first study source parameter estimates taken from 27 previous studies were combined to test the assumption that the earthquake stress drop is roughly a constant, independent of earthquake size. 200 estimates of stress drop and seismic moment from eastern North American earthquakes were combined. It was found that the estimated stress drop from the 27 studies increases approximately as the square-root of the seismic moment, from about 3 bars at 10^{20} dyne-cm to 690 bars at 10^{25} dyne-cm. These results do not support the assumption of a constant stress drop when estimating ground motion parameters from eastern North American earthquakes.

In the second study, broadband seismograms recorded by the United States National Seismograph Network and cooperating stations have been analysed to determine Q_{Lg} as a function of frequency in five regions: the northeastern U. S. (NEUS), southeastern U. S. (SEUS), central U. S. (CUS), northern Basin and Range (BR), and California and western Nevada (CN). In each of the five regions simultaneous inversions using Fourier amplitude spectra from horizontal recordings were computed to determine the whole path attenuation, the site responses, and the source spectra. This study examines the resulting whole path attenuation and presents the site responses. In the NEUS, Q_{Lg} is found to increase from roughly 850 at 2 Hz to 1500 or greater at 15 Hz. Unlike some previous studies, Q_{Lg} in the CUS is found to be nearly identical to Q_{Lg} in the NEUS, at least from 2 to 10 Hz. Q_{Lg} in the SEUS is approximately 20% lower on average than Q_{Lg} in the CUS or NEUS. Below 2 Hz, Q_{Lg} determined from the central and eastern United States inversions increases up to roughly 1350 at 1 Hz. Thus, Q_{Lg} in the central and eastern United States is not modeled particularly well by a Q of the form, $Q = Q_0 f^{\eta}$ (f is the frequency, η a constant). However, the unusual frequency dependence of Q_{Lg} in the central and eastern United States at low frequencies may be due to systematic biases caused by the difficulty in measuring Q_{Lg} at low frequencies when Q is relatively large. Q_{Lg} in the western United States is significantly lower than Q_{Lg} in the central and eastern United States. Q_{Lg} in CN is modeled well by the approximate relation $Q_{Lg} = 240 f^{0.5}$ from 0.34 to 5.5 Hz; Q_{Lg} in the BR is similar and is modeled well by the approximate relation $Q_{Lg} = 240 f^{0.4}$ from 0.75 to 8.0 Hz.

In the third study, using spectral analysis, estimates have been made for the anelastic attenuation of four regional phases, and estimates have been made for the source parameters of 27 earthquakes, including the M_b 5.6, 14 April 1995, West Texas earthquake. The attenuation determined for the phase with the largest amplitudes, Lg, is in good agreement with previous estimates for the central and eastern United States. Assuming a single corner frequency source model, the stress drops determined in this study range from about 1 to 100 bars, with the stress drop of the West Texas earthquake in the range of a few bars to a few tens of bars. These values for stress drop are consistent with other studies of small CEUS earthquakes (less than about magnitude 4), but the stress drop for the West Texas earthquake is somewhat low compared to studies of large CEUS earthquakes.

TABLE OF CONTENTS

LIST OF FIGURES

LIST OF TABLES

EXECUTIVE SUMMARY

The purpose of this three-year project has been to conduct investigations of central and eastern United States earthquakes to improve our ability to predict ground motions in the central and eastern United States from future earthquakes. In many cases, the investigations included data from earthquakes in southeastern Canada, as this region is considered to have similar seismic characteristics to the eastern United States.

For this report, the project has been separated into four distinct sections, the first three sections provide the details of three separate studies, while the last section consists of a table summarizing the data set that was collected from the United States National Seismograph Network (USNSN) during the course of the project. The three separate analyses are of varying lengths and complexities and are presented in order of the most recently conducted to the earliest conducted.

The most recent study is presented in the first section of this report. This study is also the briefest of the three analyses that were conducted. The study tests the constant stress drop hypothesis that has often been used to model earthquake ground motion. According to the constant stress drop hypothesis, earthquake ground motions can be predicted based on the assumption that the stress drop of an earthquake is roughly a constant, independent of the size of that earthquake. The constant stress drop hypothesis is a very simple and useful assumption for ground motion modelers to make. It allows the ground motion of large earthquakes to be predicted from smaller earthquakes by scaling laws assuming a constant stress drop. This is a great advantage since smaller earthquakes are more numerous, giving the researcher more data to include in the analysis.

In order to predict ground motion using the constant stress drop hypothesis, it is also necessary to have a source model that predicts how ground motion will scale. A number of early studies found reasonable success modeling earthquake ground motions using a simple, Brune (1970) source model (e.g. Hanks and McGuire, 1981; Boore 1983; Somerville et al., 1987). However, some recent studies, using larger and more recent data sets, have questioned the validity of this method (e.g. Boore and Atkinson, 1992; Atkinson and Boore, 1995).

The study presented in Section I studies this issue by compiling the results from 27 prior studies of central and eastern North American earthquake source parameters. The 27 studies used in the analysis were the result of a literature search conducted to find studies which provided estimates of seismic moment and stress drop for central and eastern North American earthquakes. The source parameter estimates from the 27 studies were combined to test whether the results from studies to date support a constant stress drop hypothesis. No attempt was made to assess the validity of the results from the studies, nor whether the assumptions made in the various studies might conflict with each other. The purpose of this study was solely to test whether previous studies support or contradict the constant stress drop hypothesis—not whether the results of these previous studies provide valid estimates of earthquake source parameters.

The results of this compilation are clear and do not support the use of the constant stress drop hypothesis for predicting ground motion from central and eastern North American earthquakes. It is found that the average estimated stress drop from these studies is not constant, increasing by a factor of over 200 for seismic moments ranging from 10^{20} to 10^{25} dyne-cm. These results indicate that the constant stress drop hypothesis should not be used to predict ground motion from future central and eastern United States earthquakes without carefully considering the possible breakdown of the constant stress drop hypothesis.

Following this study a more in-depth analysis is presented, which analyzes data collected from the USNSN as part of this project. This second study examines the attenuation and site responses of USNSN stations for the regional phase, *Lg*. Generally, the ground motion recorded from an earthquake can be broken down into three components: the source effect, the path effect (including attenuation), and the site effect. The prediction of ground motion from an earthquake is often made easier and more reliable by estimating each of these three effects separately. The study in Section II involves a combined analysis of data from various sources, paths, and station locations, in order to separate the three effects. The study presents the results of the attenuation and site responses.

The study in Section II uses the *Lg* phase because it is the most commonly recorded phase in the central and eastern United States and because low seismic-wave attenuation in the central and eastern United States makes ground motion from the *Lg* phase a potential threat at relatively large epicentral distances (e.g. Nuttli, 1981). For comparison purposes, the analysis also examines attenuation of the *Lg* phase in the western United States.

A number of studies have previously examined the attenuation of the *Lg* phase in the United States (see references listed in Section II). Although much work has been done to study *Lg* attenuation across the United States, the acquisition of three-component, broadband data from the United States National Seismograph Network (USNSN) and cooperating stations allows the attenuation to be re-examined in light of this high-quality data. For example, it is often assumed that the frequency dependence of Q_{Lg} can be modeled as $Q_{Lg} = Q_0 f^{\eta}$. With this new data set it is possible to examine the frequency dependence of Q_{Lg} without making any a priori assumptions about the mathematical form that it will take. Another issue that this data set can help to resolve is the extent and amount of the intra-regional variation of Q_{lg}.

For the purposes of the study, the data were divided into five regions: the northeastern United States (NEUS), the central United States (CUS), the southeastern United States (SEUS), California and Nevada (CN), and the Basin and Range province (BR). Earthquakes that originated in southeastern Canada and were recorded in the northeastern United States were included as part of the NEUS data set.

Large differences are found in the attenuation of the *Lg* phase between the western United States and the central and eastern United States. Significant differences in Q_{Lg} are also found for different frequency ranges. In the NEUS, Q_{Lg} is found to increase from roughly 850 at 2 Hz to 1500 or greater at 15 Hz. Unlike some previous studies, Q_{Lg} in the CUS is found to be nearly identical to Q_{Lg} in the NEUS, at least from 2 to 10 Hz. Q_{Lg} in the SEUS is approximately 20% lower on average than Q_{Lg} in the CUS or NEUS. Below 2 Hz, Q_{Lg} determined from the central and eastern United States inversions increases up to roughly 1350 at 1 Hz. Thus, Q_{Lg} in the central and eastern United States is not modeled particularly well by a Q of the form, $Q=Q_0 f^{\eta}$ (f is the frequency, η a constant). However, the unusual frequency dependence of Q_{Lg} in the central and eastern United States at low frequencies may be due to systematic biases caused by the difficulty in measuring Q_{Lg} at low frequencies when Q is relatively large.

Q_{Lg} in the western United States is significantly lower than Q_{Lg} in the central and eastern United States. Q_{Lg} in CN is modeled well by the approximate relation $Q_{Lg} = 240 f^{0.5}$ from 0.34 to 5.5 Hz; Q_{Lg} in the BR is similar and is modeled well by the approximate relation $Q_{Lg} = 240 f^{0.4}$ from 0.75 to 8.0 Hz.

The study presented in Section III of this report is the first analysis that was conducted using the USNSN data set for this project. The data used in that study dates from 1 January 1992 to 12 July 1995, and includes recordings from 185 earthquakes, ranging from 3.0 to 5.6 in magnitude, recorded at 22 USNSN stations. This study analyzes the four principal regional phases found in the central and eastern United States—*Pg*, *Lg*, *Sn*, and *Pn*—as well as a limited number of recordings from the direct phase, *Sg*.

This study examines the same general issue as the previous study, namely the separation of ground motion into site, path, and source effects. However, whereas the previous study used simultaneous inversions of the data, the study in Section III uses least-squares best-fits to individual Fourier amplitude spectra of the data. This study also assumes a Brune (1970) source spectral model. Because of this the study in Section III is not as potentially useful as the study presented in Section II; however, the results can still be compared to the many earlier studies which used similar techniques on different data sets, and so are of some interest.

Along with attenuation and site response estimates, the study in Section III presents estimates for the source parameters of the 27 best-recorded earthquakes, including the M_b 5.6, 14 April 1995, West Texas earthquake. Assuming a single corner frequency source model, the stress drops determined in this study range from about 1 to 100 bars, with the stress drop of the West Texas earthquake in the range of a few bars to a few tens of bars. These values for stress drop are consistent with other studies of small CEUS earthquakes (less than about magnitude 4), but the stress drop for the West Texas earthquake is somewhat low compared to studies of large CEUS earthquakes.

Also in this study, a recently proposed source spectral model (Atkinson and Boore, 1995), which has two corner frequencies, was tested against data from the six largest earthquakes in the NSN data set with variable results. A comparison of the model to the Lg spectra of the largest earthquake, the West Texas earthquake, shows the model underpredicting spectral amplitudes in an intermediate-frequency range. Because the data set contains only one earthquake >M 5, however, no conclusive results are drawn.

Finally, Section 4 of this report presents a table summarizing the data collected during the time of the project. The data is available as both instrument-corrected and uncorrected seismograms. This data set includes 347 recordings of the predominant phase, *Lg*, from 207 earthquakes in central and eastern North America as recorded at 25 USNSN stations. The method that was used to process and reduce the data is also described.

1. SOURCE PARAMETER ANALYSIS OF CENTRAL AND EASTERN NORTH AMERICAN EARTHQUAKES USING A COMBINATION OF RESULTS FROM PREVIOUS STUDIES

1.1 INTRODUCTION

One of the most important goals of earthquake ground motion prediction is to find the simplest source model that can accurately predict the shape of the Fourier amplitude spectrum of the earthquake source. As early as 1970, Brune proposed a simple, two-parameter model for the earthquake source spectrum. In the displacement spectrum, this model consists of the low-frequency spectral amplitude and a single corner frequency. Following Brune's work, efforts were made to use this model to predict ground motion with initially promising results (e.g. Hanks and McGuire, 1981; Boore 1983; Somerville, 1987). In order to determine the scaling of earthquake parameters with earthquake size, these initial studies generally assumed that the stress drop was a constant, independent of the size of the earthquake.

It would be extremely useful if the Brune source model with a constant stress drop could accurately model earthquake ground motion, because of the simplicity and ease of use of this model. However, more recent studies based on larger and better data sets have concluded that, at least for eastern North America, the earthquake source spectrum is too complicated to be modeled by the Brune source model with a constant stress drop (Boore and Atkinson, 1992; Atkinson and Boore, 1995).

In order to investigate this issue more fully, the present study compiles the results from previous studies of eastern North American earthquakes to examine one aspect of this issue: Do the results of studies to date support a constant earthquake stress drop, independent of the size of the earthquake?

This study does not assess the validity of the methods of the various studies to estimate the stress drops, which is a notoriously difficult parameter to measure accurately. Also, no attempt is made to determine whether the assumptions made in the various studies are consistent with one another. Instead, the question this study attempts to answer has been narrowly focused to address whether the results to date, given the assumptions under which they were made, indicate that a constant stress drop with earthquake size is a reasonable hypothesis to make. In other words, is it possible to justify, based on the presently available results, a constant stress drop hypothesis?

It is found that the results do not support a constant stress drop; instead, the estimated stress drop increases approximately as the square root of the seismic moment. For a seismic moment of 10^{20} dyne-cm, the average estimated stress drop is only 3 bars, while for a seismic moment of 10^{25} dyne-cm, the average estimated stress drop is 690 bars. This indicates that a constant stress drop model should only be used with extensive justification to estimate ground motion parameters for eastern North America, unless the range in seismic moments is very narrow.

1.2 PREVIOUS STUDIES

As a first step in finding source parameter studies with information about eastern North American earthquakes, back issues of the *Bulletin of the Seismological Society of America* were examined as far back as 1980. Source parameters were compiled from the studies discovered in this manner, and then the reference lists of these studies were examined for other likely papers. Besides these studies, an additional source of references was found in an EPRI report (Schneider, 1994). Of the papers discovered in this manner, only the studies that clearly listed both stress drop and seismic moment for eastern North American earthquakes were used.

A total of 27 studies were found that listed 200 source parameter estimates (Table 1). Earthquakes were included that occurred in the central and eastern United States as well as southeastern Canada. The study with the most source parameter estimates is that of Boatwright (1994), with 84 separate estimates. This accounts for 42% of all the estimates in the present study; however, excluding the source parameter estimates from the Boatwright study does not significantly alter the results, as will be shown. Not including Boatwright's paper, the source parameter estimates are spread out over a number of different studies. There are 7 studies that each have estimates for 8 to 17 earthquakes, totaling another 84 estimates, and there are 19 studies with estimates for between 1 and 5 earthquakes, for another 32 estimates.

1.3 RESULTS AND CONCLUSIONS

The results are most clearly seen on a log-log plot of stress drop versus seismic moment (Figure 1). The estimated stress drop is seen to increase significantly with seismic moment. A best-fit line through the data produced the following result:

$$\log(M_0) = (2.15 \pm 0.13) \log(\sigma) + (18.9 \pm 0.2) \quad (1)$$

where M_0 is the seismic moment in dyne-cm, and σ is the stress drop in bars.

Because over 40% of the data points that determined the above best-fit line come from a single study (Boatwright, 1994), those data points were removed and the best-fit line was re-calculated. The results were not significantly different:

$$\log(M_0) = (2.32 \pm 0.15) \log(\sigma) + (19.1 \pm 0.3) \quad (2)$$

In both cases, the best-fit line has a slope of close to 2, corresponding to a square-root increase of the estimated stress drop with seismic moment. Although a square-root function is not usually considered a rapidly increasing function, it must be kept in mind that seismic moments in many studies typically vary by a factor of 1000 or more. This produces a large change in the stress drop even assuming a square-root function. In the present analysis, using Equation 1, a seismic moment of 10^{20} dyne-cm yields an average estimated stress drop of 3 bars, while a seismic moment of 10^{25} dyne-cm has an average estimated stress drop of 690 bars, an increase of more than a factor of 200.

Note that if we attempt to extrapolate these results to higher seismic moments, the stress drop quickly increases to physically unreasonable values. For example, for an earthquake with moment-magnitude 7.5 ($2.2\ 10^{27}$ dyne-cm), the stress drop would be 8500 bars according to Equation 1. Thus it would be unwise to use Equation 1 to attempt to estimate ground motion.

It must be concluded that the use of the constant stress drop model for eastern North American earthquake is not validated based on the combination of the results of previous studies. While the stress drop may appear roughly constant over a relatively small range in seismic moment, when the data is combined for studies with a wide range in seismic moment, the estimated stress drop is seen to increase significantly. It is concluded that the assumption of a constant stress drop should be used with caution when estimating ground motions for eastern North American earthquakes whenever there is any appreciable range of seismic moment involved.

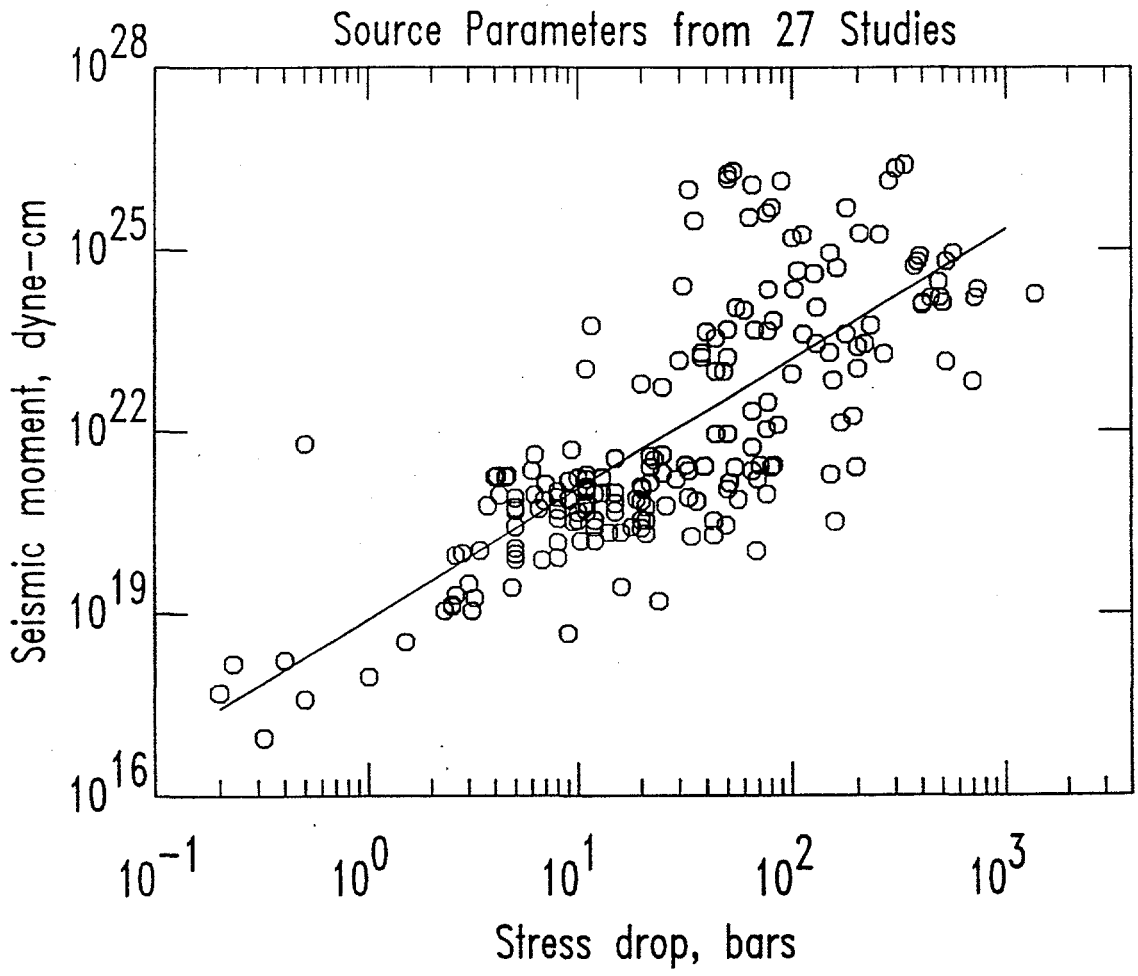

Figure 1. Average estimated stress drop versus seismic moment for Eastern North American earthquakes. The average estimated stress drop is plotted versus the seismic moment from a compilation of 27 different studies of eastern North American earthquakes. The best-fit line through the data is given in the text and shows that the estimated stress drop increases significantly with seismic moment.

Table 1. Source parameters (listed in no particular order).

Stress Drop (bars)	Seismic Moment (x 10^{20} dyne-cm)	Source
86	130	Atkinson and Boore (1995)
113	4000	"
53	2 10^{6}	"
149	2000	"
154	710	"
190	180	"
517	63000	"
517	1400	"
25	550	Lamontagne et al. (1994)
177	5.0 10^{5}	Atkinson (1993)
130	2800	"
278	1.4 10^{6}	"
379	63000	"
130	11000	"
102	22000	"
106	45000	"
483	16000	"
230	5600	"
48	1000	"
77	22000	"
89	1.4 10^{6}	"
38	2000	"
177	4000	"
63	3.5 10^{5}	"
126	40000	"
149	89000	"
51	14	Boatwright (1994)
82	27	"
21	5.7	"
20	7.0	"
76	9.1	"
10	3.5	"
12	2.7	"
29	16	"
7	13	"
11	12	"
8	10	"
11	6.6	"
9	15	"
8	8.0	"
76	110	"
5	7.8	"
50	91	"
15	35	"
25	20	"

11	19	"
13	17	"
44	90	"
16	2.2	"
19	7.6	"
11	10	"
15	4.8	"
54	25	"
15	6.5	"
5	4.9	"
50	11	"
32	27	"
8	5.1	"
23	33	"
22	14	"
25	40	"
157	3.3	"
36	7.0	"
33	22	"
12	9.2	"
14	2.2	"
13	9.5	"
11	11	"
8	1.5	"
18	2.7	"
10	17	"
22	25	"
20	12	"
77	310	"
5	5.5	"
5	0.97	"
39	26	"
0.5	61	"
22	38	"
15	9.6	"
26	5.9	"
20	3.5	"
21	3.4	"
11	4.8	"
5	1.2	"
6	22	"
33	8.1	"
12	1.6	"
9	7.4	"
10	4.7	"
5	2.7	"
4.5	17	"
11	16	"
167	140	"

150	19	"
56	7.5	"
43	2.0	"
65	54	"
9	7.7	"
43	3.4	"
20	2.6	"
80	25	"
12	3.5	"
69	16	"
34	1.9	"
21	2.1	"
71	27	"
693	670	"
49	2.9	"
8	3.7	"
35	$3.1\ 10^5$	Bent (1992)
31	25000	Boatwright and Choy (1992)
82	6700	"
558	88000	"
65	220	Boore and Atkinson (1992)
65	22	"
16	0.28	Xie et al. (1991)
8	0.85	"
5	0.79	"
160	50000	Somerville et al. (1990)
44	1000	Glassmoyer and Borcherdt (1990)
1	0.0085	"
3.1	0.11	"
0.32	0.00087	"
4.8	0.27	"
0.4	0.016	"
0.23	0.014	"
0.20	0.0046	"
0.5	0.0036	"
1.5	0.033	"
265	1900	Nabelek and Suarez (1989)
4.2	8.6	Feng and Ebel (1996)
9.5	3.3	"
6.5	5.3	"
6.9	7.2	"
6.7	0.77	"
4.5	17	"
10.3	1.6	"
6.2	8.8	"
2.8	0.99	"
10.7	5.4	"
20.2	11	"
2.6	0.92	"

68	1.1	Fletcher (1995)
196	25	"
24	0.16	"
8.9	0.046	"
6.2	40	"
300	$2.2\ 10^5$	Somerville et al. (1987)
80	$5.1\ 10^5$	"
60	10000	"
400	12000	"
200	1100	"
100	$1.6\ 10^5$	"
100	900	"
400	13000	"
20	620	"
30	1500	"
50	4800	"
500	13000	"
200	2500	"
11.6	5600	Shin and Herrmann (1987)
3.7	5.9	"
10.9	1100	"
9.3	49	"
4	17	"
4.1	18	"
4.6	18	"
3.2	0.18	"
3.4	1.1	"
2.6	0.20	"
2.5	0.14	"
2.5	0.13	"
3.0	0.31	"
2.3	0.11	"
33	$1.0\ 10^6$	Wetmiller et al. (1988)
50	$1.5\ 10^6$	"
65	$1.2\ 10^6$	Choy and Boatwright (1988)
50	$1.8\ 10^6$	"
76	$4.2\ 10^5$	Somerville (1986)
329	$2.5\ 10^6$	"
111	$1.8\ 10^5$	"
475	29000	"
709	16000	"
438	16000	"
55	11000	"
67	4700	"
216	2800	"
38	1700	"
299	$2.2\ 10^6$	Ebel et al. (1986)
730	22000	"
251	$1.8\ 10^5$	Hasegawa and Adams (1990)

203	1.9 10^5	Liu and Kanamori (1980)
388	78000	Ou and Herrmann (1990)
40	4400	"
1385	18000	Nabelek (1988)
365	53000	Choy et al. (1983)
77	4600	Herrmann et al. (1982)
50	1700	Hasegawa and Wetmiller (1980)
44	3500	Taylor et al. (1989)

2. ATTENUATION OF Lg WAVES ACROSS THE CONTIGUOUS UNITED STATES: DATA FROM THE NATIONAL SEISMOGRAPH NETWORK AND COOPERATING STATIONS

2.1 INTRODUCTION

First identified by Press and Ewing (1952), the regional phase, *Lg*, can be considered either as a surface-wave phase consisting of higher modes of Rayleigh and Love waves (e.g. Oliver and Ewing, 1957, 1958; Knopoff et al., 1973), or as the superposition of post-critically reflected *S* waves trapped in the continental crust (e.g. Bouchon, 1982; Olsen et al., 1983; Campillo, 1990).

From either viewpoint, the properties of the *Lg* phase are important because they provide a means of analysing crustal structure. In the central and eastern United States, the *Lg* phase has additional significance for earthquake hazard analyses, since strong-motion and locally recorded data are rare, and since low seismic-wave attenuation makes ground motion from the *Lg* phase a potential threat at relatively large epicentral distances (e.g. Nuttli, 1981). In the western United States, the *Lg* phase has additional significance since the phase is often studied as a means of discriminating earthquake and explosion sources (e.g. Walter et al., 1995).

Practically any use of the *Lg* phase requires some knowledge of the attenuation of the phase with distance. The attenuation of seismic waves within the earth can generally be separated into three components: geometrical, intrinsic or anelastic, and scattering. This study corrects for geometrical attenuation and estimates the remaining attenuation, which may be due to intrinsic attenuation, scattering attenuation, or a combination of the two. No attempt is made to differentiate between the two possible mechanisms, although Mitchell (1980, 1995) has argued that *Lg* attenuation, even measured from the *Lg* coda, is dominated by intrinsic rather than scattering attenuation. It should also be noted that Q_{Lg} is a measure of the decay of the *Lg* phase, and is not necessarily a direct measure of the Q of shear waves in the crust (e.g. Hwang and Mitchell, 1987; Mitchell, 1991).

The first measurements of *Lg* attenuation in the United States used data predominantly from the World Wide Standard Seismograph Network (WWSSN) and Long Range Seismic Measurement (LRSM) stations; Q values, assuming a group velocity of 3.5 km/s, were found to be approximately 900 to 1400 in the central and eastern United States near 1 Hz (Sutton et al., 1967; Nuttli, 1973; Street et al., 1976; Bollinger, 1979). Sutton et al. (1967) also provided an early estimate of 200 for Q_{Lg} near 1 Hz in the western United States. The greater attenuation (lower Q) in the western United States compared to the central and eastern United States had been reported as early as 1962 by Romney et al., based on observed amplitudes of ground motion from the GNOME explosion in New Mexico.

Subsequent studies have analysed data over broader frequency ranges. In the central and eastern United States (and including eastern Canada), most studies of direct *Lg* have found Q_{Lg} to increase gradually with frequency from about 0.5 to 10-20 Hz (Nuttli, 1981; Dwyer et al., 1983; Hasegawa, 1985; Chun et al., 1987; Gupta and McLaughlin, 1987; Shin and Herrmann, 1987; Atkinson and Mereu, 1992; Atkinson and Boore, 1995). Often the frequency dependence of Q_{Lg} is modeled according to $Q_{Lg} = Q_0 f^{\eta}$, where η in the central and eastern United States is typically 0.2 - 0.4 in this frequency range. Q_{Lg} has also been estimated from coda Q for the central and eastern United States, usually with comparable results (Singh and Herrmann, 1983; Woodgold, 1990), although Pulli (1984) found that the frequency dependence of coda Q in New England could change with lapse time.

Studies over similar frequency ranges for the western United States have confirmed the significantly lower Q values in the west compared to the central and eastern United States, and have also found a somewhat more rapid increase of Q_{Lg} with frequency such that η is approximately 0.35 - 0.7 (Nuttli, 1981; Singh and Herrmann, 1983; Chavéz and Priestley, 1986; Xie and Mitchell, 1990a). These studies include measurements from both direct *Lg* and *Lg* coda. Studies outside the United States have confirmed that, in general, stable continental regions have relatively high Q_{Lg} values and relatively low η values, compared to tectonically active regions (e.g. Hwang and Mitchell, 1987).

Besides the observed differences of Q_{Lg} between the western United States and the central and eastern United States, some of the aforementioned studies have examined variations of Q_{Lg} within each of these regions. As early as 1976, Street found 1 Hz *Lg* attenuation in the northeastern United States to be greater than attenuation in the central United States, based on Nuttli's (1973) results, while Bollinger (1979) found 1 Hz *Lg* attenuation in the southeastern United States to be consistent with the results of Nuttli (1973).

More recent studies of Q_{Lg} variability include Singh and Herrmann (1983), who measured *Lg* coda Q and found significant variations within the western United States and within the central and eastern United States. Gupta and McLaughlin (1987), using a similar technique to the one presented here, also found evidence for variation of Q_{Lg} within the central and eastern United States. On a smaller scale Woodgold (1990) has found variations in *Lg* coda Q in eastern Canada, and Shi et al. (1995) have found variations in Q_{Lg} within the northeastern United States.

Although much work has been done to study *Lg* attenuation across the United States, the recent acquisition of three-component, broadband data from the United States National Seismograph Network (USNSN) and cooperating stations allows this issue to be reexamined in light of this high-quality data. For example, it is often assumed that the frequency dependence of Q_{Lg} can be modeled as $Q_{Lg} = Q_0 f^{\eta}$. With this new data set it is possible to examine the frequency dependence of Q_{Lg} without making any a priori assumptions about the mathematical form that it will take. Another issue that this data set can help to resolve is the extent and amount of the intra-regional variation of Q_{Lg}.

This study presents the results of inversions using direct *Lg* from the USNSN and cooperating stations. This study adds to the body of knowledge of *Lg* attenuation in the United States, including its variation with frequency and region. Estimated site responses of USNSN and cooperating stations are also presented.

2.2 DATA FROM THE USNSN AND COOPERATING STATIONS

All of the USNSN and cooperating stations had three-component velocity sensors; all of the sensors except two were broadband (Table 2). A total of 36 stations, 88 events, and 270 recordings were used in the analysis of 5 different regions: the northeastern United States (NEUS), the southeastern United States (SEUS), the central United States (CUS), the northern Basin and Range (BR), and California and western Nevada (CN). Because of the paucity of data in the SEUS, some overlap was necessary between that region and the NEUS and the CUS. Of the seven stations used in the SEUS inversions, one station (MIAR) was also used in the CUS inversions, and one station (MCWV) was also used in the NEUS inversions. Figure 2 shows the station and event locations and the ray paths.

The recordings used for the central and eastern United States inversions were written over a four-year period, from 1992 through 1995. An attempt was made to include all earthquakes that were well-recorded at two or more stations; the data also include two mine bumps (Table 3). Since the installation of USNSN stations was phased in over time, most of the central and eastern United States data were recorded in 1994 and 1995. The NEUS inversions include a number of earthquakes that occurred in southeastern Canada but were recorded in the NEUS. Data from the western United States were recorded between October, 1994 and September, 1995, and in January, 1996 (Table 4). The western United States data set is a subset of the data available during that time and includes a seismic event that was probably a mine collapse (Pechmann et al., 1995). Much more broadband data is available for the western United States than was used in this study.

To reduce complications due to variations of geometrical spreading with epicentral distance, only recordings at epicentral distances greater than 150 km and less than 1000 km were used. The average ray path distance was 455 km for the NEUS, 558 km for the CUS, 461 km for the SEUS, 357 km for CN, and 437 km for the BR.

For each of the recordings, the horizontal components were first corrected for instrument response, and then were rotated to transverse using the locations from either the QED or PDE catalogs obtained from the U. S. Geological Survey in Golden, Colorado. In a small number of recordings, only one horizontal component was available due to instrument malfunction; in those cases the horizontal component was used in place of the transverse rotated component. The *Lg* phase was identified on the seismograms by computing the expected arrival time for a group velocity of 3.6 km/s. A window was chosen to include the predominant energy from the phase; because of the dispersive nature of the *Lg* waves, the window size increased with distance, and was typically 10 to 20 s for distances less than 250 km, and about 40 to 60 s for distances close to 1000 km. Once a window for the *Lg* phase was chosen, the mean value of the window was removed, a 5% Hanning taper was applied, and the Fast Fourier Transform was computed.

The frequency range that could be used varied widely depending on the recording. In order to determine the useable frequency range for a particular recording, a second window of the same length as the *Lg* window was taken directly in front of the *Lg* window. This window preceding the *Lg* window consisted of instrument noise as well as the *P* coda, the *Sn* coda, and sometimes the direct *Sn*. By comparing the *Lg* window with the preceding window, a range of frequencies was chosen over which the *Lg* signal was clearly dominant (Figure 3).

For shorter distances, less than about 250 km, the separation between the *Lg* arrival and the *Sn* arrival is short enough that what is taken as the *Lg* window also contains much of the direct *Sn*. However, this is not believed to be a significant problem, since the *Lg* phase usually dominates the *Sn* phase, and since only 18% of the spectra in this data set had epicentral distances less than 250 km.

The useable frequency range was sometimes as low as 0.1 Hz and sometimes as high as 16 Hz; however, typical values were from 0.5 to 6 Hz. Only for the CN inversions were frequencies below 0.4 Hz used.

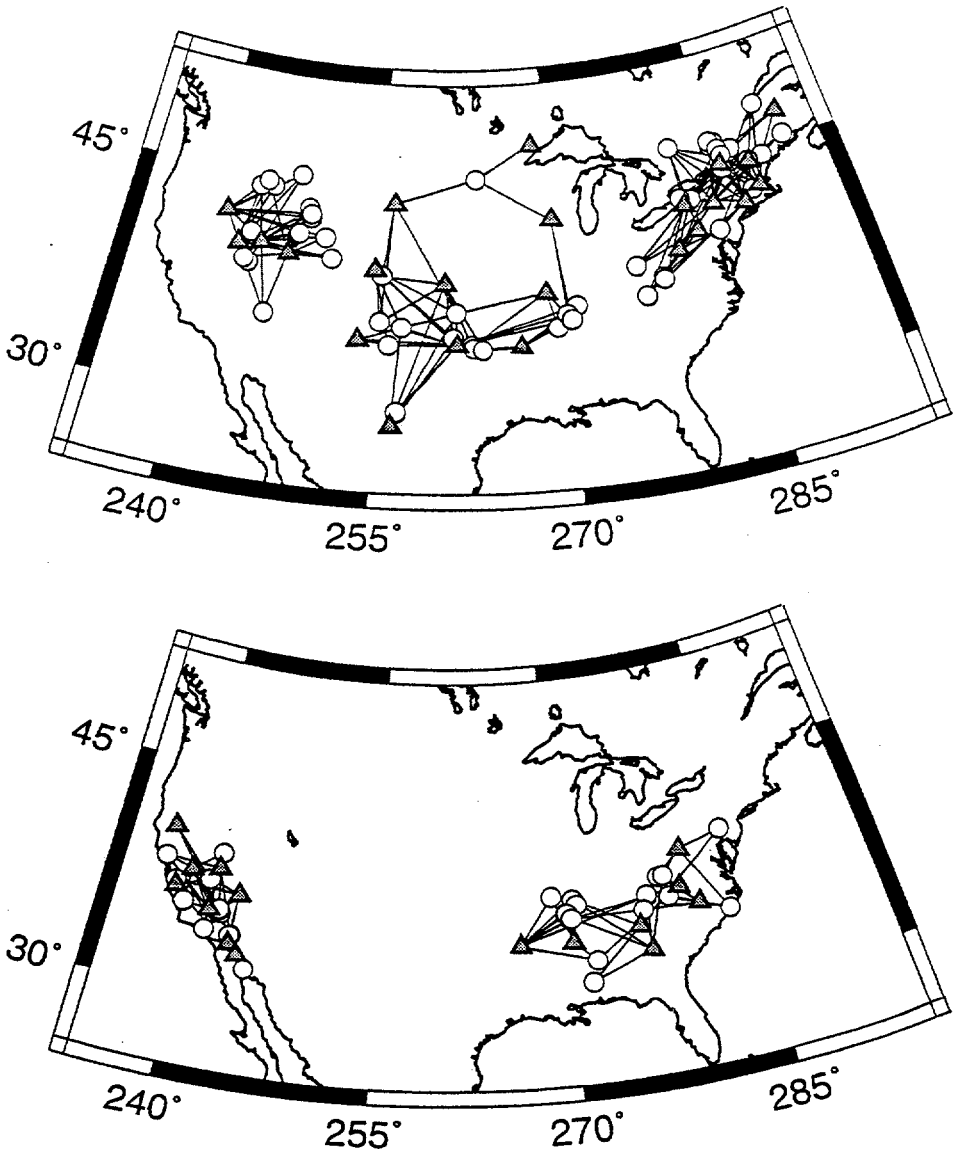

Figure 2. Station and earthquake locations. Locations of stations (triangles) and earthquakes (circles). The five regions (northeastern U.S., southeastern U.S., central U.S., northern Basin and Range, and California and western Nevada) are shown on two maps to more clearly show the different regions.

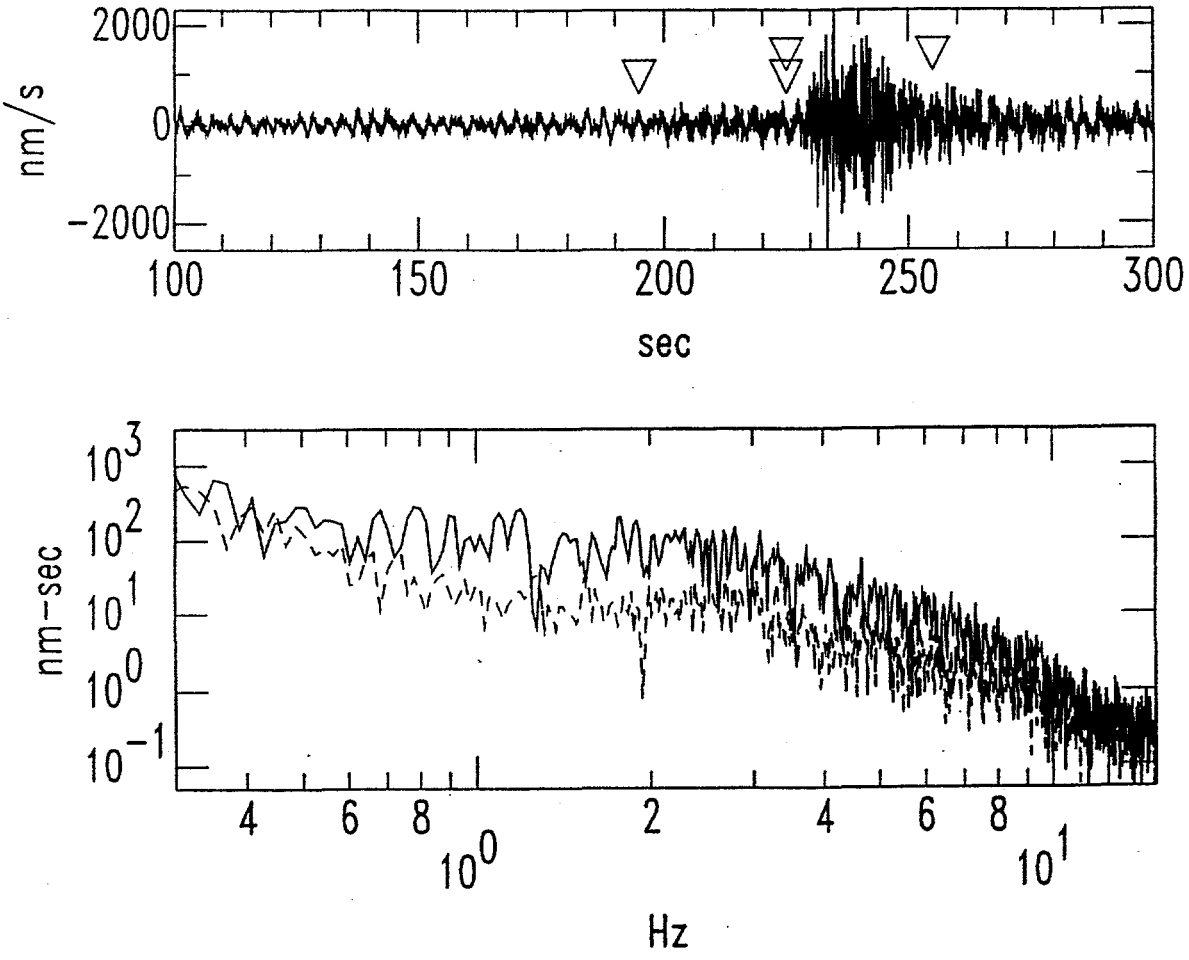

Figure 3. Example of the data. The example shows a seismogram with the *Lg* and noise window (top), and the FFTs of the two windows (bottom). Seismogram has been high-pass filtered at 0.3 Hz; the FFTs are unfiltered. The earthquake is a magnitude 3.6 event recorded at MCWV with an epicentral distance of 580 km. The *Lg* window is above the noise from approximately 0.6 to 8.0 Hz.

Table 2. Stations used in Section 2 analysis. RSNY and RSSD have short-period sensors; all other stations have broadband sensors. STS-1 and STS-2 are manufactured by Streckheisen; CMG-3, CMG-3N, CMG-4 by Guralp; KS-36000, KS-36000I, and S-750 by Geotech.

Location	I.D.	Latitude (N)	Longitude (W)	Sensor type	Inversions used for
Albuquerque, NM	ALQ	34.9425	106.4575	STS-1	CUS
Binghamton, NY	BINY	42.1993	75.9861	CMG-3N	NEUS
Blacksburg, VI	BLA	37.2113	80.4210	CMG-3N	SEUS
Battle Mountain, NV	BMN	40.4314	117.2217	CMG-3N	BR
Cedar Bluff, KS	CBKS	38.8140	99.7373	CMG-3N	CUS
Caribou, ME	CBM	46.9325	68.1208	CMG-3N	NEUS
Cathedral Cave, MO	CCM	38.0556	91.2445	STS-1	CUS
Chapel Hill, NC	CEH	35.8908	79.0927	CMG-3N	SEUS
Columbia College, CA	CMB	38.0350	120.3850	STS-1	CN
Dugway, UT	DUG	40.1950	112.8133	CMG-3N	BR
Elko, NV	ELK	40.7448	115.2387	CMG-3	BR
Ely, MN	EYMN	47.9461	91.4950	CMG-3N	CUS
Godfrey, GA	GOGA	33.4111	83.4666	CMG-3N	SEUS
Golden, CO	GOL	39.7002	105.3711	CMG-3	CUS
Harvard, MA	HRV	42.5063	71.5583	STS-1	NEUS
Isabella, CA	ISA	35.6633	118.4733	STS-1	CN
Jewell Farm, WI	JFWS	42.9148	90.2488	STS-1	CUS
Lisbon, NH	LBNH	44.2401	71.9258	CMG-3N	NEUS
Lakeside, CT	LSCT	41.6783	73.2243	STS-2	NEUS
Lajitas, TX	LTX	29.3338	103.6669	KS-36000	CUS
Mont Chateau, WV	MCWV	39.6581	79.8456	CMG-3N	SEUS, NEUS
Mount Ida, AK	MIAR	34.5457	93.5730	CMG-3N	CUS, SEUS
Mina, NV	MNV	38.4328	118.1531	CMG-3	CN
Murphy, NC	MYNC	35.0738	84.1278	CMG-3N	SEUS
Oxford, MI	OXF	34.5118	89.4091	CMG-3N	SEUS
Pinyon Flat, CA	PFO	33.6091	116.4552	STS-1	CN
Adirondack, NY	RSNY	44.5483	74.5300	S-750	NEUS
Black Hills, SD	RSSD	44.1204	104.0361	S-750	CUS
San Andreas Geo. Obs., CA	SAO	36.7650	121.4450	STS-1	CN
Superstition Mountain, CA	SMTC	32.9490	115.7200	STS-2	CN
Standing Stone, PA	SSPA	40.6358	77.8880	KS-36000I	NEUS
Topapah Spring, NV	TPNV	36.9286	116.2236	CMG-4	CN
Whiskeytown Dam, CA	WDC	40.5800	122.5397	STS-2	CN
Wichita Mountains, OK	WMOK	34.7378	98.7810	CMG-3N	CUS
Wild Horse Valley, OR	WVOR	42.4339	118.6367	CMG-3N	BR
Yorkshire, NY	YSNY	42.4758	78.5375	CMG-3N	NEUS

Table 3. Earthquakes used in the inversions for the central and eastern United States. Locations are from the QED or PDE catalogs of the U. S. Geological Survey, whichever catalog location was used to rotate the seismograms to transverse. * indicates a mine bump.

Origin time	Latitude (N)	Longitude (W)
1992 12/17 07:18	34.744	97.581
1993 01/21 19:46	36.222	89.617
1993 03/16 07:38	35.670	90.550
1993 04/28 22:40	36.190	89.440
1993 07/16 10:54	31.779	88.326
1993 07/30 22:30	45.260	74.110
1993 09/23 06:45	46.06	74.6
1993 11/16 09:31	45.182	73.495
1993 11/30 03:07	35.9	103.1
1994 01/16 00:42	40.327	76.007
1994 01/16 01:49	40.330	76.037
1994 02/05 14:55	37.370	89.180
1994 03/12 10:43	42.782	77.876
1994 08/06 19:54	35.067	76.751
1994 09/16 04:22	45.3	68.200
1994 09/16 04:36	45.3	68.2
1994 09/16 04:53	45.3	68.2
1994 09/16 07:01	45.3	68.2
1994 09/25 00:53	47.77	69.96
1994 09/26 14:23	37.0	88.9
1994 10/02 11:27	42.36	72.26
1994 11/20 19:33	44.37	70.59
1994 12/25 19:06	39.290	104.788
1995 01/18 15:51	34.51	97.49
1995 02/15 15:53	45.90	75.04
1995 02/19 12:57	39.09	83.62
1995 03/02 05:33	44.23	74.43
* 1995 03/11 08:15	36.98	83.16
* 1995 03/11 09:50	37.00	83.19
1995 03/19 18:36	34.70	104.06
1995 04/05 05:31	35.20	99.03
1995 04/14 00:32	30.2	103.3
1995 04/15 14:33	30.2	103.3
1995 05/24 15:42	38.1	81.6
1995 05/25 14:22	43.0	78.8
1995 05/27 19:51	36.1	89.5
1995 05/28 15:28	33.2	87.8
1995 06/01 01:06	30.3	103.3
1995 06/01 04:49	34.4	96.7
1995 06/16 12:13	44.3	71.9
1995 06/26 00:36	36.7	81.4
1995 06/29 09:27	36.5	89.8
1995 07/04 03:59	36.2	104.8
1995 07/20 02:10	36.5	89.7
1995 07/28 05:47	46.2	75.0
1995 07/31 00:47	37.7	90.8

1995 08/17 23:18	36.1	89.4
1995 08/20 16:15	45.4	73.2
1995 09/12 03:59	45.6	74.4
1995 09/15 00:31	36.9	98.8
1995 09/21 23:03	45.1	74.2
1995 10/10 07:19	46.4	78.8
1995 10/20 15:57	45.8	96.9
1995 10/26 00:37	37.0	83.2
1995 11/04 19:04	37.9	81.5
1995 11/23 13:00	38.1	82.0
1995 12/15 10:16	36.1	83.6
1995 12/15 15:49	38.1	81.6

Table 4. Earthquakes used in the inversions for the western United States. Locations are from the QED or PDE catalogs of the U. S. Geological Survey, whichever catalog location was used to rotate the seismograms to transverse. * indicates probable mine collapse (Pechmann, 1995).

Origin time	Latitude (N)	Longitude (W)
1994 10/03 14:00	32.056	114.941
1994 10/17 01:46	42.478	111.076
1994 10/19 00:49	35.49	117.47
1994 10/29 08:03	39.25	116.07
1994 10/29 08:10	39.28	116.07
1994 11/20 04:31	34.01	116.28
1994 11/29 01:43	43.39	111.34
1994 12/20 12:55	35.86	120.51
1995 01/28 06:26	44.51	114.83
* 1995 02/03 15:26	41.56	109.70
1995 03/04 17:15	39.5	118.1
1995 03/05 00:07	37.6	118.8
1995 03/05 02:48	37.6	118.8
1995 03/17 13:35	44.42	116.09
1995 03/20 12:46	40.20	108.99
1995 04/03 12:58	39.47	116.53
1995 04/04 05:08	34.28	117.48
1995 04/06 13:35	44.41	116.06
1995 04/11 12:20	44.83	115.41
1995 07/25 19:34	43.007	111.106
1995 07/27 17:04	41.641	111.981
1995 08/12 23:50	41.247	116.282
1995 09/04 14:14	38.6	122.7
1995 09/05 20:27	34.2	116.4
1995 09/14 10:59	35.8	117.6
1995 09/14 08:22	37.1	121.5
1995 09/20 23:27	35.7	117.6
1995 09/24 21:55	45.5	112.4

2.3 SIMULTANEOUS INVERSION TECHNIQUE

Following a standard approach, each spectrum is assumed to be divisible into three components:

$$A_{ij}(f) = S_j(f) * P_{ij}(f) * R_i(f) \qquad (3)$$

where f is the frequency, $A_{ij}(f)$ is the Fourier amplitude spectrum of the *ith* recording of the *jth* source, $S_j(f)$ is the source term, $P_{ij}(f)$ is the path effect, and $R_i(f)$ is the receiver term, the site effect. No term is included for the instrument response since the data are calibrated prior to computing the Fast Fourier Transforms.

In equation (3), two assumptions have been made: first, that the source term is independent of the recording site; and, second, that the site effect is independent of the event location. The assumption that the source term is independent of the recording site can not be met exactly, since the radiation pattern of the source will vary depending on the focal mechanism and directivity of the source. However, the *Lg* phase, since it consists of post-critically reflected rays from a variety of take-off angles, will have some natural averaging that should reduce the effects of the variation of the source term due to the radiation pattern. Additional averaging will occur as the number of events and stations is increased. Similarly, the assumption that the site effect does not vary with event location can not be met exactly. Again, however, the nature of the *Lg* phase will lead to some natural averaging.

No functional form is assumed for either the source or the site terms. The path effect is assumed to be modeled by:

$$P_{ij}(f) = \frac{e^{-\gamma(f) r_{ij}}}{r_{ij}^{n}} \qquad (4)$$

where r_{ij} is the epicentral distance, n determines the geometrical attenuation, and $\gamma(f)$ is the attenuation coefficient. The attenuation coefficient determined in this method is an average value over the region from which the data is taken.

The attenuation coefficient, $\gamma(f)$, is related to the quality factor of attenuation, $Q(f)$, according to:

$$\gamma(f) = \frac{\pi f}{Q(f) U} \qquad (5)$$

where U is the group velocity. The *Lg* phase arrives over a range of group velocities, with the largest amplitudes typically near 3.5 km/s. Accordingly, $U$is assumed to be 3.5 km/s in order to determine $Q(f)$ from $\gamma(f)$.

To determine $\gamma(f)$ using equation (4), the geometrical spreading parameter, n, is assumed to be 0.5, as appropriate for the spectral decay of the *Lg* phase beyond about 150 km (e.g. Campillo et al., 1984). In theory, n could be included in the inversion as one of the model parameters to be determined rather than taking on an assumed value. In practice, however, the trade-off between $\gamma$and n was too close to successfully determine both these parameters.

Substituting equation (4) into equation (3) and taking the natural logarithm gives:

$$\ln[S_j(f)] + \ln[R_i(f)] - \gamma(f) r_{ij} = \ln[A_{ij}(f)] + n \ln[r_{ij}] \qquad (6)$$

If we assume that the frequency interval is sufficiently small so that the terms in the equation can be assumed to be constant, then equation (6) defines a linear inverse problem

$$\mathbf{G}\,\mathbf{m} = \mathbf{d} \qquad (7)$$

where $\mathbf{d}$ is the data vector, whose elements consist of $\ln[A_{ij}] + n \ln[r_{ij}]$, $\mathbf{m}$ is the model vector, consisting of $-\gamma r_{ij}$ and each $\ln[S_j]$ and $\ln[R_i]$, and $\mathbf{G}$ is a matrix relating $\mathbf{m}$ to $\mathbf{d}$ through equation (6).

The least-squares solution can be found according to:

$$\mathbf{m} = [\mathbf{G}^T\mathbf{G}]^{-1}\mathbf{G}^T\mathbf{d} \qquad (8)$$

The errors in the model parameters are estimated from the diagonal elements of the covariance matrix

$$\text{cov}\,\mathbf{m} = \sigma_d^2[\mathbf{G}^T\mathbf{G}]^{-1} \qquad (9)$$

where σ_d^2 is the variance of the data.

The size of the frequency interval to be used represents a trade-off between resolution and error; a larger frequency interval includes more data and therefore reduces the estimated errors in the model parameters, but also means reduced resolution. The sizes of the frequency intervals that were used were found by testing different size intervals, and choosing the smallest interval that still gave an acceptably small error.

As formulated in equation (6), there is not enough information to uniquely determine a solution; at least one additional constraint must be applied. If one of the sites can be considered to be a reference site; that is, a hard-rock site, then that site response can be constrained to be 1.0. (Actually the constraint must be linear, so that the log of the site response is constrained to be 0.0.)

In the present study, with numerous stations spread over large distances, it is difficult to identify one site and call it a reference site. Instead, the log-average site response is constrained to be 0.0. In one sense this is clearly not a valid constraint, since the "average" site will not have zero site attenuation, and therefore the average site response would be expected to fall with increasing frequency. Note, however, that the value for Q derived from the inversions will be identically the same whether a single site is chosen to be a reference site, or whether the log-average site response is taken to be 0.0. The values of the site responses will, of course, change depending on the chosen constraint.

The solutions to the inverse problem were computed using singular-value decomposition. Singular-value decomposition has the advantage that small singular values indicate the presence of non-uniqueness. This sometimes happened in the present study for a particular frequency range when there was only a small amount of data at one of the stations. When this occurred, the data from that station were removed from the inversion for that particular frequency range. Figure 4 shows several example fits to the spectra using the method described above.

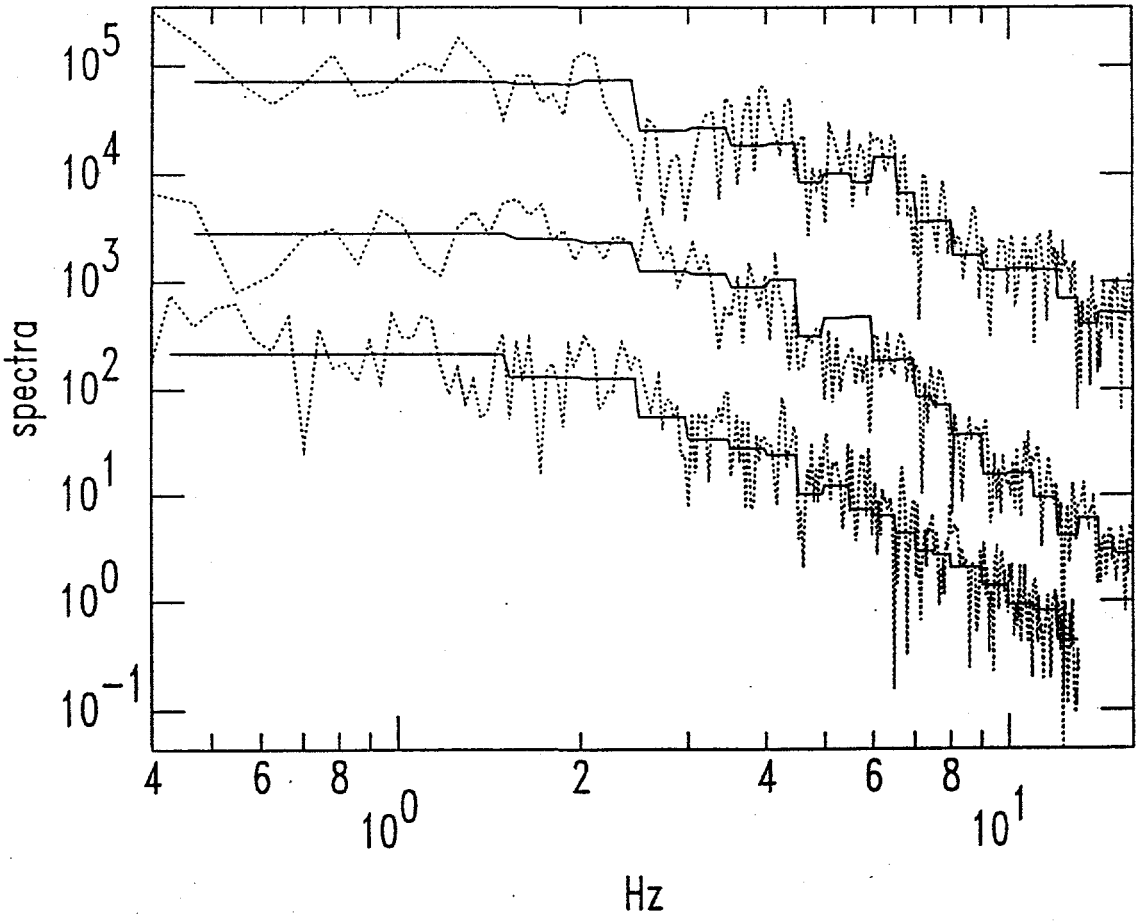

Figure 4. Example of the fits to the FFTs. The quality of the fits shown is typical of the results; the frequency range that could be fit for these FFTs is greater than is available for most of the data.

2.4 INVERSION RESULTS: $Q(f)$

Five areas in the United States were chosen based on the availability of data and on the expectation of finding measureable differences between the areas in *Lg* attenuation. Three areas (NEUS, SEUS, and CUS) were included from the central and eastern United States and two areas (BR and CN) from the western United States (Figure 3). Nine sites, 28 events, and 87 spectra were used in the NEUS inversions; 10 sites, 21 events, and 52 spectra were used in the CUS inversions; 7 sites, 19 events, and 42 spectra were used in the SEUS inversions; 8 sites, 17 events, and 53 spectra were used in the CN inversions; 4 sites, 15 events, and 42 spectra were used in the BR inversions.

Large differences in *Lg* attenuation are found between the western United States and the central and eastern United States; however, only relatively minor differences are observed within the central and eastern United States and within the western United States. Table 5 lists the results of the inversions, and Figure 5 shows the values of Q_{Lg} determined for each of the five regions. Q_{Lg} in the central and eastern United States is significantly greater than in the western United States for all common frequencies. At the highest frequencies for which there are common results, 5 to 8 Hz, the average Q_{Lg} from all three of the regions in the central and eastern United States is 1000 ± 50, nearly double the average Q_{Lg} of 530 ± 20 determined in the same frequency range for the two regions in the western United States.

From 2 to 5 Hz, Q_{Lg} determined for the central and eastern United States is nearly constant, while Q_{Lg} in the western United States decreases with decreasing frequency. Averaging the Q_{Lg} values from 4.5 to 5.5 Hz gives 960 ± 50 for the central and eastern United States inversions and 510 ± 40 for the western United States inversions, roughly a factor of two difference. From 1.5 to 2.5 Hz, the average Q_{Lg} value for the central and eastern United States drops only slightly to 850 ± 30, while the average Q_{Lg} value for the western United States in the same frequency range is 320 ± 20, a factor of 2.6 difference.

Q_{Lg} in the western United States continues to decrease at frequencies below 2 Hz, falling to 230 ± 30 at 0.75 Hz. Q_{Lg} in the central and eastern United States, however, increases below 2 Hz; the average value for the three central and eastern United States areas is 1330 ± 230 between 0.75 and 1.0 Hz. This would make Q_{Lg} almost six times greater in the central and eastern United States than in the western United States in this frequency range.

The values of Q_{Lg} determined in the central and eastern United States at or below 1 Hz should be viewed with some caution, however, since there is the increased possibility of systematic biases affecting the results. The estimated errors for Q_{Lg} in the central and eastern United States at or below 1 Hz are relatively large. This occurs even though the sizes of the frequency intervals at low frequencies have been increased to reduce the errors (Table 5 and Figure 5). These large error terms at low frequencies are due to the difficulty in determining Q when the frequency is relatively small and Q is relatively large. These are also the most likely conditions under which systematic biases might become significant.

Although large differences are observed between Q_{Lg} in the central and eastern United States and the western United States, only small variations are found within each of these two regions. In the central and eastern United States, Figure 5 shows considerable overlap for the Q_{Lg} values for the NEUS, SEUS, and CUS inversions at all common frequencies. If we compute an average Q_{Lg} value for each of the three regions between 2 and 6 Hz, where Q_{Lg} is approximately constant, we find $Q_{Lg} = 770 \pm 40$ for the SEUS, $Q_{Lg} = 970 \pm 20$ for the NEUS, and $Q_{Lg} = 980 \pm 60$ for the CUS. The results for the NEUS and CUS are identical within the errors; Q_{Lg} in the SEUS is approximately 20% lower than Q_{Lg} in the NEUS or the CUS.

Below 2 Hz, both the NEUS and SEUS inversions show an increase in Q_{Lg} whereas the CUS inversions do. Because of the large errors in determining Q_{Lg} at these low frequencies, these apparent differences probably should not be considered significant. To gain a better understanding of the behavior of Q_{Lg} at low frequencies, the data from all three central and eastern United States regions were combined and a new inversion computed. This is believed appropriate since the differences in Q_{Lg} between the three regions are relatively small at most frequencies. Above 8 Hz, practically the only data available was from the NEUS, so above 8 Hz the inversion results are nearly identical to the those of the NEUS inversions. Below 8 Hz, the results are a combination of between 18 to 24 stations depending on the frequency range. The resulting values of Q_{Lg} are shown in Figure 6 along with two attempts to find approximate mathematical relations to model the results.

The dashed line in Figure 6 shows an attempt to model Q_{Lg} according to the standard form, $Q = Q_0 f^{\eta}$, with $Q_0 = 550$ and $\eta = 0.4$. This form is seen to give a reasonably good fit from 2 to 16 Hz. Below 2 Hz, however, the Q_{Lg} value determined from the inversions increases from 840 ± 60 at 1.9 Hz to 1420 ± 230 at 0.86 Hz, a much larger value than the 518 that the model estimate, based on $Q = 550\, f^{0.4}$, would give. As stated above, the values of Q_{Lg} below 2 Hz may be affected by systematic errors. On the other hand, if we accept these values it is not difficult to find a functional form that does a good job of fitting the entire frequency range. A simple Boltzmann relaxation mechanism (see, e.g., Liu et al., 1976) is a reasonably good model:

$$Q = K\frac{1+(2\pi f\tau)^2}{2\pi f\tau} \qquad (10)$$

where K is a constant related to the relaxed and unrelaxed elastic moduli, and τ is the period of the relaxation mechanism. Assuming $K = 400$ and $\tau = 0.053$ (corresponding to a frequency of 3.0 Hz), a reasonably good fit can be obtained at all frequencies as evidenced by the solid line in Figure 6.

In contrast to the results for the central and eastern United States, the values of Q determined for the western United States can be well modeled by the standard functional form, $Q = Q_0 f^{\eta}$, at all frequencies (Figure 7). For California and western Nevada, the results are well modeled with $Q_0 = 240$ and $\eta = 0.5$; for the northern Basin and Range, the results are well modeled with $Q_0 = 240$ and $\eta = 0.4$. The results for the two areas within the western United States are very similar to each other, with little variation in the Q values at any of the common frequencies.

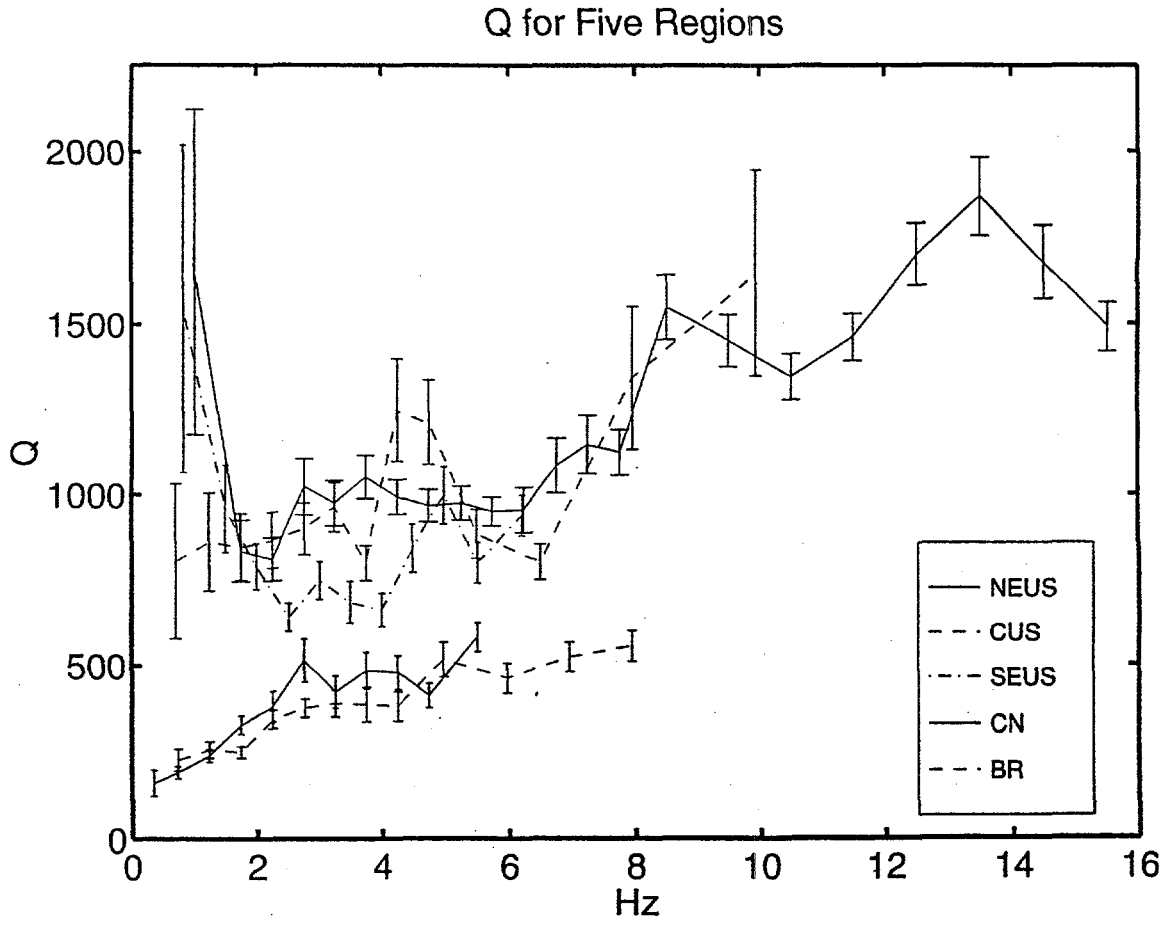

Figure 5. *Q* plotted vs. the average frequency for each of five regions. The three regions with the highest values of *Q* are from the central and eastern United States; the two regions with the lowest values of *Q* are from the western United States. Error bars in this and subsequent figures are two standard deviations in length.

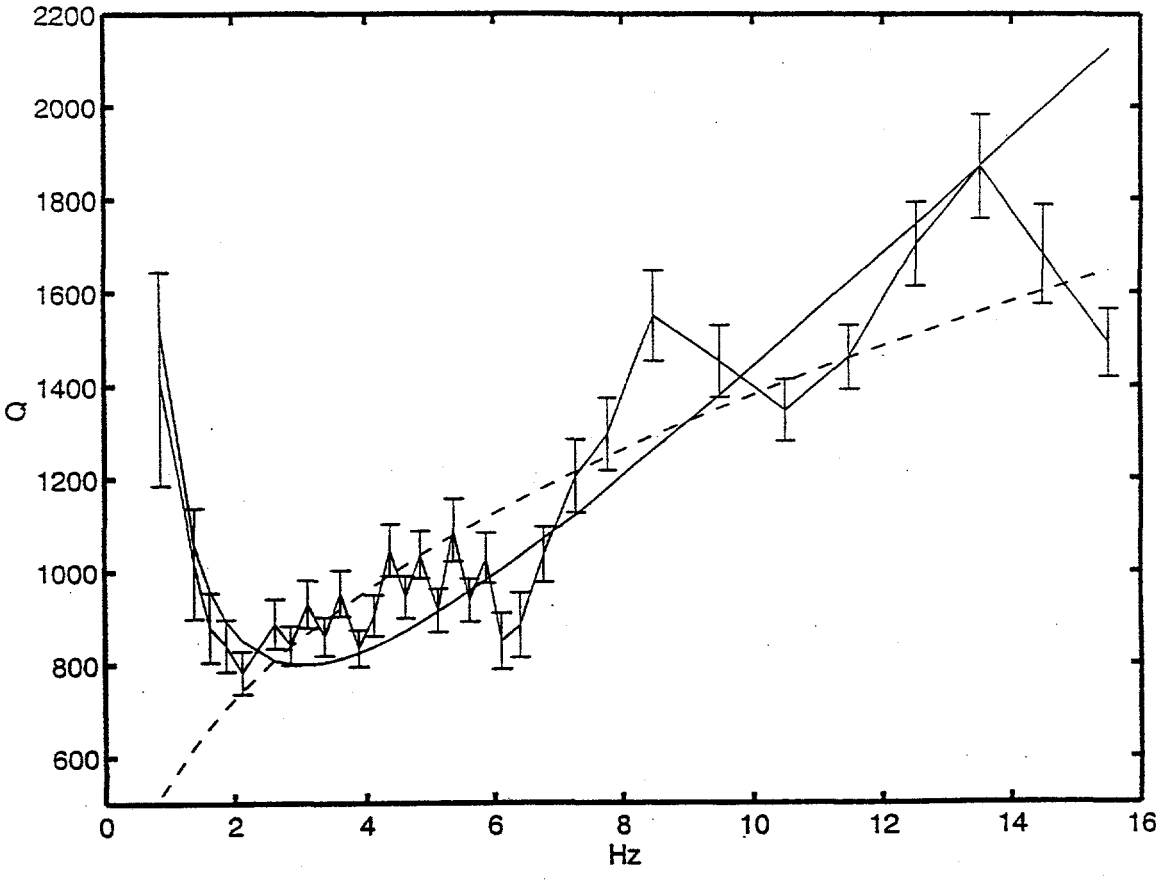

Figure 6. Q plotted vs. the average frequency combining the three regions in the central and eastern United States. The two smooth curves are different models that attempt to fit the results: dashed line is $Q = 550\, f^{0.4}$, solid line is a Boltzmann relaxation mechanism (see text).

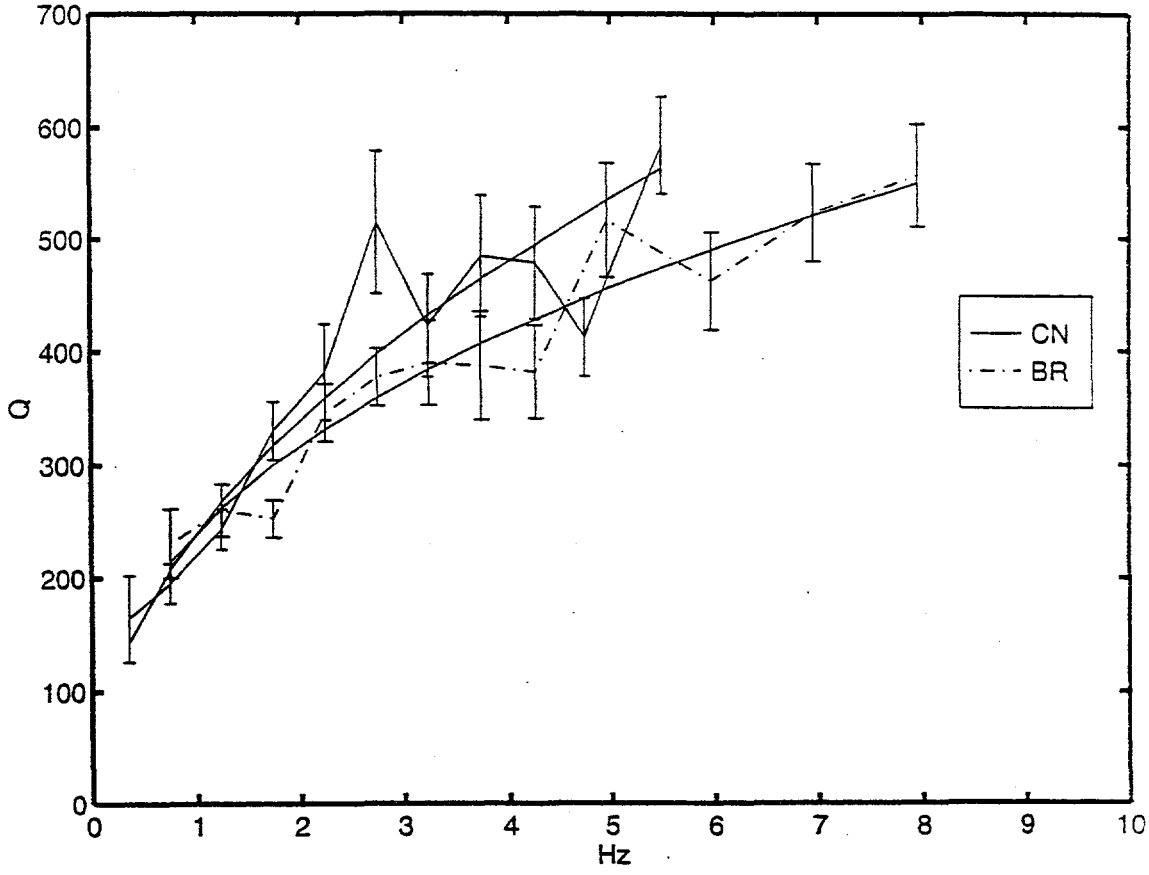

Figure 7. Q plotted vs. frequency for two western United States regions. Smooth curves are: for CN, $Q = 240 f^{0.5}$; for the BR, $Q = 240 f^{0.4}$.

Table 5. Inversion results for *Lg* Q in the five regions studied.

Freq. interval (Hz)	Avg. freq. (Hz)	No. of stations	$\gamma(10^{-3}\ km^{-1})$	Q
Northeastern U. S. (NEUS):				
0.4 - 1.5	1.02	9	0.55 ± 0.16	1654 ± 472
1.5 - 2.0	1.75	9	1.89 ± 0.20	836 ± 89
2.0 - 2.5	2.25	9	2.48 ± 0.15	813 ± 63
2.5 - 3.0	2.76	9	2.41 ± 0.20	1025 ± 84
3.0 -3.5	3.24	9	2.99 ± 0.20	975 ± 67
3.5 - 4.0	3.75	9	3.20 ± 0.20	1053 ± 65
4.0 - 4.5	4.26	9	3.85 ± 0.20	993 ± 52
4.5 - 5.0	4.75	9	4.40 ± 0.22	968 ± 48
5.0 - 5.5	5.26	8	4.84 ± 0.25	975 ± 50
5.5 - 6.0	5.74	8	5.42 ± 0.24	951 ± 42
6.0 - 6.5	6.25	8	5.87 ± 0.40	955 ± 66
6.5 - 7.0	6.76	8	5.57 ± 0.42	1088 ± 83
7.0 - 7.5	7.24	8	5.65 ± 0.43	1151 ± 87
7.5 - 8.0	7.76	8	6.18 ± 0.38	1128 ± 69
8.0 - 9.0	8.50	7	4.92 ± 0.30	1551 ± 96
9.0 - 10.0	9.49	7	5.86 ± 0.31	1453 ± 76
10.0 - 11.0	10.5	6	7.00 ± 0.35	1348 ± 66
11.0 - 12.0	11.5	6	7.06 ± 0.33	1462 ± 69
12.0 - 13.0	12.5	6	6.59 ± 0.35	1704 ± 90
13.0 - 14.0	13.5	6	6.48 ± 0.39	1870 ± 112
14.0 - 15.0	14.5	6	7.74 ± 0.49	1680 ± 106
15.0 - 16.0	15.5	6	9.33 ± 0.45	1491 ± 72
Central U. S. (CUS):				
0.4 - 1.0	0.71	10	0.80 ± 0.22	806 ± 226
1.0 - 1.5	1.25	10	1.30 ± 0.21	862 ± 141
1.5 - 2.0	1.75	10	1.86 ± 0.21	847 ± 97
2.0 - 2.5	2.25	10	2.33 ± 0.22	867 ± 81
2.5 - 3.0	2.75	10	2.75 ± 0.23	901 ± 75
3.0 - 3.5	3.24	10	3.02 ± 0.23	963 ± 73
3.5 - 4.0	3.75	10	4.20 ± 0.27	801 ± 51
4.0 - 4.5	4.26	10	3.05 ± 0.37	1251 ± 150
4.5 - 5.0	4.75	9	3.51 ± 0.36	1215 ± 124
5.0 - 6.0	5.50	8	5.57 ± 0.44	886 ± 71
6.0 - 7.0	6.50	8	7.25 ± 0.47	805 ± 52
7.0 - 9.0	7.96	6	5.32 ± 0.82	1344 ± 209
9.0 - 11.0	9.94	5	5.41 ± 0.98	1649 ± 298

Table 5 (continued). Inversion results for *Lg* Q in the five regions studied.

Southeastern U. S. (SEUS):				
0.4 - 1.25	0.84	7	0.49 ± 0.15	1543 ± 477
1.25 - 1.75	1.51	7	1.41 ± 0.19	960 ± 129
1.75 - 2.25	1.99	7	2.26 ± 0.19	792 ± 67
2.25 - 2.75	2.50	7	3.49 ± 0.23	643 ± 42
2.75 - 3.25	3.00	7	3.59 ± 0.26	751 ± 54
3.25 - 3.75	3.49	7	4.55 ± 0.40	688 ± 60
3.75 - 4.25	4.00	7	5.40 ± 0.39	665 ± 48
4.25 - 4.75	4.49	7	4.78 ± 0.39	843 ± 70
4.75 - 5.25	4.98	7	4.48 ± 0.38	999 ± 85
5.25 - 5.75	5.51	6	6.16 ± 0.46	802 ± 60
5.75 - 6.75	6.22	6	5.95 ± 0.37	939 ± 59
Northern Basin and Range (BR)				
0.5 - 1.0	0.75	4	2.92 ± 0.39	231 ± 31
1.0 - 1.5	1.25	4	4.31 ± 0.39	260 ± 23
1.5 - 2.0	1.75	4	6.22 ± 0.41	253 ± 17
2.0 - 2.5	2.25	4	5.82 ± 0.43	346 ± 26
2.5 - 3.0	2.75	4	6.54 ± 0.44	378 ± 25
3.0 - 3.5	3.24	4	7.46 ± 0.71	391 ± 37
3.5 - 4.0	3.75	4	8.67 ± 1.07	388 ± 48
4.0 - 4.5	4.26	4	9.99 ± 1.07	382 ± 41
4.5 - 5.5	4.97	4	8.64 ± 0.85	517 ± 51
5.5 - 6.5	5.98	4	11.6 ± 1.09	463 ± 44
6.5 - 7.5	6.96	4	11.9 ± 0.99	524 ± 44
7.5 - 8.5	7.96	3	12.8 ± 1.06	557 ± 46
California and western Nevada (CN):				
0.0 - 0.5	0.35	8	1.93 ± 0.45	164 ± 38
0.5 - 1.0	0.74	8	3.42 ± 0.31	195 ± 18
1.0 - 1.5	1.24	8	4.59 ± 0.34	243 ± 18
1.5 - 2.0	1.75	8	4.75 ± 0.37	330 ± 26
2.0 - 2.5	2.24	7	5.27 ± 0.58	382 ± 42
2.5 - 3.0	2.74	7	4.78 ± 0.59	515 ± 64
3.0 - 3.5	3.24	6	6.88 ± 0.74	423 ± 45
3.5 - 4.0	3.75	6	6.94 ± 0.77	485 ± 54
4.0 - 4.5	4.26	6	7.97 ± 0.83	479 ± 50
4.5 - 5.0	4.74	6	10.3 ± 0.86	413 ± 34
5.0 - 6.0	5.51	5	8.47 ± 0.63	584 ± 43

2.5 INVERSION RESULTS: SITE RESPONSES

The site responses determined in the inversions are shown in Figures 8-12. Each of these site responses was determined with the constraint that the log-average site response be 0.0, so these responses can be thought of as the ratio of the site response for the particular site to the average site response of all stations used in the inversions. A site response that is equal to 1.0, therefore, indicates a site response that is equal to the average site response. Because of this, the site responses presented here are not the true site responses. Nonetheless, these estimated site responses can be used as a starting point for these sites and are also a useful measure of the relative differences between the site responses.

The ratio of the largest to smallest site amplification for any particular frequency was typically a factor of 3 to 10, and in some cases was as large as a factor of 20. At some sites the responses show peaks and holes, presumably corresponding to near-surface resonances, but do not systematically increase or decrease. At other sites the site response systematically increases or decreases with frequency. Site responses that increase systematically probably represent sites with lower than average attenuation in the near-surface, while site responses that decrease systematically probably represent sites with higher than average attenuation in the near surface. This near-surface attenuation would not be included in the whole path Q as determined in the inversions, and is usually modeled using the parameter t^* or κ according to, $e^{-\pi f t^*}$ (e.g. Anderson and Hough, 1984). No attempt was made to determine t^* for each site, although relative t^* values could be estimated from the slopes of these site responses.

It is interesting to compare the site responses determined for the two stations that were included in more than one region. These two stations are MCWV, which was included in both the NEUS and SEUS inversions, and MIAR, which was included in both the CUS and SEUS inversions. For site MCWV, the site amplification determined from the NEUS inversions is greater than that determined from the SEUS inversions by approximately a factor of 2 (Figures 8 and 9). Similarly, the amplification at site MIAR is greater by roughly a factor of 2 for the CUS inversions compared to the SEUS inversions (Figures 9 and 10). This indicates that the average site amplification determined from the NEUS and CUS inversions is roughly two times lower than the average site amplification determined from the SEUS inversions. This is apparently due to one or more of the sites in the SEUS having large site amplifications that significantly increase the average site response. Both stations GOGA and BLA show large site amplifications for the SEUS inversions.

It is also interesting to compare the shapes of the two estimates of the site responses at sites MIAR and MCWV. For MCWV, both the NEUS and SEUS inversions show a broad peak from roughly 2 to 5 Hz. For MIAR, however, the SEUS inversions show a minimum at approximately 3.5 Hz, while the CUS inversions yield a maximum near the same frequency. These comparisons show the difficulty in determining site responses when no suitable reference sites exist.

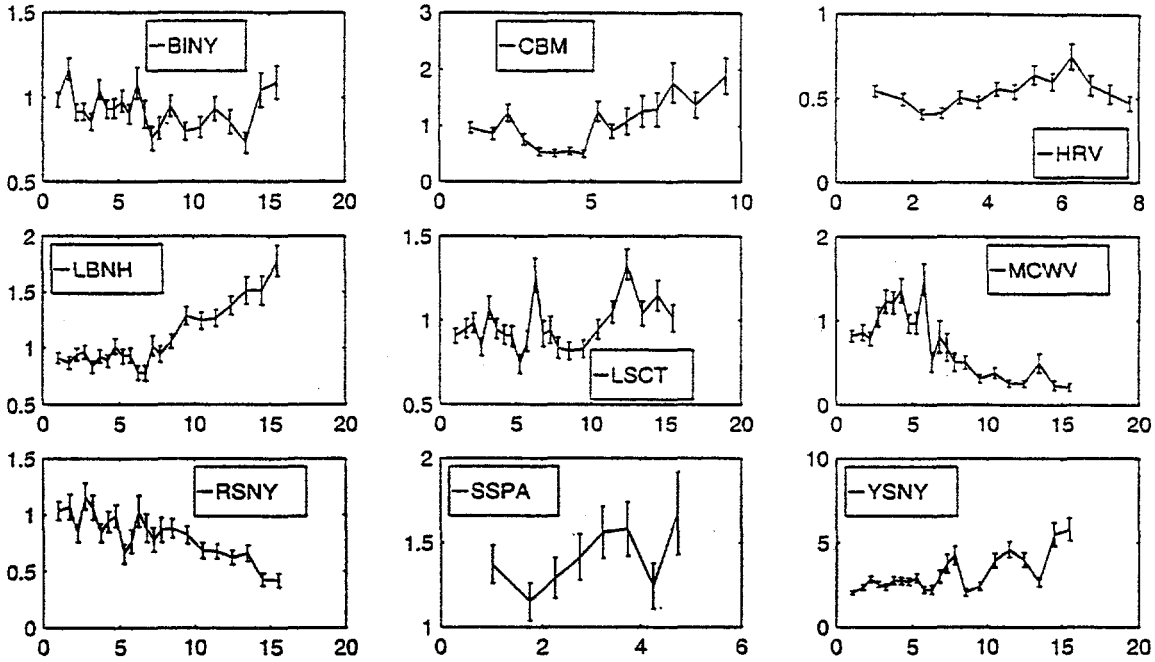

Figure 8. Site responses from the inversions for the northeastern United States.

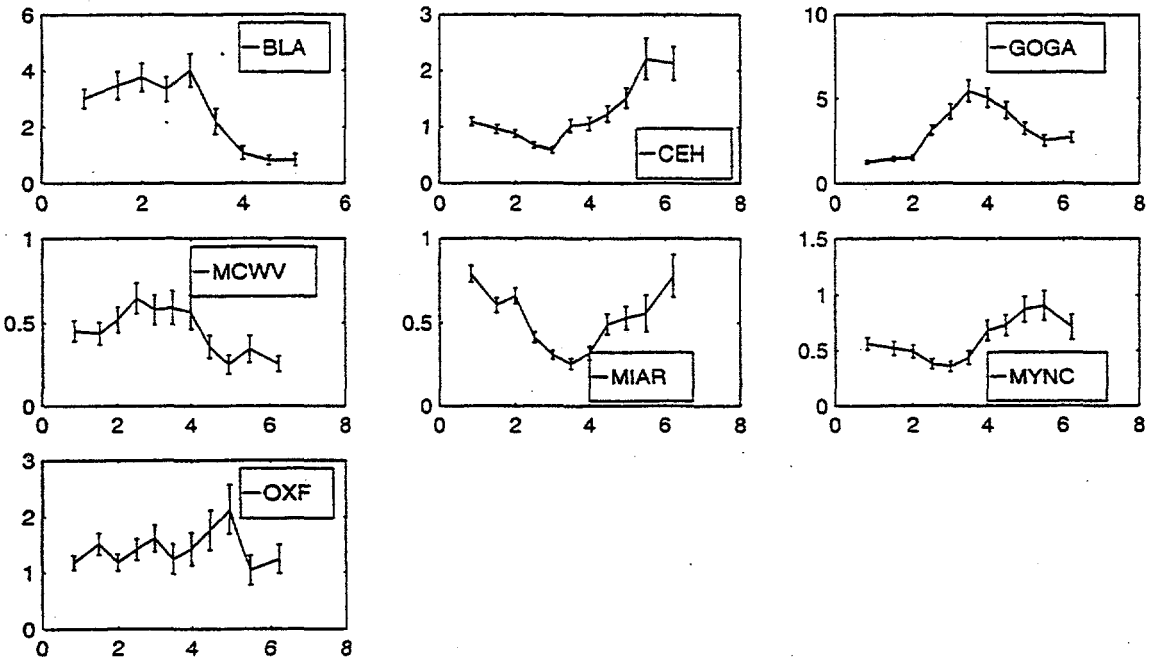

Figure 9. Site responses from the inversions for the southeastern United States.

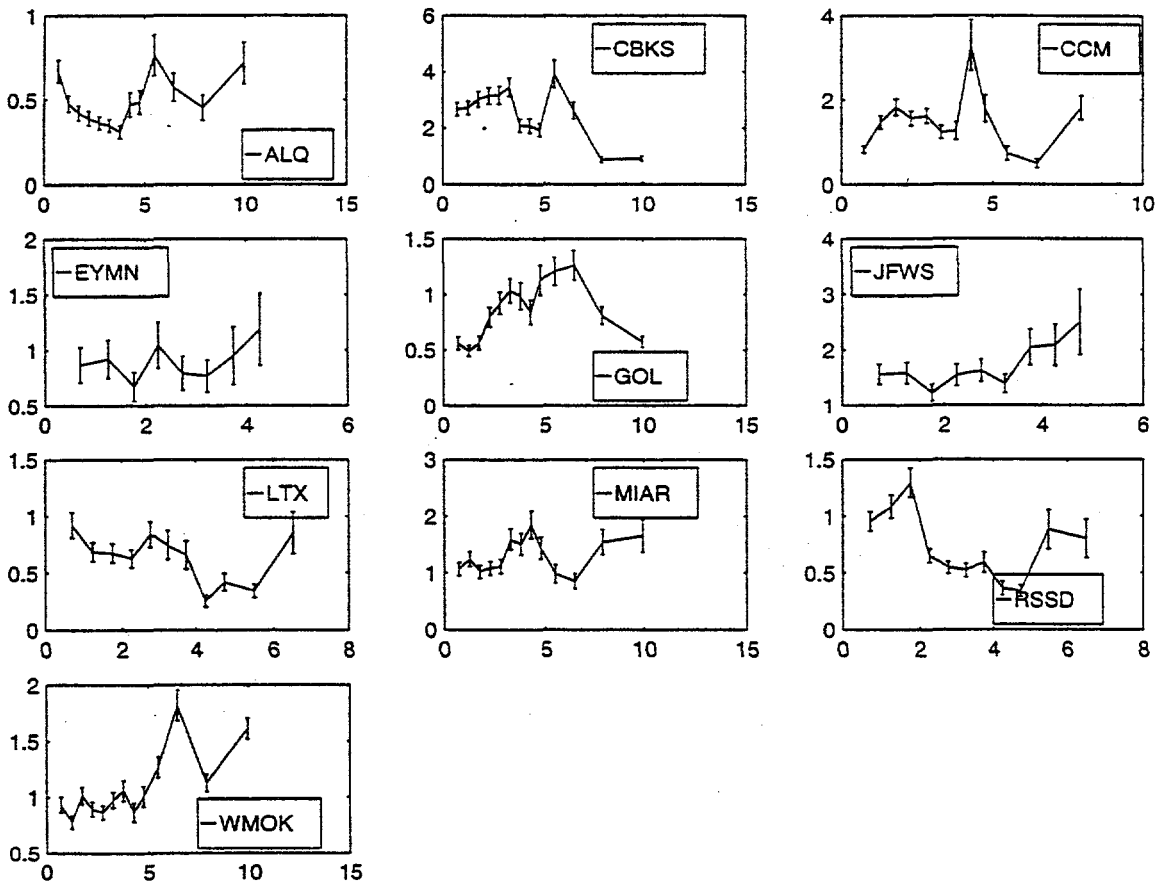

Figure 10. Site responses from the inversions for the central United States.

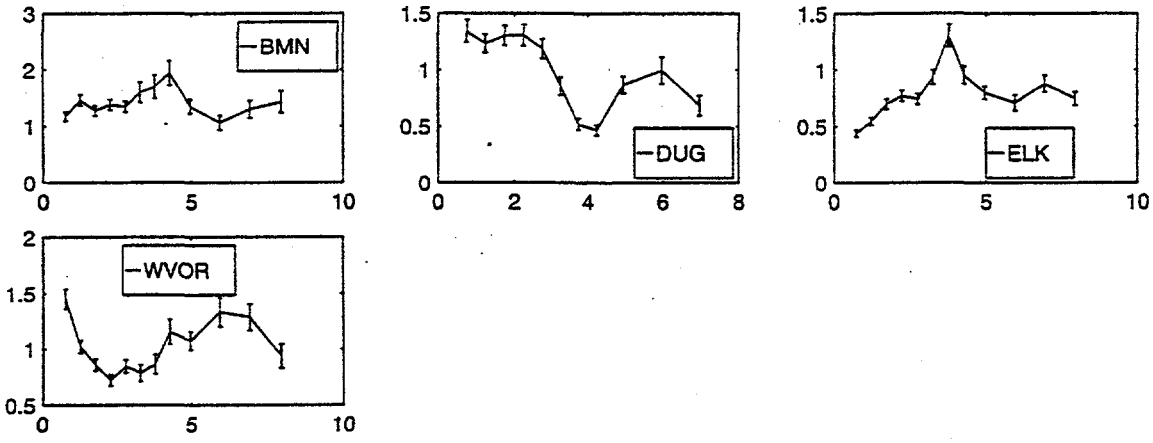

Figure 11. Site responses from the inversions for the northern Basin and Range.

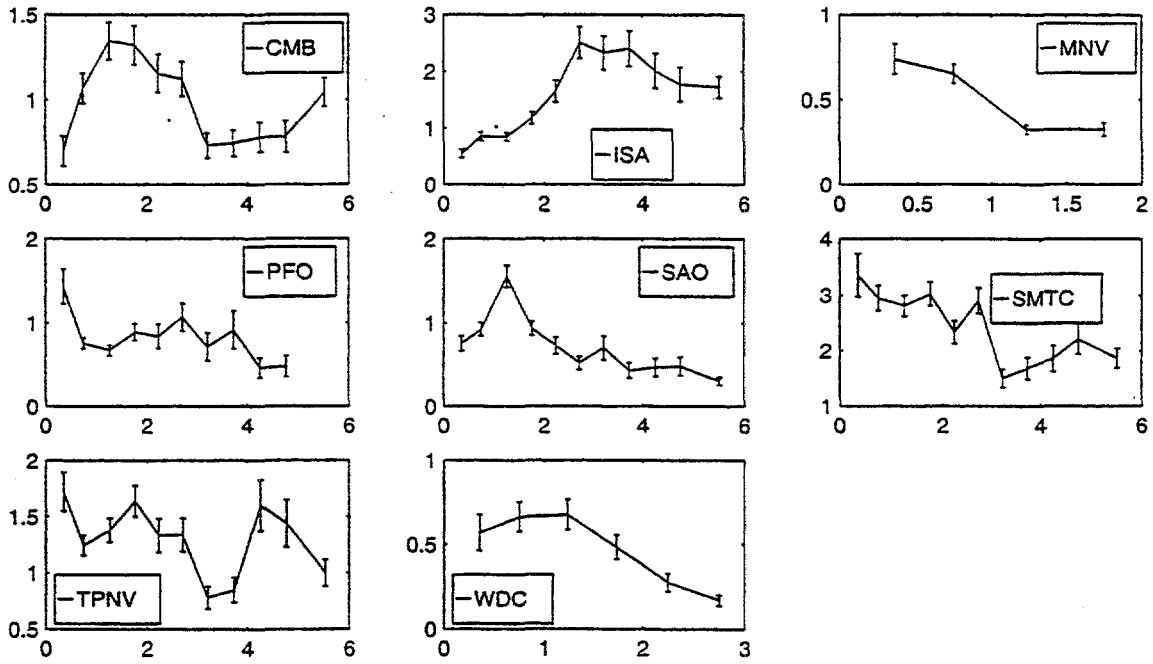

Figure 12. Site responses from the inversions for California and western Nevada.

2.6 DISCUSSION AND CONCLUSIONS

The results of Q_{Lg} measurements in this study are generally similar to previously published results. For example, the values of Q_{Lg} determined in this study for the BR, as approximated by $Q_{Lg} = 240 f^{0.4}$, are in close agreement with the values of 200-230 $f^{0.45\text{-}0.7}$ obtained by Chavéz and Priestley (1986), 210-300 $f^{0.3\text{-}0.4}$ obtained by Xie and Mitchell (1990a), and 200-350 $f^{0.3\text{-}0.5}$ obtained by Singh and Herrmann (1983). The values of Q_{Lg} determined for CN, as approximated by $Q_{Lg} = 240 f^{0.5}$, are in reasonably close agreement with 200 $f^{0.7}$ obtained by Nuttli (1981) for southern California, and slightly larger than the values of 150 $f^{0.4\text{-}0.5}$ obtained by Singh and Herrmann (1983) for California.

Due to the importance of the *Lg* phase for seismic hazard analysis in the central and eastern United States (and in eastern Canada, as well) numerous studies of Q_{Lg} have been conducted for eastern North America (see the Introduction for references). Modeling Q_{Lg} as $Q_0 f^{\eta}$, Q_0 determined in these studies typically ranges from 500-1200 and η from 0.2 to 0.5.

The gradual increase in Q_{Lg} for the central and eastern United States seen in this study from roughly 2 to 16 Hz is in keeping with the results of previous studies. Excluding frequencies below 2 Hz, the Q_{Lg} values obtained in this study for the central and eastern United States can be approximately modeled by $Q_{Lg} = 550 f^{0.4}$ (Figure 6). These values of Q_0 and η are within the range of previously determined values for the central and eastern United States, although Q_0 is toward the low end of previous values and η is toward the high end. This result, however, depends on the frequency range. Examining Figure 6 it is apparent that the measured increase of Q_{Lg} with frequency for the central and eastern United States is more gradual from 2 to 7 Hz than it is from 7 to 16 Hz. From 2 - 7 Hz, Q_{Lg} is better modeled by $Q_{Lg} = 700 f^{0.2}$, and from 7 - 16 Hz, Q_{Lg} is better modeled by $Q_{Lg} = 350 f^{0.6}$.

Comparing the result for the central and eastern United States to the western United States in the 2 to 7 Hz range, η in the central and eastern United States is lower than η in the western United States, in keeping with the results of previous studies. The above results also suggest that in the central and eastern United States η increases with frequency above about 7 Hz, at least for the NEUS where most of the high frequency data has been derived.

An interesting result of this study is the relatively small variations found in Q_{Lg} within the central and eastern United States and within the western United States. Differences in Q_{Lg} within the central and eastern United States had been identified as early as twenty years ago, when Street (1976) found greater attenuation, by a factor of 1.6, in the northeastern United States compared to the results of Nuttli (1973) for the central United States. Studying a wider frequency range, Nuttli (1981) and Singh and Herrmann (1983) found a similar result, with Q_{Lg} in the central United States greater than Q_{Lg} in the eastern United States by a factor of two or less. On the other hand, Gupta and McLaughlin (1987) found the opposite result, with Q_{Lg} in the central United States roughly two times smaller than Q_{Lg} in the eastern United States, at least near 1 Hz.

In contrast to these results, this study has found no significant difference in Q_{Lg} between the NEUS and the CUS. Indeed, the average Q_{Lg} value between 2 and 6 Hz for the NEUS (970 ± 20) is identical within the errors to the CUS value (980 ± 60). In the SEUS, Q_{Lg} (770 ± 40) was found to be lower by about 20% than in the NEUS or the CUS; however, even this result should be viewed with some caution. While the standard deviations appear to indicate a significant difference between the SEUS and the NEUS and CUS Q_{Lg} values, these standard deviations measure the random errors only, and not systematic biases. In particular, the amount of bias that would result from the choice of particular station locations is unknown. The bias due to station locations could result in apparent regional variations in Q_{Lg} that do not actually exist.

As within the central and eastern United States, little significant difference has been found in Q_{Lg} values for different areas within the western United States. Based on previous results that found greater attenuation in tectonically active regions compared to stable regions (e.g. Hwang and Mitchell, 1987), it was thought that Q_{Lg} might vary in the western United States based on the rate of tectonic and seismic activity. Accordingly, two areas were chosen for study, one of relatively high tectonic and seismic activity (California and western Nevada), and one having a lower rate of tectonic and seismic activity (northern Basin and Range). At most frequencies, however, Q_{Lg} was not found to vary significantly between CN and the BR. What small variation there is indicates a slightly larger Q_{Lg} for CN than for the BR, opposite of the expected result.

The lack of significant variation of Lg attenuation between the two western United States regions appears to indicate that the rate of tectonic and seismic activity is not the sole determinant of the level of Lg attenuation. Alternatively, the relatively large areas of the regions examined may be masking variations in Q_{Lg} in the western United States which might correlate with tectonic activity on a smaller scale.

Another unusual feature of this study is the increase of Q_{Lg} seen for the central and eastern United States below 2 Hz (Figures 5 and 6). This raises a question about the applicability of the commonly held assumption that the frequency dependence of Q_{Lg} can be modeled by $Q_{Lg} = Q_0 f^{\eta}$, which for positive values of η yields a Q_{Lg} that increases with frequency. Instead, the results of this study are modeled better by a standard relaxation mechanism with a minimum in Q_{Lg} near 3.0 Hz. However, the difficulty of determining Q_{Lg} at low frequencies when Q_{Lg} is large suggests that the high Q_{Lg} below 2 Hz may be due to unknown and relatively subtle systematic biases in the method or the data analysis.

As an illustration of the difficulty in accurately determining Q_{Lg} at 1 Hz, one can consider the difference in spectral amplitude that the standard $Q_{Lg} = Q_0 f^{\eta}$ model and the relaxation mechanism model would produce. At 1 Hz, using $K = 400$ and $\tau = 0.053$ in equation (6), gives $Q_{Lg} = 1330$; for $Q_{Lg} = 550 f^{0.4}$, $Q_{Lg} = 550$ at 1 Hz. For a distance of 400 km, using $Q = 1330$ from the relaxation mechanism, the spectral amplitude would be reduced by 24%; for $Q = 550$ from the standard model, the spectral amplitude would be reduced by 48%. The difference in spectral amplitude produced by the two values of Q_{Lg} is a factor of 1.5. Such a factor is relatively small given the fluctuations in spectra that are typically seen in Fast Fourier Transforms.

Finally, although this studies calls into question the amount of the variation of Q_{Lg} within the western United States and within the central and eastern United States, there are certain to be some variations within each of these regions, especially on smaller scales. The method described in this paper could be easily modified to perform a tomographic inversion for Q_{Lg}. This type of inversion has been computed for Lg coda waves (Xie and Mitchell, 1990b; Mitchell, 1995), but not direct waves. Using the method described in this study would allow inversions to be performed at different frequencies without any assumption about the functional form of $Q(f)$, and, since the method is a linear inversion, would allow simple estimations of the errors in the modeled Q_{Lg} values.

3. ANALYSIS OF ATTENUATION, SITE RESPONSE, AND SOURCE PARAMETERS IN THE CENTRAL AND EASTERN UNITED STATES USING THE REGIONAL PHASES Pn, Pg, Sn, and Lg

3.1 INTRODUCTION

The paucity of earthquake recordings for the central and eastern United States makes seismic hazard analysis difficult. This lack of data is due, in part, to the relatively low rate of earthquake activity in the region, but is also due to a lack of instrumentation. The National Seismograph Network (NSN), which has been installed over the last five years, is increasing the data available for study from the central and eastern United States (CEUS).

The NSN data set examined in this study spans the dates from 1 January 1992 to 12 July 1995 and includes recordings from 185 earthquakes recorded at 22 CEUS stations. The magnitudes range from less than 3.0 up to 5.6, and epicenters vary from 9 km to about 3000 km, with most of the data between 150 and 1250 km epicentral distance.

In order to analyze this data set, the Fourier amplitude spectra of various phases have been computed. The predominant phases in the data set are the regional phases: Pg and Lg, postcritically reflected waves trapped in the crust, and Sn and Pn, waves that extend down to and travel through the uppermost mantle. Also included in the data are a few local recordings (less than about 100 km epicentral distance) of direct S and P waves, called Sg and Pg, and S phases (at epicentral distances greater than about 1500 km) that travel deeper within the mantle than Sn. A total of 616 spectra were computed for this study.

Of the four predominant phases—Pg, Lg, Pn, and Sn—Lg, since it has the largest amplitudes, is the most important phase for direct hazard analysis, with Sn of some potential significance. All of the phases are important, however, for understanding the structure of the earth and the properties of the earthquake source, factors that are critical to predicting ground motion and, therefore, seismic hazard.

In this study, the details of the data set will first be discussed, followed by an examination of the variation of regional phase propagation in the central and eastern United States. After that, the methods for analyzing the spectra and the results of that analysis will be discussed.

One of the important factors that determines seismic hazard is the attenuation of seismic waves with distance in the earth. Average CEUS Q values for the crust and uppermost mantle have been determined for P and S waves from the data. These values are compared to a few recordings, included in the data set, from the western United States (WUS), where attenuation is generally larger by a factor of two to three over attenuation measured at CEUS stations.

For CEUS data and a frequency-independent Q, Q_P is found to be roughly equal to Q_S in the crust and uppermost mantle, with an average crustal value for frequency-independent Q of approximately 900. In the uppermost mantle, Q values are more poorly constrained, but exceed Q values from the crust with average values near 5000. Measurements assuming frequency-dependent Q are also discussed and given in this report. S wave attenuation measured for epicentral distances greater than about 1500 km increases dramatically, possibly indicating that the ray paths travel through the low-velocity zone of the mantle at these distances.

Lg Q values determined in this report are generally in good agreement with previous estimates of CEUS attenuation (e.g. Bollinger, 1979; Nuttli, 1983; Dwyer et al., 1983; Hasegawa, 1985; Chun et al., 1987; Gupta et al., 1987; Shin and Herrmann, 1987; Atkinson and Mereu, 1992; Boatwright, 1994).

CEUS earthquake source parameters, including seismic moment and stress drop, have also been estimated for all earthquakes for which spectra were computed at at least four NSN stations (17 earthquakes for S waves and 19 for P waves). This analysis is based on a single corner frequency source spectral model (Boatwright, 1984) similar to models proposed originally by Aki (1967) and Brune (1970). It is found that for earthquakes ranging from seismic moments of 10^{20} to 10^{24} dyne-cm, earthquakes scale with an approximately constant stress drop, not increasing with seismic moment as suggested, for example, by Street et al. (1975), Street and Turcotte (1977), Nuttli (1983), Chael (1987), and Chun et al. (1989b).

The constant stress drop scaling is in agreement with other studies of CEUS earthquakes (e.g. Somerville et al., 1987; Boore and Atkinson, 1987; Boore and Atkinson, 1989; Johnston, 1994). However, the stress drops determined in this study, primarily between 1 and 100 bars, are significantly lower than those found in Somerville et al. (1987), Boore and Atkinson (1987), or Johnston (1994), all of which find average stress drops near 100 bars.

An additional complication in the source modeling is the possibility that the simple source spectral models first proposed by Aki (1967) and Brune (1970) may not adequately model the data (e.g. Boatwright and Choy, 1992; Atkinson, 1993; Boatwright, 1994; Atkinson and Boore, 1995; Haddon, 1995). In order to assess this possibility, the Lg spectra of the six largest (magnitude 4.0 to 5.6) and best-recorded earthquakes in the data set were compared to the more complicated source model proposed in Atkinson and Boore (1995). The results are somewhat mixed. The spectra of three of the earthquakes (magnitudes 4.2, 4.3, and 4.6) were well modeled by the Atkinson and Boore model. There were discrepancies, however, between the model and the data for the two smallest earthquakes (both magnitude 4.0) and the largest earthquake (magnitude 5.6).

Finally this study presents some preliminary results of the estimation of site response for NSN stations in the central and eastern United States.

3.2 DATA

Table 6 shows a summary of the data set by phase, and Table 7 shows a detailed breakdown of the data by earthquake. The largest number of spectra (180) were computed for the Lg phase, which generally has the largest-amplitude wavetrain for the body-wave phases from 100 km to >2000 km epicentral distance. Only 34 Sn spectra were computed; the Sn phase often has weak amplitudes, and the Sn wavetrain can be lost in the coda of the P waves.

In addition, 130 Pn spectra, 104 Pg spectra, and 65 Sg spectra have been computed. Many of the Pg and Sg spectra are from relatively small earthquakes, locally recorded by only one station.

All of the 22 CEUS stations whose recordings are used in this report recorded three components. Most of the stations are equipped with CMG-3 broadband sensors, a few have Streckheisen STS-1 or STS-2 broadband sensors, and two have short-period sensors. Most of the data are recorded at 40 samples/s, while some of the data are recorded at 20 samples/s.

All of the data were obtained through the Internet from the U S Geological Survey in Golden, Colorado via File-Transfer Protocol. The data for 1994 and 1995 were collected on an ongoing basis using the Automatic Data Request Manager (Buland, 1992). Ray paths projected to the surface for all of the data are shown in Figure 13.

Before computing the spectra, the phases are picked on the seismograms (Figure 14) using a travel time table appropriate to the CEUS (Nuttli et al., 1969). For P waves the vertical component is used, and for S waves the horizontal components are rotated to transverse. The signal of each phase is windowed so as to include the majority of energy for that phase. A noise window of equal length to and just before the signal window is also taken. A 5% taper is applied to each window.

The noise of the first-arriving P wave, then, is the ambient noise. (The first-arriving P wave is usually Pn for this data set, but for distances less than about 175 km it is Pg.) The noise for Pg, when it arrives second, is the coda of Pn. The noise for Sn is the Pn and Pg codas, and the noise for Lg is the Sn coda, which may actually be dominated by the Pn and Pg codas if the Sn phase is weak.

The window lengths for Pn are typically about 5 s at 250 km, increasing to about 10 s at 1250 km, and are typically 20 s for the few recordings beyond 1500 km distance. Typical window lengths for Pg range from 4 s for distances less than 100 km up to about 10 s at 1000 km. Pg is observed only rarely above 700 km epicentral distance.

Typical Sn window lengths vary from 7 s at 300 km to 15 s at 1000 km; Lg window lengths vary from about 15 s at 300 km to 35 s at 1200 km, with windows over 2000 km of typically 75 s. Care is taken in choosing the Lg window lengths in order not to include significant surface-wave energy.

After computation of the signal and noise Fast Fourier Transforms, the signal and noise spectra are compared visually to determine the frequency range over which the signal exceeds the noise (Figure 15). The usable frequency range for Pn spectra is typically 1 to 16 Hz out to 1000 km. For distances beyond 1500 km the frequency range drops to typically 0.5 to 5 Hz. For Pg spectra, the typical frequency range that is used is again 1 to 16 Hz. For Sn spectra, the typical frequency range is 1 to 12 Hz. For Lg spectra, the frequency range is typically 0.3 to 12 Hz at 300 km, decreasing to 0.3 to 8 Hz at 500 km, 0.3 to 4 Hz at 1000 km, and 0.04 to 2 Hz beyond 1500 km.

Once the spectra have been computed, they are corrected for instrument response using calibrations obtained from the Automatic Data Request Manager.

At distances from roughly 100 to 250 km, the arrival of the Pn and Pg phases and the Sn and Lg phases is nearly coincident. In these cases windows are taken over both the Pn and Pg phases and the Sn and Lg phases. These spectra are labeled as "Pn + Pg" and "Sn + Lg" in Table 6.

For the shorter epicentral distances, several hundred km, the windows of Pn and Sn are long enough that they may contain the bounces off the Moho, PmP and SmS. If a clear phase arrival was seen between Pn and Pg, the windows were taken so as to exclude this arrival from the signal windows.

Table 6. Data summary by phase.

Phase	Number of Spectra
P_n, P	130
P_g	104
$P_n + P_g$	57
L_g	180
S	7
S_n	34
$S_n + L_g$	39
S_g	65
Total	616

Table 7. Data summary by earthquake.

Time (UTC)	Lat. (N)	Lon. (W)	Mag.	Stations and phases of computed spectra
1992 01/03 04:21	33.946	82.465	3.2	CEH (P_n, P_g)
1992 04/03 03:06	35.828	89.479	3.2	CCM (P_n, P_g)
1992 07/15 02:56	38.760	99.549	3.3	RSSD (P_n)
1992 08/21 16:31	33.050	80.116	4.4	CEH (Pn)
1992 08/26 05:41	37.360	89.680	3.2	CCM (P_{ng}, S_nL_g)
1992 09/27 17:02	28.172	88.438	3.8	MIAR (P_n, L_g)
1992 10/06 15:38	43.324	71.578	3.4	HRV (P_g, S_g); RSNY (P_{ng}, L_g)
1992 11/17 03:58	45.764	74.862	4.0	CBM (P_n); HRV (P_g, L_g)
1992 12/17 07:18	34.744	97.581	3.5	ALQ (P_g, L_g); CCM (P_n, L_g); GOL (P_n); MIAR (P_n); WMOK (P_g, S_g)
1992 12/27 10:12	37.5	89.63	3.2	CCM (P_{ng}, S_nL_g); MIAR (P_n, P_g)
1993 01/01 05:08	35.877	82.090	3.0	CEH (P_n, P_{ng}, L_g)
1993 01/08 13:01	35.830	90.030	3.5	CCM (P_n, S_nL_g); MIAR (P_n, P_g, L_g); WMOK (P_n)
1993 01/14 17:06	36.595	98.275	3.1	MIAR (P_n); WMOK (P_{ng}, S_nL_g)
1993 01/21 19:46	36.222	89.617	3.0	CCM (P_n, P_g, L_g); MIAR (P_n, P_g, L_g)
1993 02/06 02:09	36.660	89.730	3.5	CCM (P_{ng}, S_nL_g); MIAR (P_n, P_g, L_g)
1993 02/20 13:08	42.830	101.46	3.1	GOL (P_n, P_g); MIAR (S_n); WMOK (L_g)
1993 03/02 00:29	36.670	89.490	3.0	CCM (P_{ng}, S_nL_g); MIAR (P_n, L_g)
1993 03/16 07:38	35.670	90.550	3.0	CCM (P_{ng}, L_g)
1993 03/31 20:23	36.790	89.420	3.3	CCM (P_{ng}, S_nL_g)
1993 04/28 22:40	36.190	89.440	3.5	GOGA (P_n, L_g); MIAR (P_n, P_g, L_g); WMOK (P_n, S_n)
1993 05/06 01:23	46.300	75.500	3.5	RSNY (P_n, S_nL_g)
1993 06/05 12:45	45.674	96.293	4.1	GOGA (P_n, P_g); MIAR (P_n, S_n); RSSD (P_n, P_g, L_g); WMOK (P_n, S_n)

1993 07/16 10:54	31.779	88.326	3.7	GOGA (P_n, L_g); MIAR (P_n); MYNC (L_g)
1993 07/30 22:30	45.260	74.110	3.9	CBM (P_n, S_n, L_g); HRV (L_g)
1993 08/27 00:08	38.090	90.360	3.3	MIAR (P_n, S_n)
1993 08/30 05:15	46.450	75.060	3.8	CBM (P_n, L_g)
1993 09/23 06:45	46.06	74.600	3.9	BINY (P_n, S_n, L_g); CBM (P_n); LBNH (P_n, P_g, L_g)
1993 10/16 06:30	41.741	81.134	3.4	BINY (P_n, S_n); YSNY (P_{ng}, S_nL_g)
1993 11/16 09:31	45.182	73.495	3.8	BINY (P_n, L_g); CBM (P_n, L_g); HRV (P_n, P_g, L_g); LBNH (P_{ng}, S_nL_g); LSCT (P_n, L_g); MCWV (L_g); YSNY (P_n, L_g)
1993 11/30 03:07	35.900	103.10	3.6	ALQ (P_n, P_g, L_g); GOL (L_g); LTX (P_g, L_g); WMOK (P_n, P_g, L_g)
1994 01/16 00:42	40.327	76.007	4.0	LBNH (P_g, L_g); LSCT (P_{ng}, L_g); MCWV (P_n, P_g, L_g); YSNY (P_n, P_g, S_n)
1994 01/16 01:49	40.330	76.037	4.6	CEH (P_n, S_n); GOGA (L_g); LBNH (P_n, P_g, L_g); LSCT (P_n, P_{ng}, L_g); MCWV (P_n, P_g, L_g); MIAR (P_n, L_g); MYNC (L_g); YSNY (P_n, S_n)
1994 02/05 14:55	37.370	89.180	4.2	GOGA (L_g); LTX (P_n); MIAR (P_n, L_g); MYNC (P_n, L_g); WMOK (P_n, S_n)
1994 03/12 10:43	42.782	77.876	3.5	LBNH (L_g); LSCT (L_g); MCWV (L_g); YSNY (P_g, S_g)
1994 08/06 19:54	35.067	76.751	3.6	BINY (L_g); CEH (P_n, P_{ng}, L_g); MCWV (L_g); YSNY (L_g)
1994 09/02 21:00	NA	NA	NA	LBNH (P_{ng}, S_nL_g)
1994 09/02 21:23	42.800	84.543	3.4	BINY (L_g); MCWV (L_g)
1994 09/16 04:22	45.300	68.200	3.6	BINY (L_g); LBNH (P_g, L_g)
1994 09/16 04:36	45.300	68.200	NA	LBNH (P_g, L_g)
1994 09/16 04:53	NA	NA	NA	CEH (P_g, S_g)
1994 09/16 07:01a	45.300	68.200	NA	LBNH (P_n)
1994 09/16 07:01b	45.300	68.200	NA	BINY (L_g); LBNH(L_g)
1994 09/16 07:28	45.300	68.200	NA	LBNH (L_g)
1994 09/16 07:40	45.300	68.200	NA	BINY (L_g); LBNH (P_n, P_g, L_g)
1994 09/16 07:44	45.300	68.200	NA	BINY (L_g); LBNH (P_g, L_g)
1994 09/25 00:53	47.77	69.96	4.3	BINY (P_n, L_g); HRV (L_g); LBNH (P_n, L_g); MCWV (L_g)
1994 09/26 14:23	37.00	88.90	3.6	MIAR (P_g, L_g); OXF (P_{ng}, L_g); WMOK (P_n, L_g)
1994 09/27 19:09	37.99	81.55	3.3	CEH (P_n); MCWV (P_n, P_{ng}, S_n, S_nL_g)
1994 09/27 19:46	NA	NA	NA	MCWV (P_g, S_g)
1994 10/02 11:27	42.36	72.26	3.6	BINY (P_{ng}, L_g); HRV (P_g, S_g); LBNH (P_{ng}, L_g)

1994 10/03 21:19	NA	NA	NA	WMOK (P_g)
1994 10/03 21:28	NA	NA	NA	LBNH (P_g)
1994 10/14 12:43	37.97	81.62	3.5	MCWV (P_n, P_{ng}, S_n, S_nL_g)
1994 10/15 21:44	NA	NA	NA	OXF (L_g)
1994 11/18 11:21	43.821	70.951	2.6	LBNH (P_g, L_g)
1994 11/20 19:33	44.37	70.59	2.9	BINY (L_g); CBM (P_n, P_g, L_g); HRV (P_{ng}, S_nL_g); LBNH (P_g, S_g)
1994 11/20 23:32	NA	NA	NA	OXF (L_g)
1994 12/25 19:06	39.290	104.788	4.0	CBKS (P_n, L_g); RSSD (P_n, L_g)
1994 12/25 19:06b	NA	NA	NA	WMOK (P_n, L_g)
1994 01/18 15:41	NA	NA	NA	RSSD (P_g)
1995 01/18 15:51	34.51	97.49	4.0	CBKS (P_n, S_n, L_g); JFWS (P_n, S_n, L_g); MIAR (P_n, L_g); OXF (P_n); RSSD (P_n, S_n, L_g); WMOK (P_{ng}, L_g)
1995 01/22 08:24	37.05	80.789	2.7	CEH (P_{ng})
1995 02/11 05:54	40.50	94.98	3.1	JFWS (P_n, S_n); MIAR (P_n, S_n); RSSD (L_g); WMOK (P_n, S_n)
1995 02/12 16:44	44.27	70.25	2.8	LBNH (L_g, P_{ng}); RSNY (L_g)
1995 02/15 15:53	45.90	75.04	3.4	BINY (L_g); HRV (L_g); LBNH (L_g, P_n); LSCT (L_g); RSNY (P_{ng}, S_nL_g)
1995 02/15 15:59	NA	NA	NA	WMOK (L_g, P_{ng})
1995 02/17 01:13	44.17	70.24	2.7	LBNH (L_g, P_{ng})
1995 02/19 12:57	39.09	83.62	3.5	BINY (L_g); JFWS (L_g); RSNY (L_g); SSPA (L_g); YSNY (L_g)
1995 03/02 05:33	44.23	74.43	2.9	BINY (P_{ng}, S_nL_g); LBNH (P_{ng}, S_nL_g); LSCT (L_g, P_g); RSNY (P_g, S_g); YSNY (L_g)
1995 03/11 08:15	36.98	83.16	3.8	BINY (L_g, P_n); CBKS (L_g); CEH (L_g, P_n); JFWS (L_g); LSCT (L_g); MIAR (L_g, P_n); RSNY (L_g, P_n, S_n) SSPA (L_g, P_n); WMOK(L_g)
1995 03/11 09:50	37.00	83.19	3.3	MIAR (L_g); RSNY (L_g); SSPA (L_g); YSNY (L_g)
1995 03/18 22:03	NA	NA	NA	RSSD (L_g)
1995 03/18 22:06	35.425	84.922	3.3	OXF (P_n)
1995 03/18 22:15	NA	NA	NA	LTX (P_g, S_g)
1995 03/19 18:36	34.70	104.06	3.4	ALQ (S_nL_g, P_{ng}); GOL (L_g); WMOK (L_g)
1995 03/19 18:53	NA	NA	NA	LTX (P_n)
1995 03/23 11:10	36.90	99.60	2.8	CBKS (P_{ng}, S_nL_g); WMOK (P_{ng}, S_nL_g)
1995 04/05 05:31	35.20	99.03	3.0	CBKS (L_g, P_n); GOL (L_g, P_n); LTX (L_g); WMOK (P_g, S_g)
04/05 05:31 aftershock	see above	see above	NA	WMOK (P_g, S_g)

1995 04/14 00:32 West Texas	30.2	103.3	M_b=5.6	BINY (S, P_n); BMN (S, L_g, P_n); CBKS (L_g, P_n); CMB (S, L_g, P_n); FFC (S, L_g, P_n); GOL (L_g, P_g, P_n); ISA (L_g, P_n); JFWS (L_g, P_n); LSCT (S); RSNY (P_n); SAO (P_n); SSPA (S, P_n); TUC (L_g, P_n); WDC (P_n); WMOK (L_g, P_n); WVOR (S, L_g, P_n)
Aftershocks of West Texas earthquake: 04/14 02:13 to 04/17 09:45	see above	see above	varies	30 LTX (P_g); 46 LTX (S_g); 5 WMOK (P_n); 4 WMOK (S_n); 1 WMOK (L_g); 1 CBKS (L_g); 1 TUC (L_g); 1 RSSD (L_g)
1995 04/14 00:34	NA	NA	NA	RSSD (L_g, P_n)
1995 04/14 01:46	NA	NA	NA	RSSD (P_{ng}, S_nL_g)
1995 04/14 09:04	NA	NA	NA	RSSD (P_g, S_g)
1995 04/14 12:35	NA	NA	NA	RSSD (P_g, S_g)
1995 04/14 13:30	NA	NA	NA	JFWS (P_g, S_g)
1995 04/14 15:06	NA	NA	NA	RSSD (P_g)
1995 04/17 13:45	32.9	80.0	3.9	BINY (L_g); CEH (L_g, P_g, P_n, S_n); LSCT (L_g)
1995 04/17 16:27	NA	NA	NA	RSNY (P_g)
1995 04/27 00:42	36.7	89.6	2.7	OXF (L_g, P_n, P_{ng})
1995 05/03 22:17	32.7	82.1	NA	GOGA (S_nL_g)
1995 05/03 22:19	NA	NA	NA	WMOK (P_{ng}, S_nL_g)
1995 05/08 22:26	NA	NA	NA	BLA (S_n)
1995 05/08 22:34	37.6	81.2	NA	BLA (S_n, P_g); CEH (L_g, P_n)
1995 05/22 20:11	NA	NA	NA	WMOK (P_g, S_g)
1995 05/24 15:42	38.1	81.6	NA	CEH (L_g, P_n); GOGA (L_g); LSCT(L_g); SSPA (L_g, P_n)
1995 05/24 15:46	NA	NA	NA	BLA (P_g)
1995 05/24 15:48	NA	NA	NA	OXF(S_nL_g)
1995 05/25 14:08	NA	NA	NA	JFWS(P_g)
1995 05/25 14:22	43.0	78.8	3.1	BINY(L_g, P_{ng}); RSNY (L_g, P_g)
1995 05/25 14:36	NA	NA	NA	WMOK(P_{ng}, S_nL_g)
1995 05/27 19:39	NA	NA	NA	RSNY (P_{ng}, S_nL_g)
1995 05/27 19:51	36.1	89.5	3.8	BLA (L_g); CEH (L_g); JFWS (L_g, P_n); MIAR (L_g, P_n, S_n); RSNY (L_g); RSSD (L_g); WMOK (L_g, P_n, S_n)
1995 05/28 15:28	33.2	87.8	3.4	BLA (L_g); MIAR (L_g); OXF (P_{ng}, S_nL_g)
1995 05/31 16:13	37.9	81.8	NA	BLA (P_{ng}, S_nL_g)
1995 06/01 01:06	30.3	103.3	3.5	CBKS (L_g); WMOK (L_g, P_n, S_n)
1995 06/01 04:49	34.4	96.7	3.0	CBKS (L_g, P_n); MIAR (P_{ng}, L_g); WMOK (P_{ng}, S_nL_g)
1995 06/01 20:02	NA	NA	NA	WMOK (S_g)
1995 06/05 15:17	43.0	76.4	NA	BINY (P_g)

1995 06/06 21:27	36.1	89.5	3.6	MIAR (L_g, P_n, S_n)
1995 06/08 22:03	NA	NA	NA	WMOK (P_g, S_g)
1995 06/08 22:21	43.2	104.2	NA	RSSD (P_g)
1995 06/08 22:34	NA	NA	NA	WMOK (P_{ng}, S_nL_g)
1995 06/14 17:01	NA	NA	NA	EYMN (P_{ng})
1995 06/14 17:02	NA	NA	NA	BLA (P_{ng}, S_nL_g)
1995 06/16 12:13	44.3	71.9	3.8	BINY(L_g, P_g); HRV (P_{ng}, S_nL_g); LBNH (P_g, S_g); LSCT (L_g, P_g, P_n); RSNY (P_{ng}, S_nL_g)
1995 06/16 14:13	NA	NA	NA	BLA (P_{ng}, S_nL_g)
1995 06/16 14:31	NA	NA	NA	OXF(P_{ng}, S_nL_g)
1995 06/16 18:35	37.1	81.9	NA	BLA (P_{ng}); CEH (L_g, P_{ng})
1995 06/26 00:36	36.7	81.4	3.5	BINY(L_g, P_g); BLA (P_g, S_g); CEH (P_{ng}, S_nL_g); MIAR(L_g)
1995 06/29 09:27	36.5	89.8	3.1	MIAR(L_g, P_g, P_n); OXF(L_g, P_g, P_n)
1995 06/29 20:07	36.6	89.8	3.0	OXF (L_g, P_g)
1995 07/03 03:04	44.0	99.5	2.8	CBKS (P_n); RSSD (P_g, P_n)
1995 07/04 03:59	36.2	104.8	3.8	ALQ (P_{ng}); CBKS (L_g, P_g); GOL(L_g, P_g); MIAR (L_g); RSSD (P_g, L_g); WMOK (L_g, P_g)
1995 07/05 14:16	35.4	84.2	3.7	OXF (L_g, P_g)
1995 07/10 16:30	NA	NA	NA	WMOK (P_{ng}, S_nL_g)

Notes on Table 7: "P_{ng}" means a window over both the P_n and P_g phases; "S_nL_g" means a window over both S_n and L_g (probably dominated by L_g). The phase identified as "S" has lower frequency content than the phase identified as S_n and is presumably traveling deeper within the mantle than S_n; some phases labeled as P_n may also be traveling deeper than the upper mantle. Locations and magnitudes, usually m_{bLg}, are from the U.S. Geological Survey, Golden, Colorado; "NA" indicates the event was not found in the earthquake catalog.

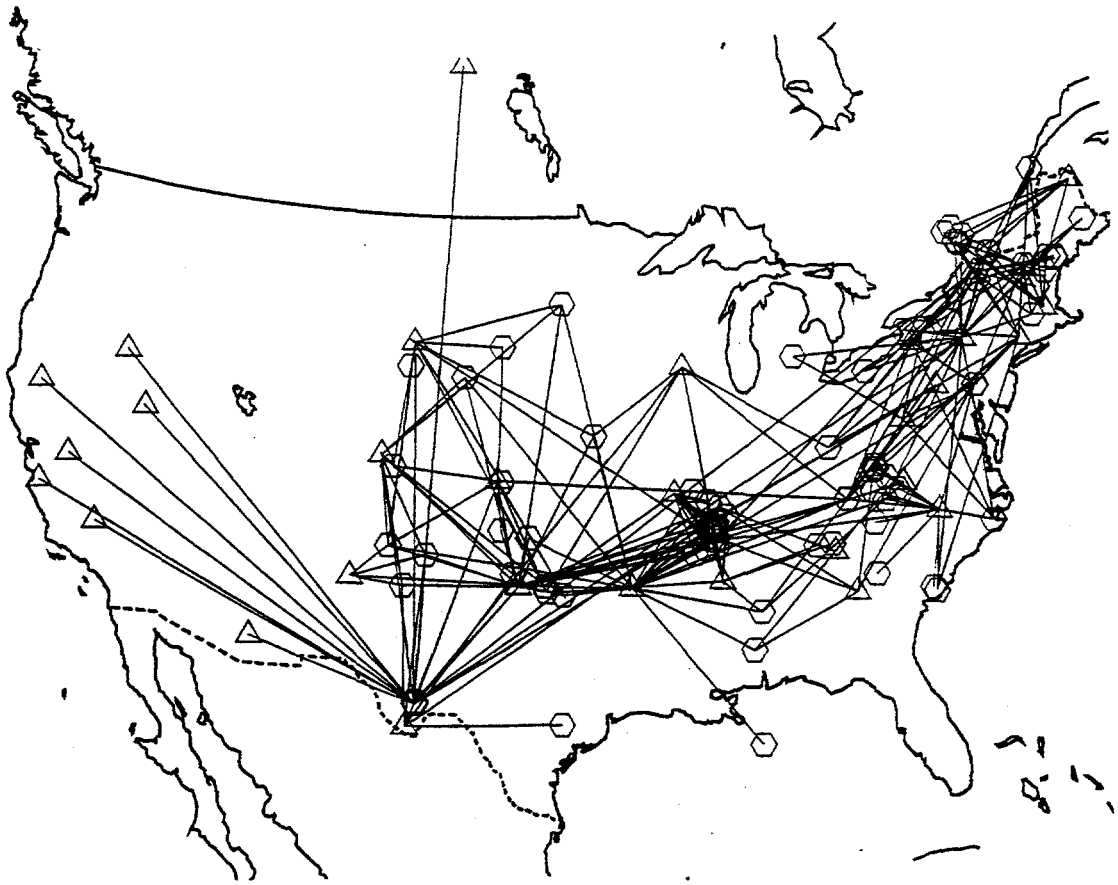

Figure 13. Ray paths projected onto the surface for NSN data collected 1 January 1992 to 12 July 1995. Circles are earthquake epicenters, triangles are station locations. Ray paths through the western United States are for recordings of the M_b 5.6, West Texas earthquake.

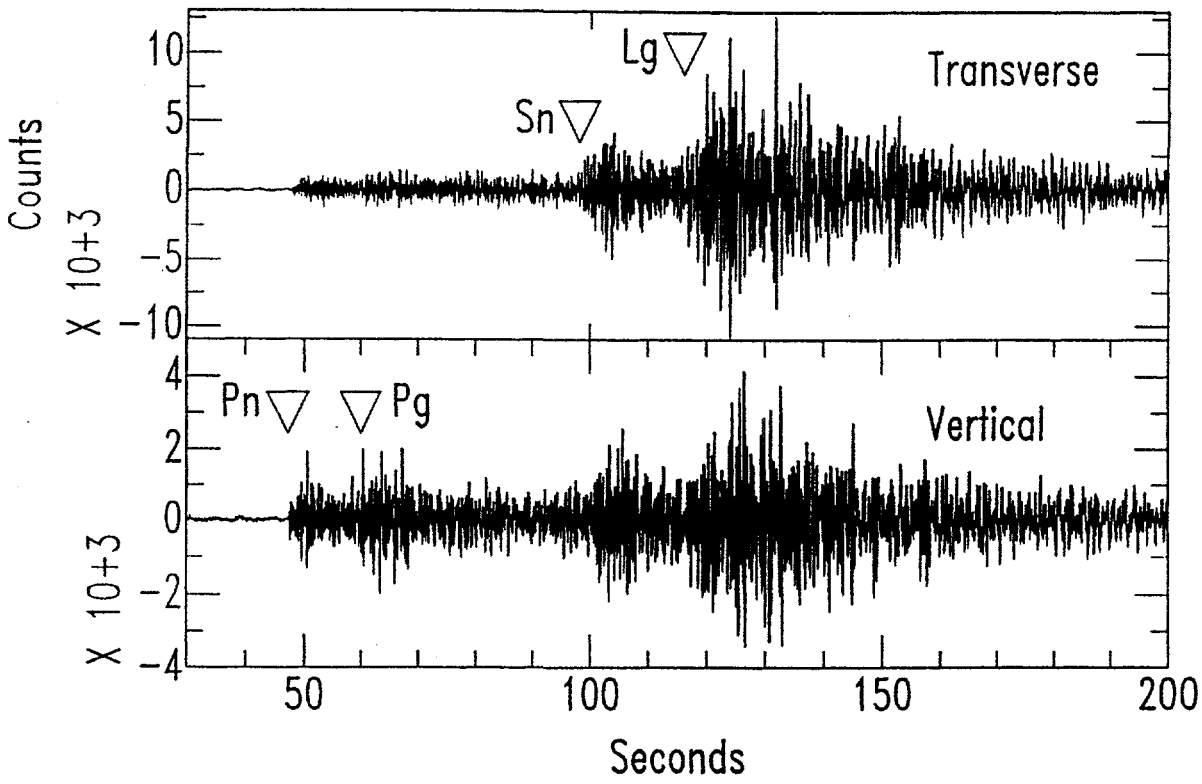

Figure 14. Example of data and phase picks. The m_{bLg} 4.0 earthquake occurred on 18 January 1995 in Oklahoma (see Table 7). The recording was made at station CBKS in Kansas, at 520 km epicentral distance. The seismograms have been high-pass filtered at 0.5 Hz.

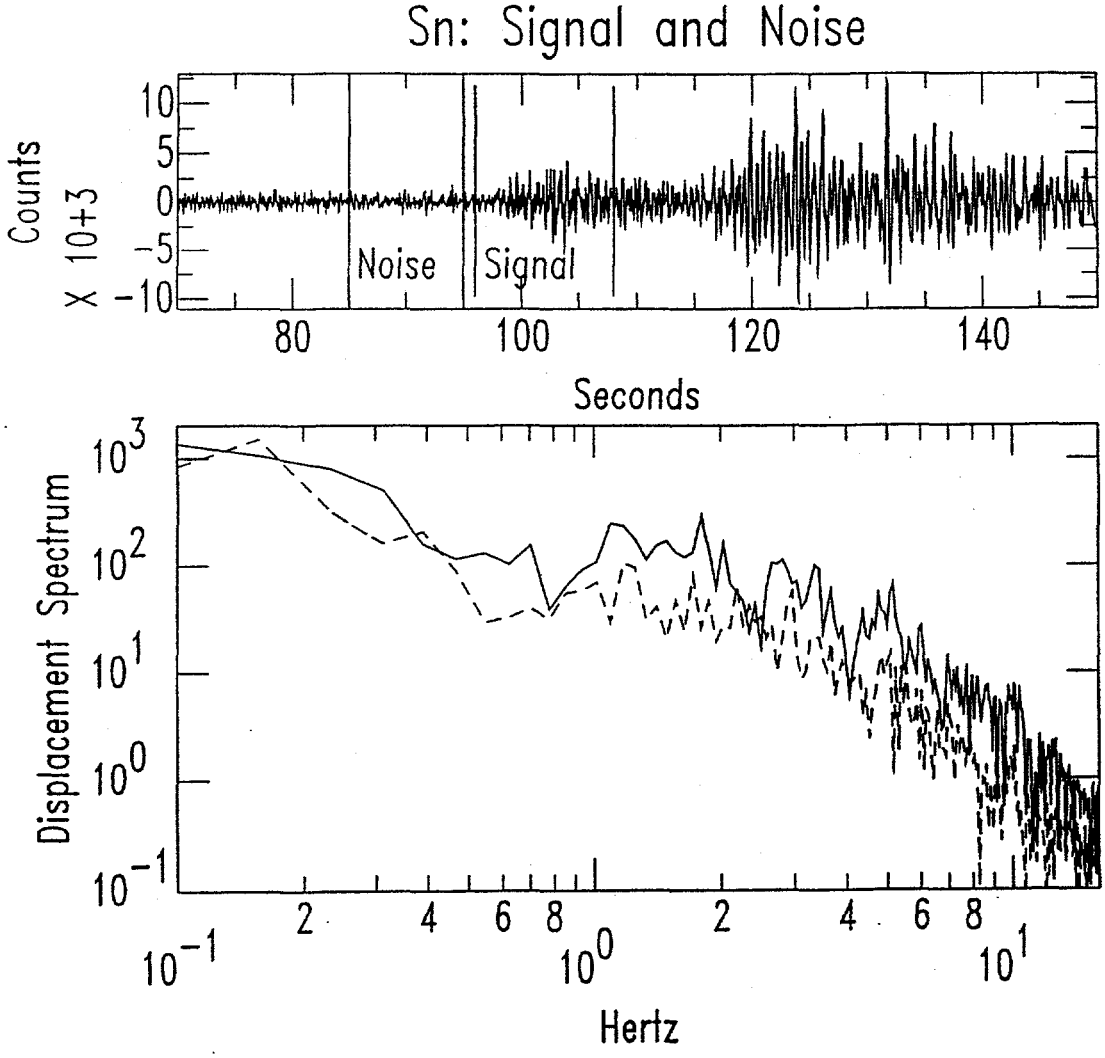

Figure 15. Example of determination of frequency range for which the signal exceeds the noise. The earthquake recording is the same as is shown in Figure 14. In this case, the Sn signal exceeds the noise from 0.5 Hz to 16 Hz.

3.3 CHARACTERISTICS OF REGIONAL PHASE PROPAGATION

Regional phases have been observed to propagate with different efficiency in different areas. For example, the Pg phase is less prominent compared to Pn in the CEUS than in the WUS (e.g. Evernden, 1967; Langston, 1982). Also, in Eurasia, Sn has been observed to propagate less efficiently compared to Lg in areas with significant topography (Zhang and Lay, 1994).

Variation of the regional phases within the central and eastern United States can also be observed from the NSN data set. Figure 16, for example, shows the Lg (top) and Sn (bottom) rays for which the amplitudes of the phases were large enough to compute spectra. Most of the Sn rays occur in the central United States region of relatively flat topography—Texas, Oklahoma, Kansas, Nebraska, South Dakota, Iowa, Missouri, and Arkansas. This variation with topography is consistent with the result of Zhang and Lay (1994) for Eurasia.

In addition, a few large amplitude Sn phases are observed in the eastern United States, generally traveling along a NNE trend, parallel to the Appalachian mountain range, and just east or west of the Appalachians.

This disruption of Sn waves at regions of significant topography could be due to variations in the depth of the Moho corresponding to variations in surface topography. The topography could also disrupt the phase directly, since many of the larger Sn amplitudes are probably surface multiple reflections (Kennett, 1985).

Similar observations can be made for Pg and Pn (Figure 17). Pg is observed to occur with largest amplitudes primarily in regions of topographic variation—near the eastern base of the Rocky Mountains, on paths traveling southwest from the New Madrid Seismic Zone underneath the Ouachita Mountains of Arkansas, and underneath the Appalachians and other mountain ranges in the Northeast, including the states of Maine, New Hampshire, Vermont, New York, Pennsylvania, and Massachusetts.

This result could be caused by the disruption of the Pn wavetrain by topography as with Sn, therefore allowing the Pg phase to be more readily observed. Alternatively, Pg propagation can be strongly attenuated in flat, shield-type areas due to the conversion of P to S waves with each surface reflection of Pg (Kennett, 1989).

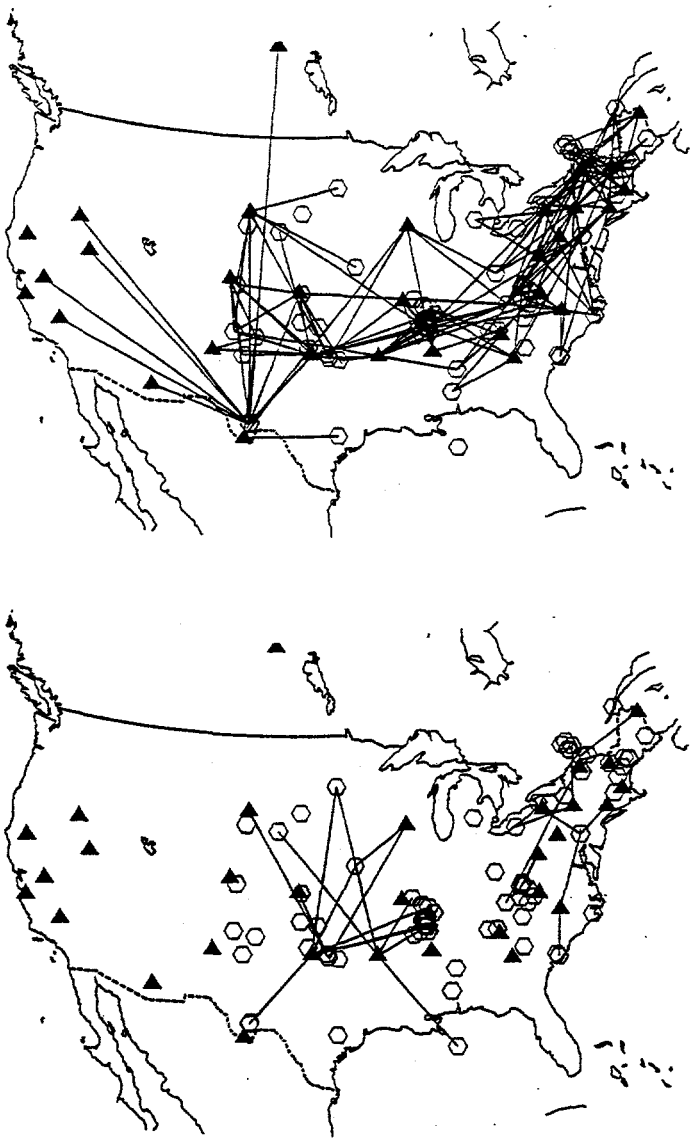

Figure 16. Lg rays (top) and Sn rays (bottom) from the NSN data set. Relatively strong Sn amplitudes were observed in the central United States and just east and west of the Appalachian mountain range.

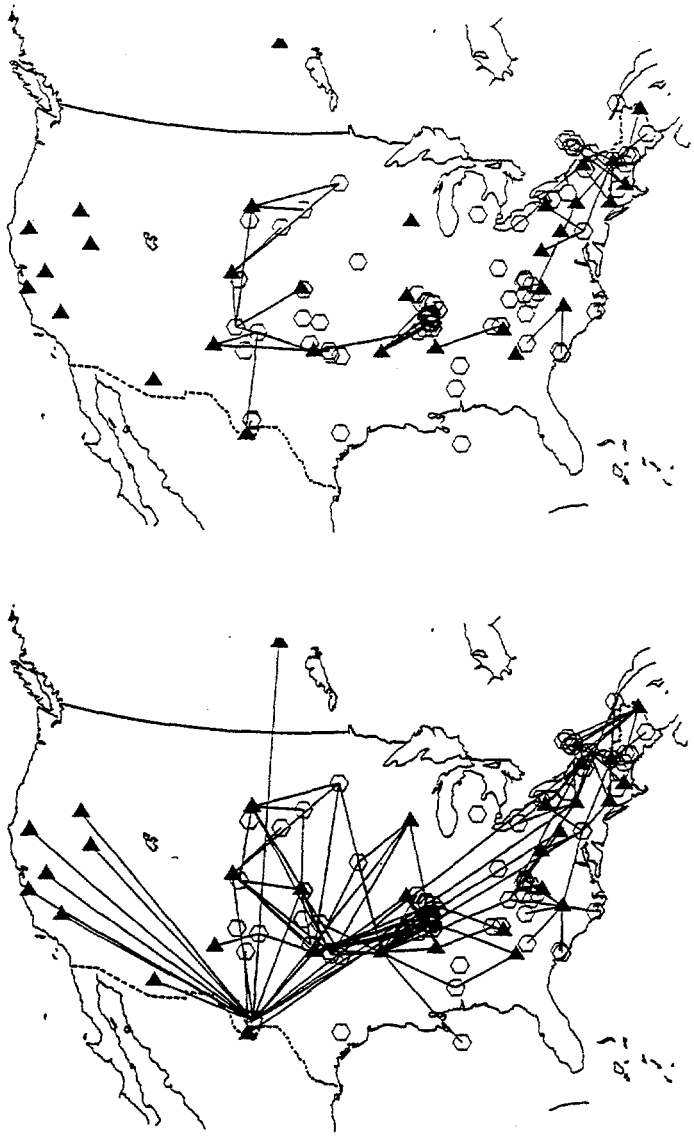

Figure 17. Pg rays (top) and Pn rays (bottom) from the NSN data set. Relatively strong Pg amplitudes occur near or underneath mountain ranges.

3.4 SPECTRAL FITTING

In order to quantitatively analyze the data, least-squares best fits were made to the earthquake spectra. Earthquake spectra are often modeled as a convolution of site, path, and source effects:

$$D(f) = S(f) * P(f) * E(f), \qquad (11)$$

where f is the frequency, D(f) is the displacement Fourier amplitude spectrum, S(f) is the site response, P(f) is the path effect, and E(f) is the source spectrum. Note that in this report we will show the displacement spectrum. Some researchers prefer to plot the acceleration spectrum rather than the displacement spectrum, especially for larger earthquakes. All of the methods of analysis adopted in this report are independent of the units chosen to plot the spectra—none of the quantitative results would change if the acceleration spectrum was used instead of the displacement spectrum.

The simplest and most widely used model for the source spectrum contains just three parameters: the low-frequency spectral asymptote, Ω_0, the falloff of the spectrum at high frequencies, γ, and the corner frequency, f_c (Aki, 1967). The low-frequency spectral asymptote, Ω_0, can be used to estimate the seismic moment (see e.g. Aki and Richards, 1980). The corner frequency and the seismic moment can then be used to estimate the stress drop (Brune, 1970). In much of this report, a three-parameter source model similar to the models of Aki (1967) and Brune (1970) will be used; this model was proposed by Boatwright (1978):

$$E(f) = \Omega_0 / [1 + (f/f_c)^{2\gamma}]^{1/2}. \qquad (12)$$

More complicated source models, in which there are two corner frequencies and an intermediate-frequency range in which the falloff is less than γ, have been proposed for CEUS earthquakes (e.g. Boatwright and Choy, 1992; Atkinson, 1993; Atkinson and Boore, 1995). We will primarily consider the model expressed in equation (12); however, a comparison between the model of Atkinson and Boore (1995) to NSN CEUS data is made later in this report.

In (12), it is widely assumed that the source spectral falloff at high frequencies, γ, is equal to 2.0, as first proposed by Aki (1967) and Brune (1970). For CEUS earthquakes, several studies have examined this issue, and generally favor $\gamma = 2$ (e.g. Boore and Atkinson, 1989; Chael, 1987, Chun et al., 1989a). This report assumes $\gamma = 2$ in equation (12).

The path effect, P(f), is modeled by an attenuation operator according to

$$P(f) = \exp(-\pi f t^*), \qquad (13)$$

where t* is a function of distance,

$$t^* = d/vQ. \qquad (14)$$

The distance from the source to the receiver is given by d, v is the velocity appropriate for the particular phase, and Q is the average quality factor of attenuation along the ray path. The parameter t* in equation (13) has also been called κ, but without the physical interpretation of equation (14) (Anderson and Hough, 1984).

Besides the frequency-dependent attenuation given in equation (13), the amplitudes of the spectra are also reduced with distance due to geometrical spreading. The effects of geometrical attenuation are taken into account when computing the seismic moment from Ω_0; this approach is valid as long as geometrical attenuation does not vary with frequency.

For this study, the site effect in equation (11), S(f), is assumed to be 1.0—that is, site effect is ignored. Of course, this is a simplification of the real earth. The probable effect of ignoring the site effect is to increase the random errors in the determination of f_c, t*, and Ω_0. If the site effect systematically increases or decreases at some of the stations, this could also cause a systematic bias in the determination of the three parameters.

Another complicating factor is that Q may vary with frequency. To account for this, Q in equation (14) is modeled according to:

$$Q = Q_0 f^{\alpha}, \qquad (15)$$

where Q_0 is Q at zero frequency, and α is a parameter to measure the frequency dependence. Three values of α were tested: $\alpha = 0.0$, 0.25, and 0.5. Little difference was found in the quality of the fits for the different α values, although $\alpha = 0.5$ did produce slightly better fits for a few of the earthquakes.

The actual fits were computed to the logarithm of the spectrum:

$$\log [D(f)] = \log[\Omega_0] - 0.5 \log[1 + (f/f_c)^{2\gamma}] - 0.43 (\pi f t^*). \qquad (16)$$

Fitting to the logarithm of the spectrum is appropriate since the variance of the Fourier spectrum is approximately log-normally distributed.

Not all of the spectra in the data set obey the simple model proposed in equations (11) - (16). In particular, the NSN station in Chapel Hill, North Carolina, CEH, produces spectra with broad peaks at intermediate frequencies (Figure 18). Apparently station CEH is affected by complicated site effects, path effects, or both, and this station is excluded from the analysis.

The inversion for the fit parameters according to equation (16) is nonlinear and some iterative method must be employed to find the least-squares best fits. In this report, the Simplex algorithm (Nelder and Mead, 1965; Caceci and Cacheris, 1984) is used. This algorithm has the advantage that convergence toward a minimum in the sum of squared residuals is guaranteed. As with all iterative methods, some initial guess is required; different initial estimates of the fit parameters were tested and, typically, the final values were found to agree to within about 5% for the different initial guesses.

The spectra can be fit to the model, equation (16), either individually or jointly. An example of an individual spectral fit and the fit parameters that resulted is shown in Figure 19. The individual fits generally produce a good match between the model and the data; however, in order to reduce the variance in the final fit parameters, especially for t*, joint fits were computed to the spectra. In these joint fits, the spectra from a single earthquake are fit under the condition that the corner frequency be the same for all the fits (Figure 20). For the joint fits, the P waves are separated from the S waves. Two separate fits are computed for earthquakes if there is enough data.

Only earthquakes for which spectra were available from four or more stations are included in the joint fits; there are 17 such earthquakes for the S waves and 19 for the P waves. For S waves, this includes 73 Lg spectra, 13 Sn spectra, 3 Sg spectra, 6 spectra from windows over both Sn and Lg, and 6 spectra of S waves believed traveling deeper in the mantle than Sn. For P waves, this includes 33 Pg spectra, 62 Pn spectra, and 12 spectra from windows over both Pn and Pg.

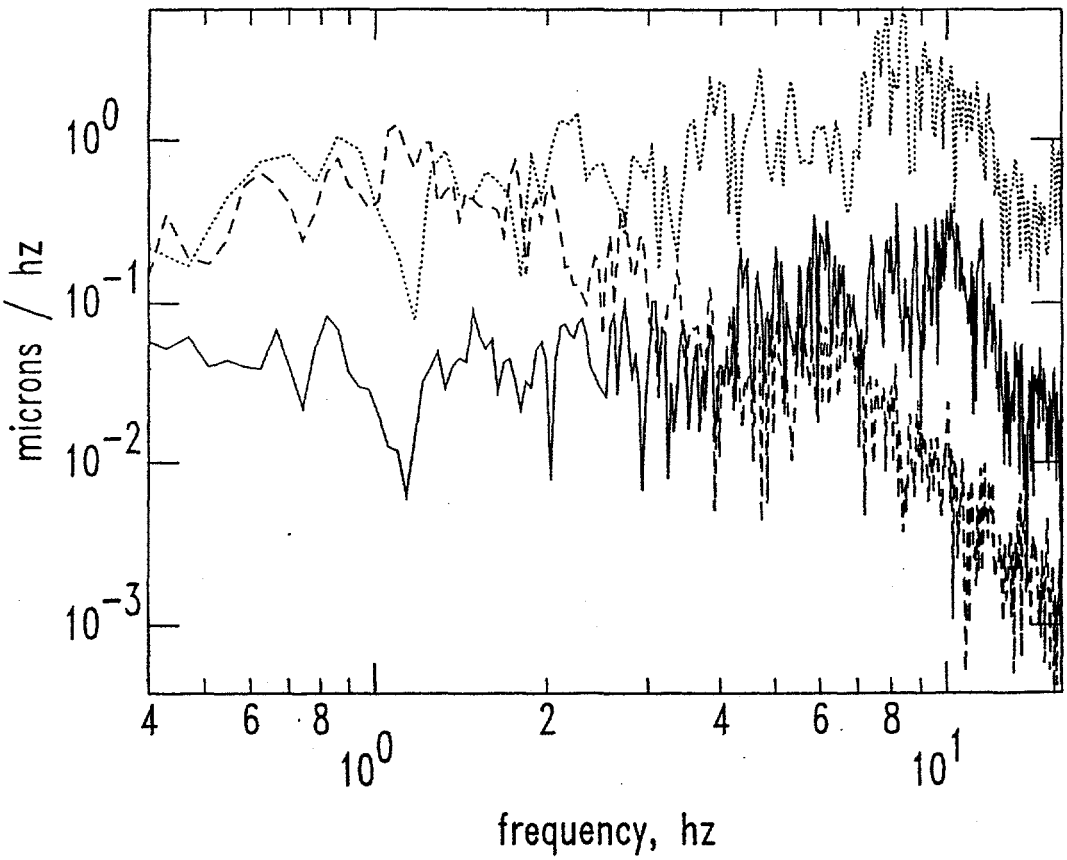

Figure 18. Examples of Lg spectra from data written at station CEH. The broad peaks in the spectra were difficult to model and this station was excluded from the analysis.

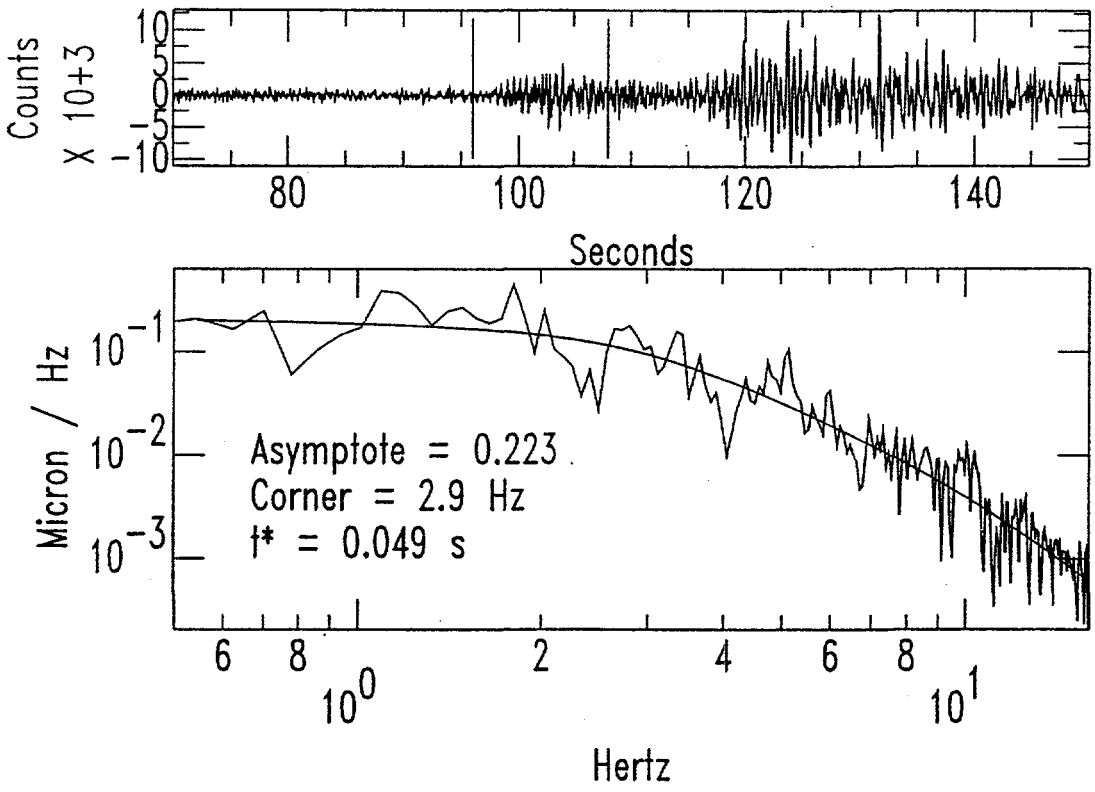

Figure 19. Example of fit to Fourier amplitude spectrum. This is the same recording shown in Figures 14 and 15.

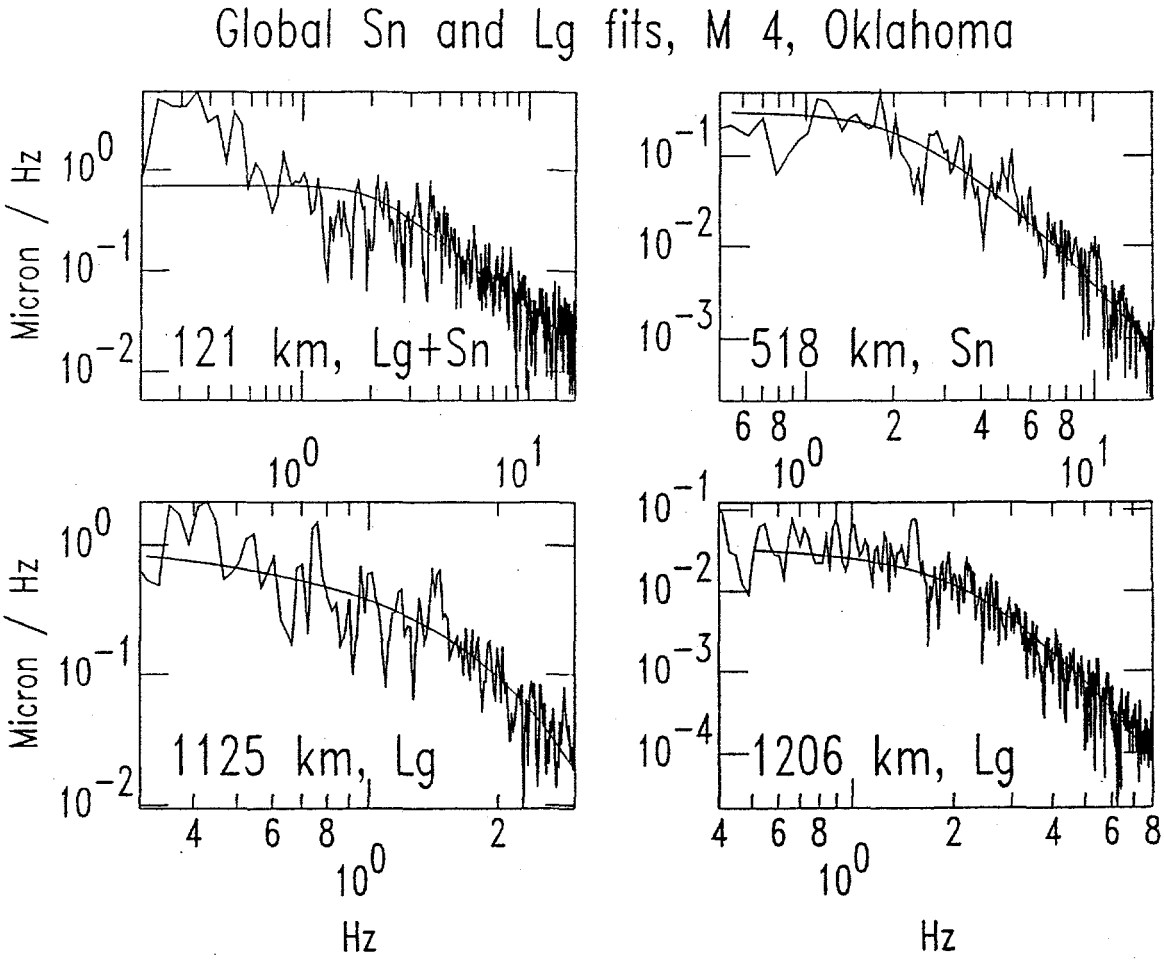

Figure 20. Example of joint fit to several spectra, assuming the source corner frequency to be the same for all the spectra. The spectrum in the upper right-hand side is the same spectrum shown in Figures 15 and 19.

3.5 COMPUTATION OF SEISMIC MOMENTS

For recordings close to the source (less than about 100 km), the seismic moment can be estimated from the low-frequency spectral asymptote, Ω_0, according to (see e.g. Aki and Richards, 1980):

$$M_0 = 4\pi\rho\, v^3\, d\, \Omega_0 / 2\, R_{\theta\phi}, \qquad (17)$$

where M_0 is the seismic moment, ρ is the density at the source, v is the velocity at the source for S or P waves, and $R_{\theta\phi}$ determines the radiation pattern of the source. The distance between the source and receiver, d, gives the geometrical spreading in this simple case, and the 2 in the denominator takes into account amplification at the free surface. This estimate of the seismic moment is used for the Pg and Sg phases within 100 km epicentral distance. Since the focal mechanisms of most of these earthquakes are not available, an average value for $R_{\theta\phi}$ of 0.32 is used (Boore and Boatwright, 1984). The density ρ is assumed to be 2.8 g/cc, the velocity for S-waves is assumed to be 3.6 km/s, and the velocity for P-waves 6.2 km/s.

While this method has been found to produce reasonable values for the seismic moments within about 100 km epicentral distance, most of the seismic moments in this study are computed for epicentral distances greater than 100 km. Beyond about 100 km, the simple d^{-1} estimate for geometrical attenuation in equation (17) may not be valid. Also, the geometrical attenuation may be different for each phase.

Since Lg, for example, consists of waves trapped in the crust, it might be more appropriate to assume a $d^{-1/2}$ attenuation, which is valid for surface waves. However, when d in equation (17) is replaced by $d^{1/2}$, and the seismic moments computed from the Lg spectra, the estimated seismic moments are found to be too small by an order of magnitude or more compared to the seismic moments estimated from the earthquake magnitudes.

The underestimation of the seismic moments may indicate that $d^{-1/2}$ geometrical attenuation for Lg is not appropriate for all distances. If, instead, the geometrical attenuation is taken to be d^{-1} for distances less than 100 km, then $d^{-1/2}$ above 100 km, the estimates of the seismic moments become more reasonable; to estimate the seismic moments in this way, $d_0(d/d_0)^{1/2}$ replaces d in equation (17), where d_0 is 100 km (Street et al., 1975). This geometrical attenuation was assumed for the Lg phase to compute the seismic moments.

Implied in the above method for computing the seismic moment is that no energy is lost from the Lg wavetrain, either through S to P conversions or by energy leaking through the Moho into the mantle. Although these assumptions are generally considered valid for Lg propagation, for Pg waves P to S conversions at the surface may be significant (Kennett, 1989), and energy leaking into the mantle may also be significant (Campillo et al., 1984).

To test this possibility, values of Ω_0 determined from the Pg phase were compared to values from the Lg phase where both were observed on the same seismogram. The variation between the two estimates of Ω_0 was quite large, probably due in part to differences in P and S wave radiation patterns; however, no systematic variation with distance was observed. Moreover, the average value of the ratio of Ω_0 between the Lg phase and the Pg phase is $6.6\,^{+0.8}_{-0.7}$, which is only slightly higher than the value of 5.2 one would expect for P wave velocity equal to $\sqrt{3}$ times the S wave velocity. For Pg, then, the seismic moments are estimated in the same way as Lg, then multiplied by a factor of 6.6.

The geometrical spreading factor that should be used for the Pn and Sn phases is more problematic. For classical head waves, we expect the amplitudes to decay as

$L^{-3/2}\ d^{-1/2}$, where $L = d - d_0$ (e.g. Fowler, 1992). If this geometrical attenuation is assumed, the seismic moments estimated from the Pn and Sn phases is two to three orders of magnitude greater than that estimated from the Lg phase or from the magnitudes. This is not too surprising since it is unlikely Pn and Sn are true head waves (e.g. Zhu et al., 1991). The observed amplitudes of Pn and Sn may be greater than true head waves because the phases are turning rays in the upper mantle (Langston, 1982), because of surface multiple reflections (Kennett, 1989), or because of multiple reflections of the waves along the underside of the Moho (Fowler, 1992).

In an attempt to estimate the geometrical attenuation for Pn and Sn, the values of Ω_0 from the Pn and Sn phases were compared to the Ω_0 values from the Lg phases. As with Pg, however, there was much scatter and no significant variation with epicentral distance. Because no trend could be observed, the determinations of the seismic moment from Pn and Sn were multiplied by an average factor determined from the Sn-Lg and Pn-Lg Ω_0 ratios, as with Pg. For Sn, the factor was $7.3\ ^{+2.2}_{-1.8}$; for Pn, the factor was $30.4\ ^{+5.3}_{-4.6}$.

Because the Lg waves dominate the fits for the S waves, this simple assumption for geometrical attenuation of the Sn phase does not have a large effect on the S wave results. The possible effects on the P wave measurements of source parameters are more difficult to assess since Pn is the dominant P-wave phase in the data set.

The estimates of the seismic moments determined from the S waves are plotted versus magnitude in Figure 21. The best fit line to the data is

$$\log M_0 = (1.37 \pm 0.11)\ M + (16.0 \pm 0.4). \qquad (18)$$

The seismic moments determined in this report are slightly low, but in reasonable agreement with the standard relationship, $\log M_0 = 1.5\ M + 16$ (Kanamori and Anderson, 1975).

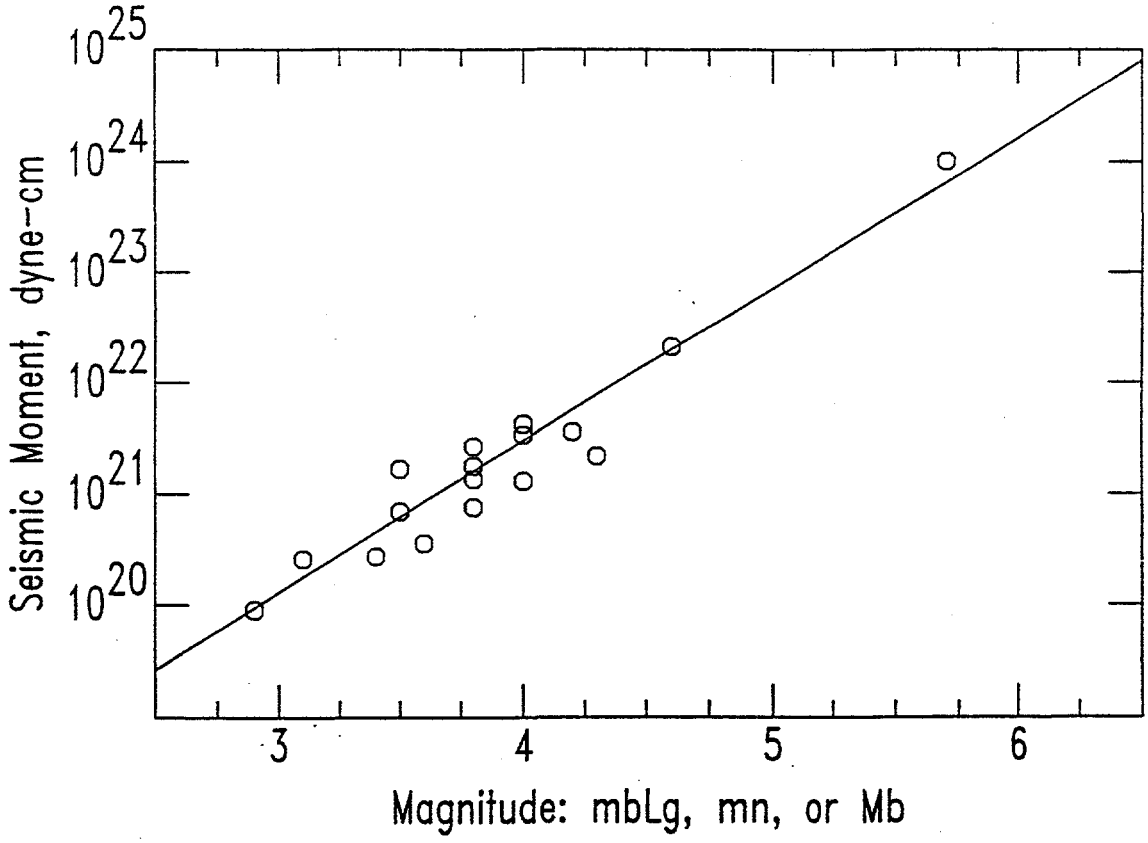

Figure 21. Seismic moment versus magnitude as determined from the joint fits to the S wave data. The magnitudes are a combination of m_{bLg}, m_N, and M_b.

3.6 ANELASTIC ATTENUATION

Besides geometrical attenuation, there is also intrinsic or scattering attenuation given by equations13-15. The parameter that determines anelastic attenuation in the fits is t*. The values of t* determined by the fits for the four regional phases are plotted versus epicentral distance in Figures 22 through 25. These figures include t* estimates for $\alpha = 0.0$ only; the figures for $\alpha = 0.5$ are similar in appearance, although there is some increased scatter in the results.

Figure 22 includes five Lg t* values determined for the western United States (WUS). These estimates of Lg t* were computed from recordings of the 14 April 1995 West Texas earthquake, which was large enough to be recorded at NSN stations out to distances >2500 km in both the eastern and western United States. Based on these estimates, it appears that Lg t* in the WUS is about two to three times Lg t* for the CEUS. Similar observations from Figure 24 indicate that Pn attenuation for the WUS is also two to three times Pn attenuation for the CEUS.

Figures 23 and 25 show t* values for Pg, Pn, Sn, and Lg determined by CEUS stations only. By computing the best-fit lines through these data, a Q for each of the phases can be estimated according to $Q = 1/(m\ v)$, where m is the slope in the figures. For Pg and Lg, the estimates yield Q in the crust; for Pn and Sn, the estimates yield Q in the uppermost mantle. For Pn in Figure 25, the best-fit line is computed over the same distance range as Sn in Figure 23. Also for Pn one outlier was removed from the data set. In the computation of Q, the velocity for Lg is assumed to be 3.6 km/s, Pg is 6.2 km/s, Sn is 4.6 km/s, and Pn is 8.2 km/s. Q values are shown in Table 8 for $\alpha = 0$ and $\alpha = 0.5$.

Table 8. Estimates of Q in the crust and uppermost mantle. Error estimates are one standard deviation.

	Q_0 crust (Lg, Pg)	Q_0 mantle (Sn, Pn)
S wave ($\alpha = 0$)	870 ± 60	5200 ± 3800
P wave ($\alpha = 0$)	970 ± 170	4800 ± 3400
S wave ($\alpha = 0.5$)	510 ± 70	>1640
P wave ($\alpha = 0.5$)	240 ± 60	760 ± 380

For frequency-independent Q ($\alpha = 0$), Q_S is approximately Q_P in both the crust (Q ~ 900) and uppermost mantle (Q ~ 5000), although the value in the mantle is poorly constrained. For frequency-dependent Q, Q_S is greater than Q_P by roughly a factor of two in both the crust and uppermost mantle.

A comparison of Q_{Lg} determined in this study to the values determined in other papers is shown in Figure 26. Q_{Lg} measured in this study is toward the low end of other estimates of Q_{Lg}, but is generally within the range of estimates from the other studies. A possible bias in the Q_{Lg} presented here is that the best-fit line was not constrained to go through the origin (Figure 23). Because the y-intercept is negative on the best-fit line, the slope may be too large, causing Q_{Lg} to be underestimated slightly.

Measurements of the Q values for the other three phases—Pn, Pg, and Sn—are rare in the central and eastern United States (see, however, Chun et al., 1989b; Zhu et al., 1991). Because of this, a comparison similar to Figure 26 cannot be made for these phases

It is also worth mentioning that for the 14 April 1995 West Texas earthquake, there are seven recordings of an S phase at epicentral distances ranging from 1700 to 3000 km. This S phase has considerably lower frequency content than Sn. Determinations of t* from these arrivals are correspondingly much larger than Sn, by roughly a factor of 50 (Figure 27). These arrivals probably travel through the low velocity zone of the mantle.

It should be emphasized that the Q values presented here are based on the assumption that the geometric attenuation is frequency-independent. Some studies have found a frequency-dependence for the geometrical attenuation of regional phases (e.g. Campillo et al., 1984; Zhu et al., 1991). It is difficult, however, to include these results in the present analysis. The effect of the frequency-dependence of geometrical attenuation on the determination of Q in this study is poorly known.

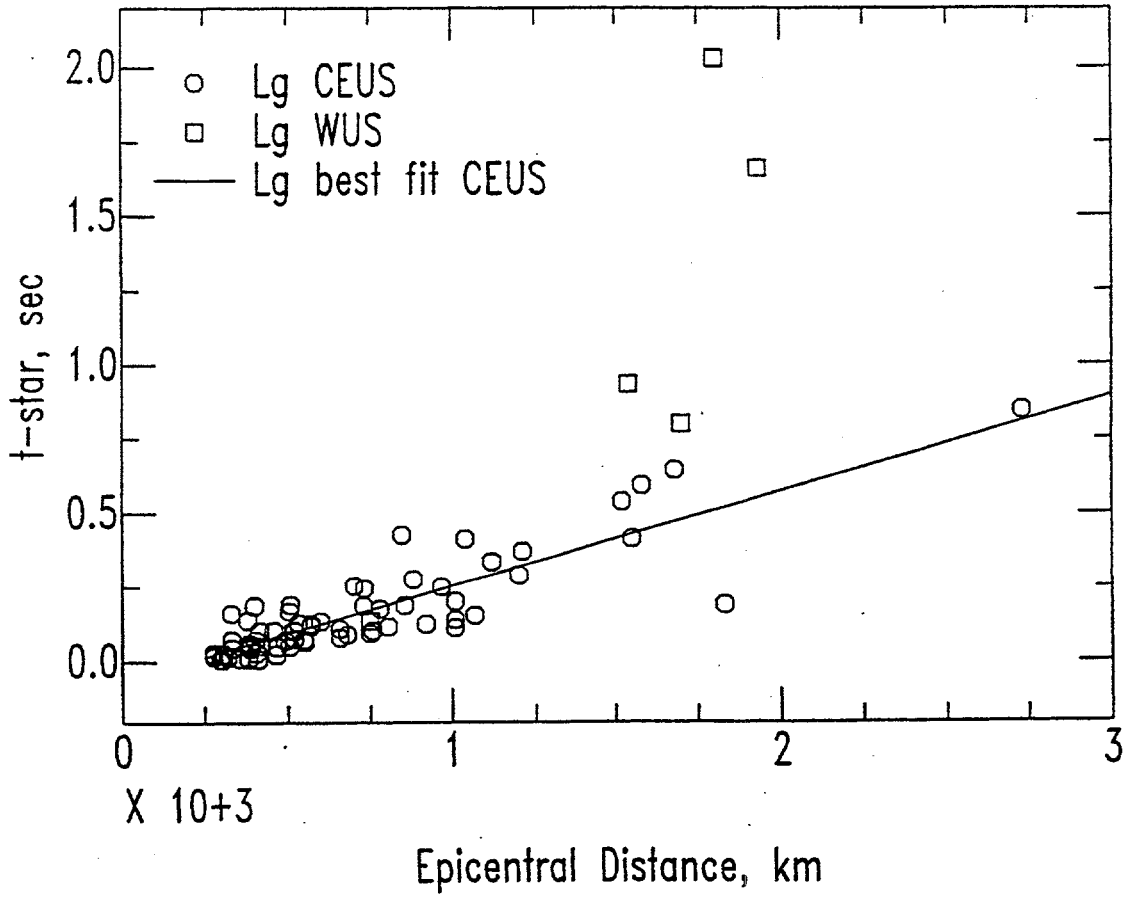

Figure 22. Lg t* versus epicentral distance. Values of Lg t* versus epicentral distance show a strong increase with distance for t* measurements in the CEUS and larger t* values for the WUS compared to the CEUS.

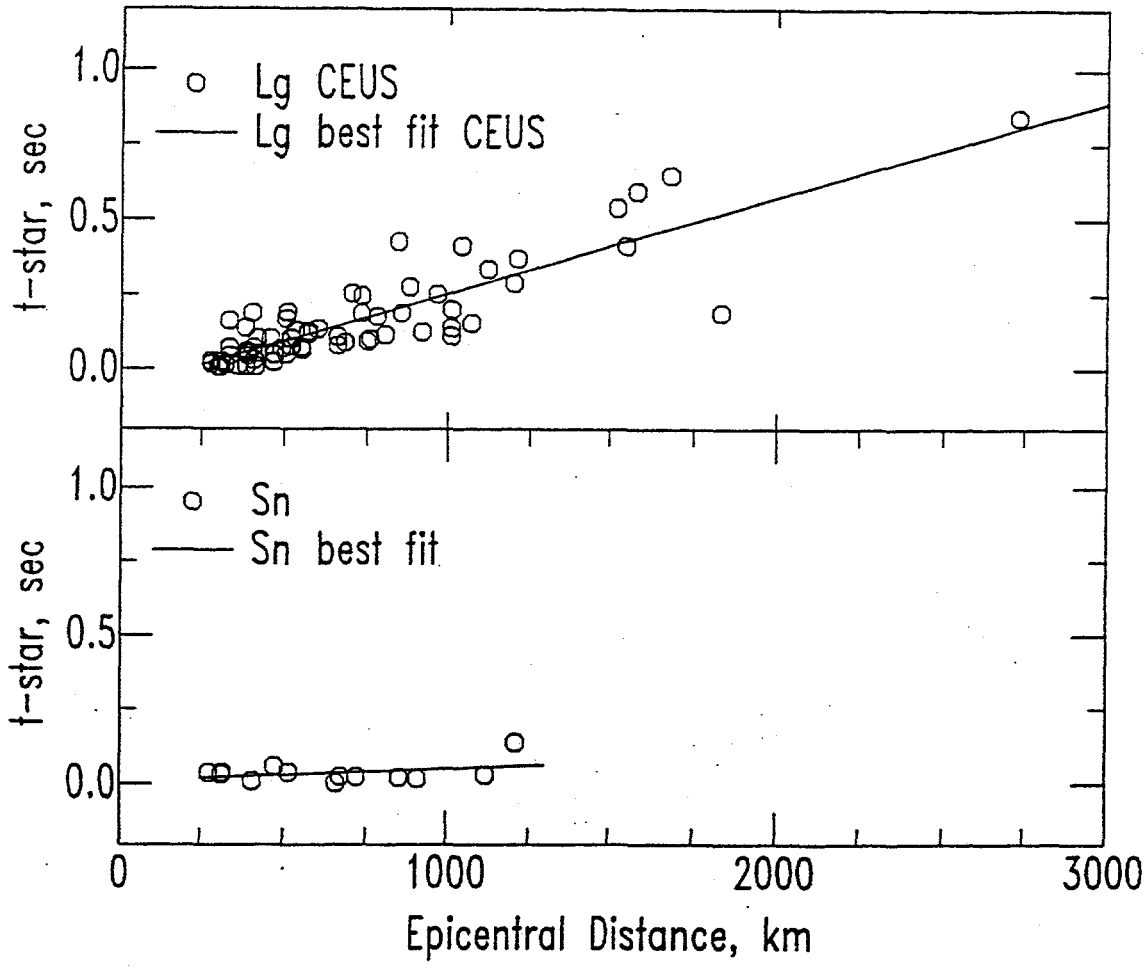

Figure 23. Measurements of t* from the joint inversion of S wave spectra. Q for Lg and Sn is estimated from the best fit lines (see text). The greater slope for the Lg phase compared to the Sn phase indicates a lower S wave Q in the crust than the uppermost mantle.

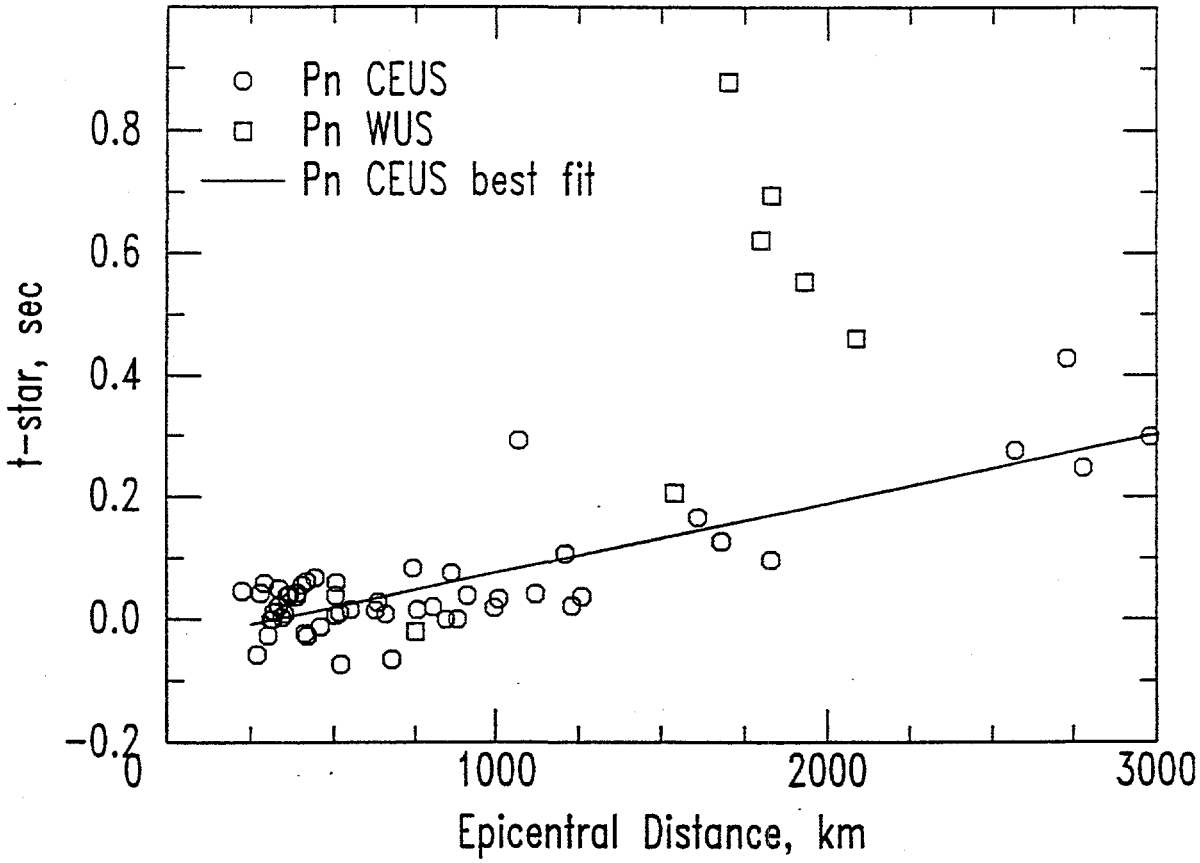

Figure 24. Pn t* versus epicentral distance. Values of Pn t* versus epicentral distance show a slight increase with distance for t* measurements in the CEUS and larger t* values for the WUS compared to the CEUS.

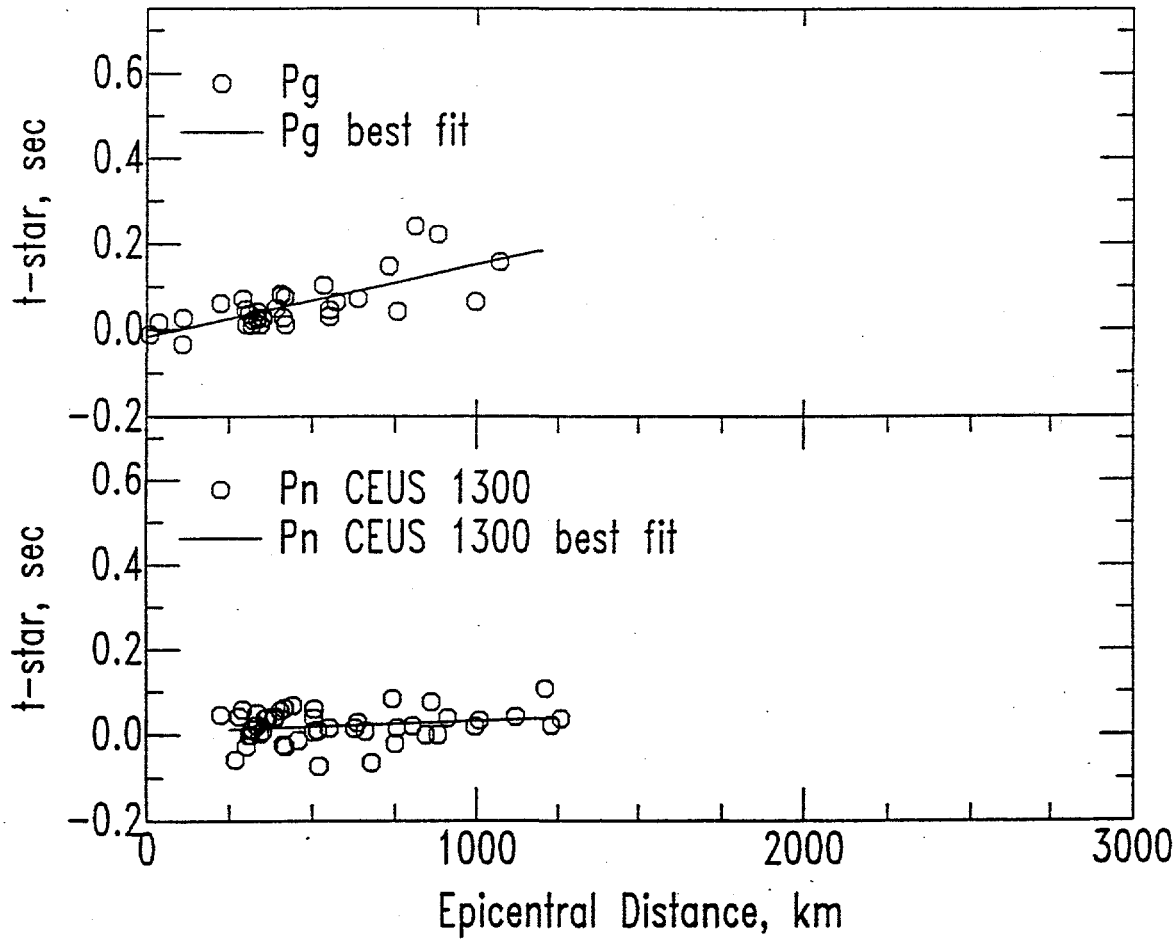

Figure 25. Measurements of t* from the joint inversion of P wave spectra. Q for Pg and Pn is estimated from the best fit lines (see text).

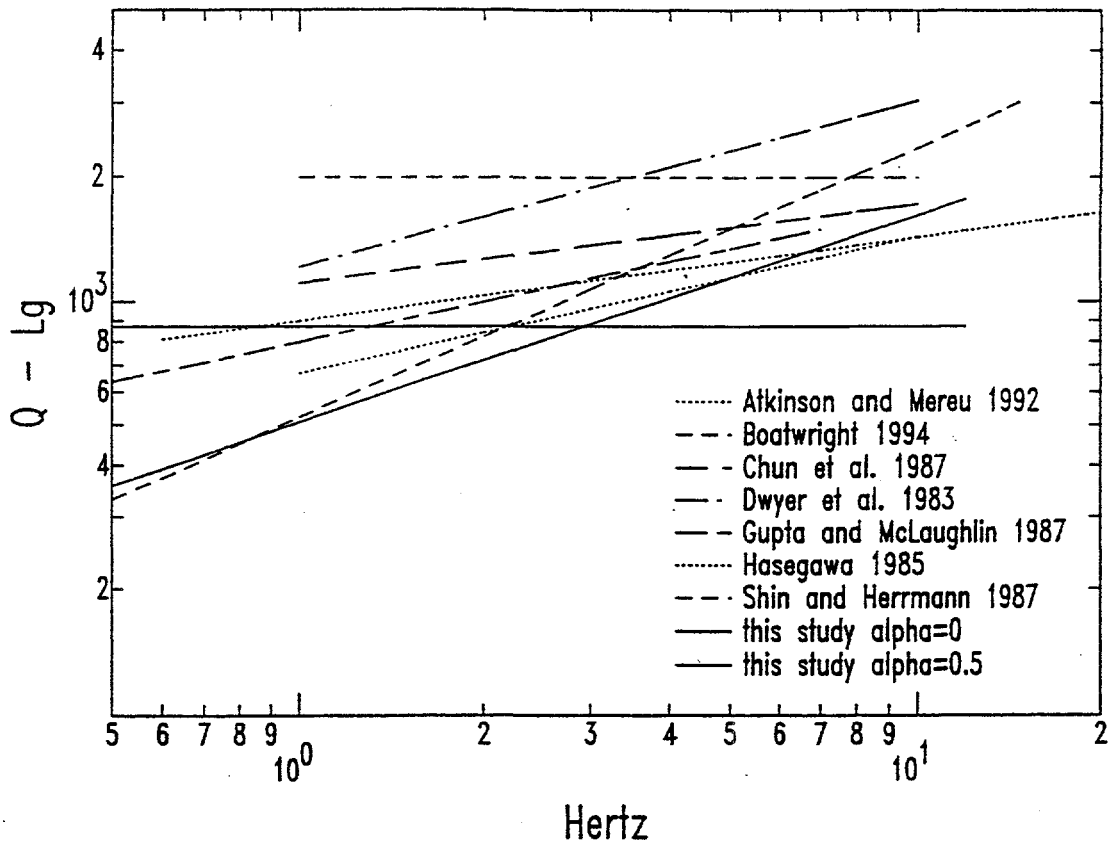

Figure 26. Comparison of Q_{Lg} determined in this study to that determined by other studies.

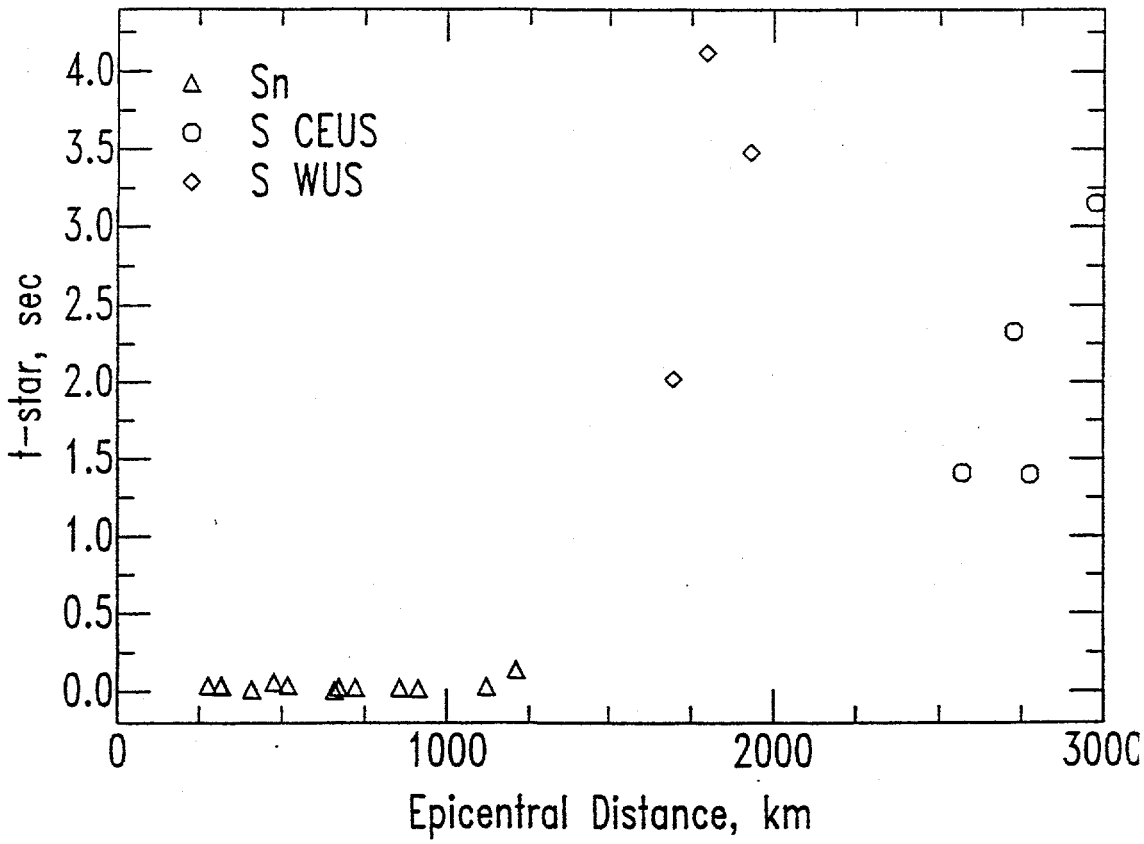

Figure 27. S wave attenuation out to 3000 km. The S phase estimates of t* beyond 1700 km epicentral distance correspond to recordings from the M_b 5.6, 14 April 1995, West Texas earthquake.

3.7 COMPARISON OF DATA TO A TWO CORNER FREQUENCY SOURCE MODEL

We now turn to examining the source spectra and source parameters. One of the assumptions made in computing the joint fits presented in this study is that a single corner frequency source model (equation 16) adequately fits the data. This assumption for CEUS earthquakes has been questioned, and a detailed two corner frequency model has recently been proposed by Atkinson and Boore (1995).

In this section the model of Atkinson and Boore (1995) is compared to the Lg spectra of earthquakes from the NSN data set. The model presented by Atkinson and Boore was validated by them for earthquakes ranging from magnitude 4 to 7. There are six earthquakes in the NSN data set with at least three high-quality Lg recordings in this magnitude range (Table 9).

In order to test Atkinson and Boore's model, the spectra are first corrected for attenuation according to the value presented in their paper: $Q_{Lg} = 670\ f^{0.33}$ (this value is close to the values presented here—Table 8). Next, the attenuation-corrected spectra are log-averaged together. This log-average is then compared to the source model of Atkinson and Boore, with the low-frequency levels of the data and the model shifted an arbitrary amount so that the low frequencies match. Information about the earthquakes—and the source parameters of the Atkinson and Boore model used to fit the data—are shown in Table 9. The parameters f_A and f_B are the two corner frequencies in the model, and ε determines the relative significance of these corner frequencies in determining the shape of the source spectrum. For a description of the derivation of these parameters and the functional form of the source model, see Atkinson and Boore (1995).

Table 9. Earthquakes and source parameters used to test the model of Atkinson and Boore.

Origin time	Magnitude	Number of CEUS Lg recordings	f_A	f_B	ε
1995 01/18 15:51	4.0 m_{bLg}	3	NA	4.8	1.0
1995 04/14 00:32	5.6 m_b	3	0.27	2.4	0.094
1994 01/16 00:42	4.0 m_n	3	NA	4.8	1.0
1994 01/16 01:49	4.6 m_n	5	0.91	3.7	0.41
1994 02/05 14:55	4.2 m_n	3	1.5	4.4	0.73
1994 09/25 00:53	4.3 m_{bLg}	3	1.3	4.2	0.63

The results are somewhat mixed. For earthquakes approaching magnitude 4.0, the model of Atkinson and Boore reduces to a single corner frequency model. For the four earthquakes close to magnitude 4.0—ranging from 4.0 to 4.3—two of the averaged spectra (Figures 28 and 29) are significantly overpredicted by the model above 2 or 3 Hz, while two of the spectra (Figures 30 and 31) are fit well by the model. This result appears to be due to variations in the source spectra of the data. In the two cases where the spectra are overpredicted, the spectra begin to fall off at lower frequencies than in the two cases where the earthquake spectra are well modeled. Thus, it is hard to imagine a source model, tied only to the magnitude, that could fit all four of these earthquake spectra—variation of some additional variation in the source model besides the magnitude, such as the stress drop, seems to be required.

For the magnitude 4.6 earthquake, the model of Atkinson and Boore does an excellent job of modeling the averaged spectrum (Figure 32).

For the magnitude 5.6 earthquake, the model of Atkinson and Boore underpredicts the averaged spectrum in an intermediate frequency range of about 0.2 to 2.0 Hz (Figure 33). This underprediction may be significant since the specified reason for using a two corner frequency model is to reduce the amplitudes at intermediate frequencies. Atkinson and Boore concluded that this intermediate-frequency amplitude reduction was required by the data they had analyzed. In this example, however the West Texas earthquake does not appear to have the reduced amplitudes at intermediate frequencies. On the other hand, since this is the only earthquake significantly above 4.0 in the NSN data set, it is difficult to draw a firm conclusion.

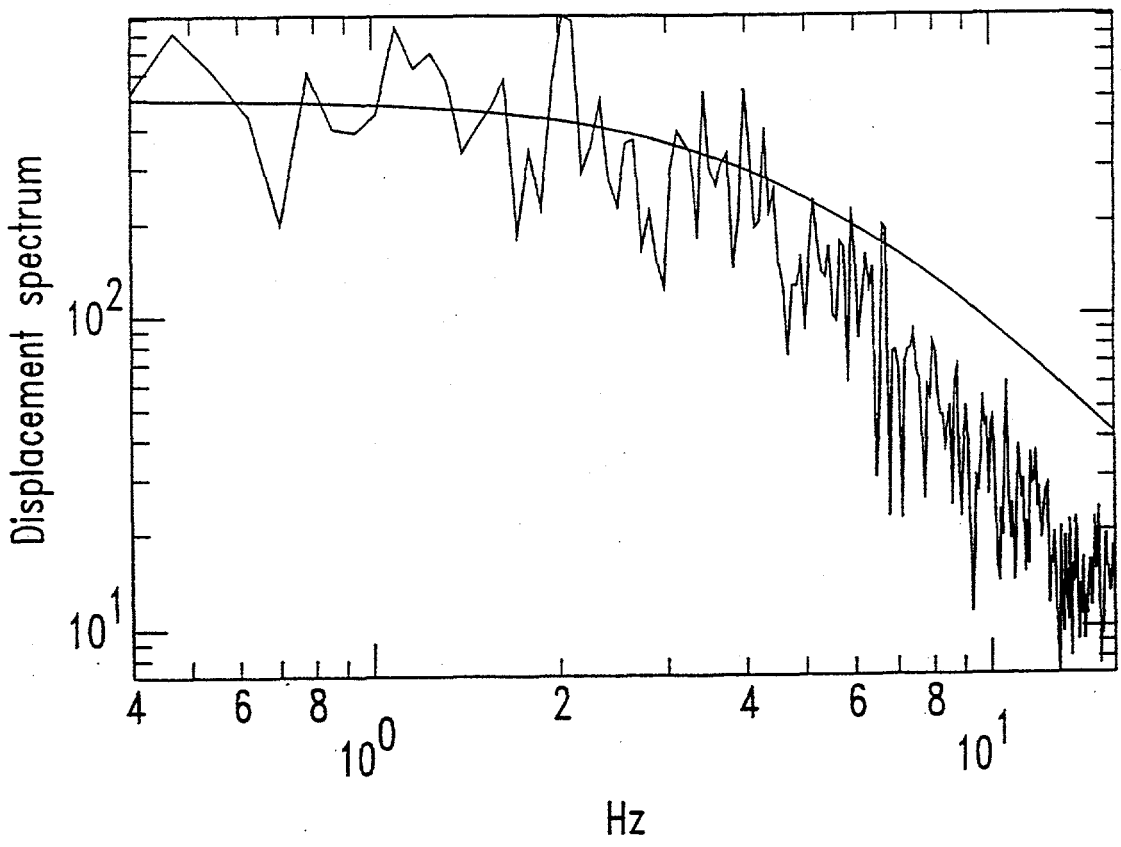

Figure 28. Comparison of Atkinson and Boore (1995) model to magnitude 4.0 Oklahoma earthquake (see Table 9 and text).

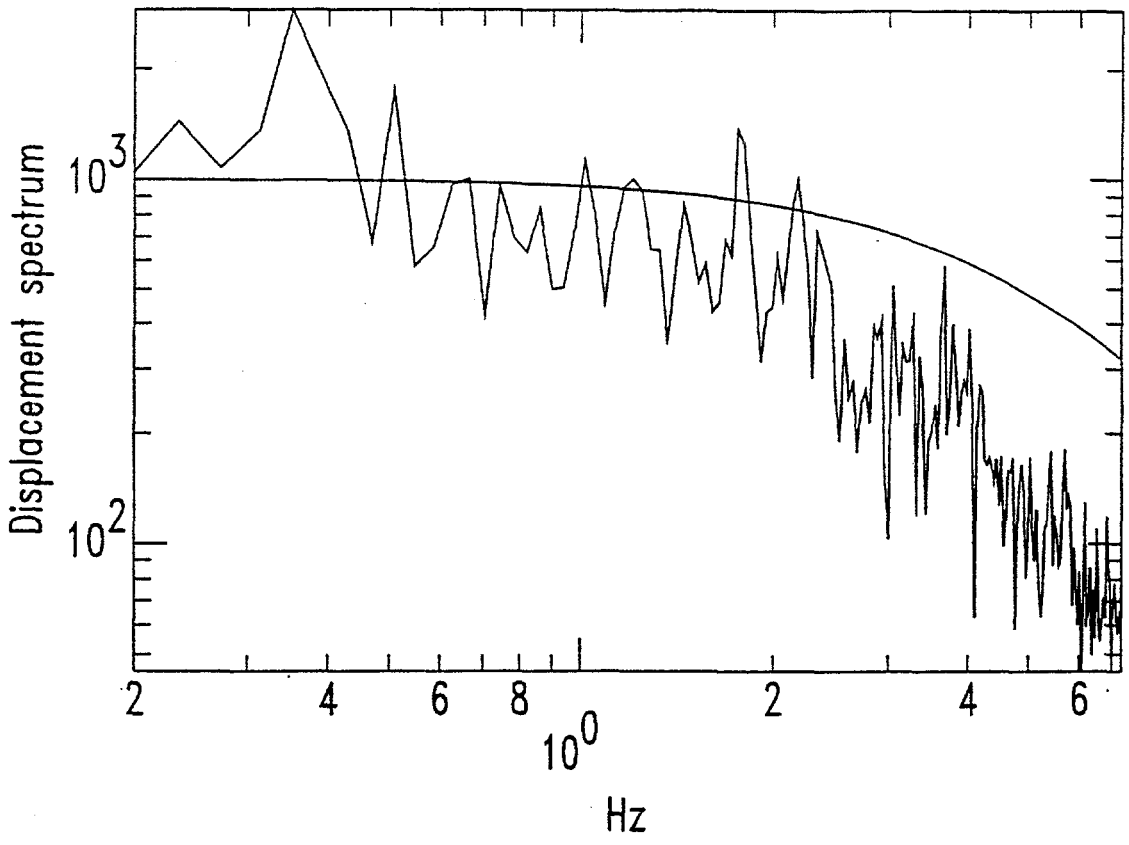

Figure 29. Comparison of Atkinson and Boore (1995) model to magnitude 4.0 Pennsylvania earthquake (see Table 9 and text).

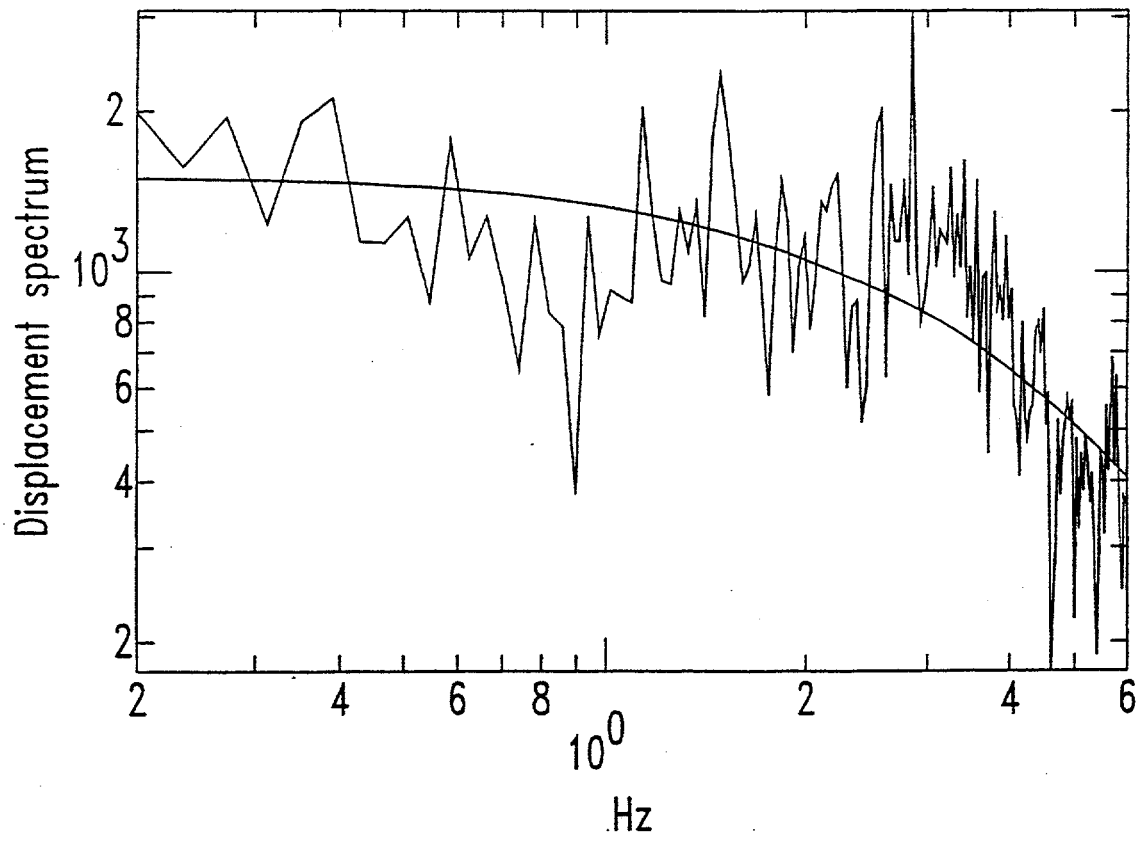

Figure 30. Comparison of Atkinson and Boore (1995) model to magnitude 4.2, New Madrid Seismic Zone earthquake (see Table 9 and text).

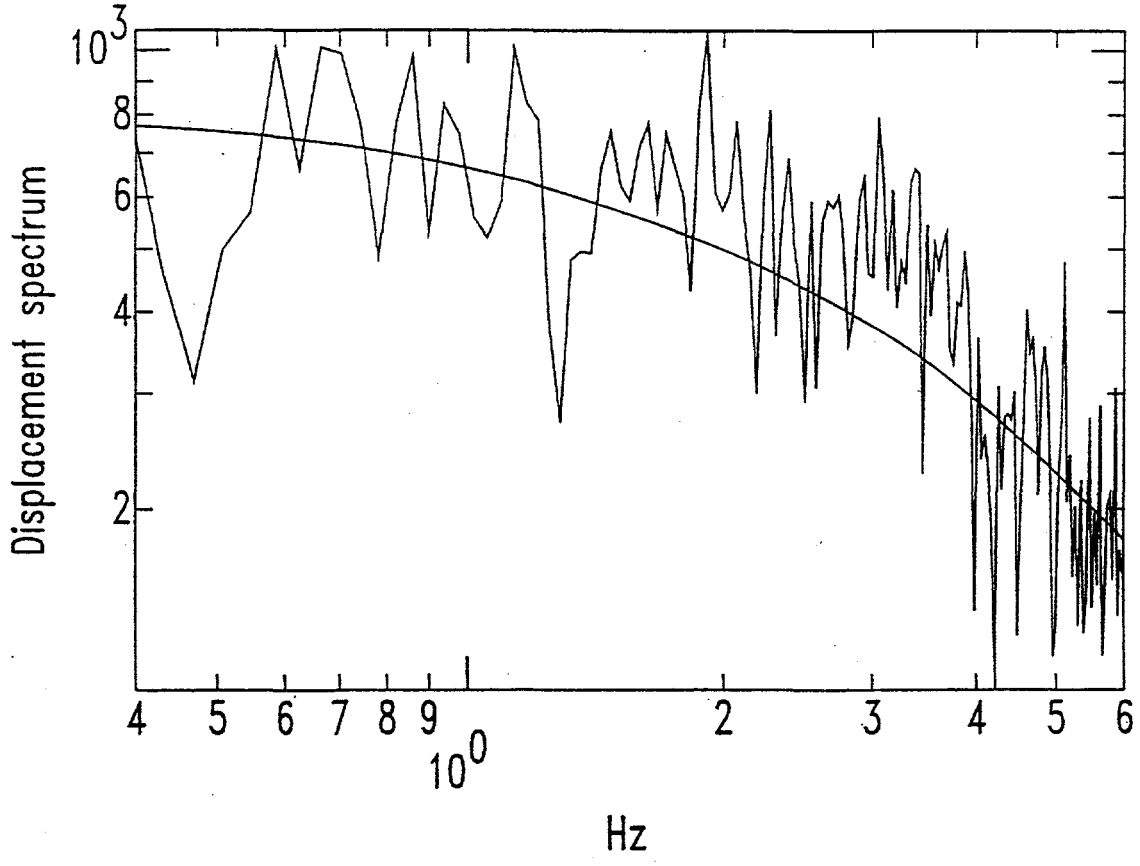

Figure 31. Comparison of Atkinson and Boore (1995) model to magnitude 4.3 southeastern Canada earthquake (see Table 9 and text).

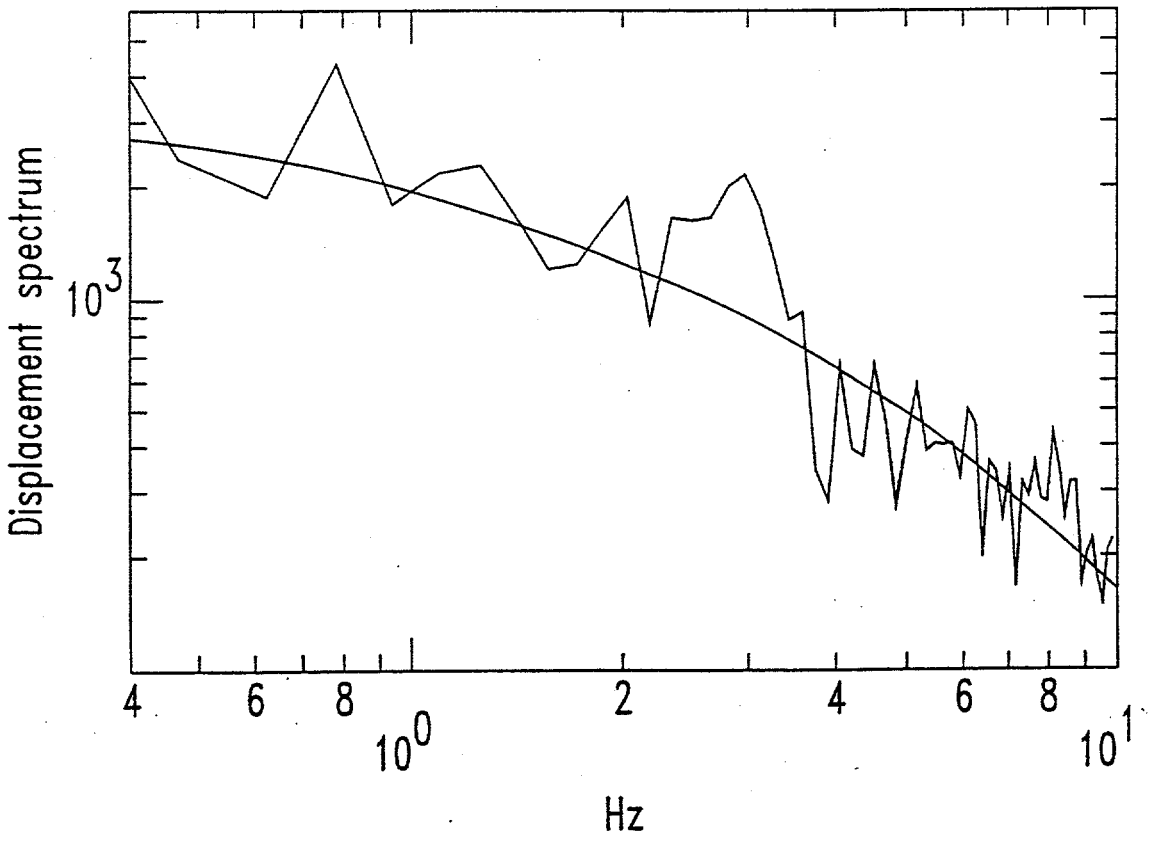

Figure 32. Comparison of Atkinson and Boore (1995) model to magnitude 4.6 Pennsylvania earthquake (see Table 9 and text).

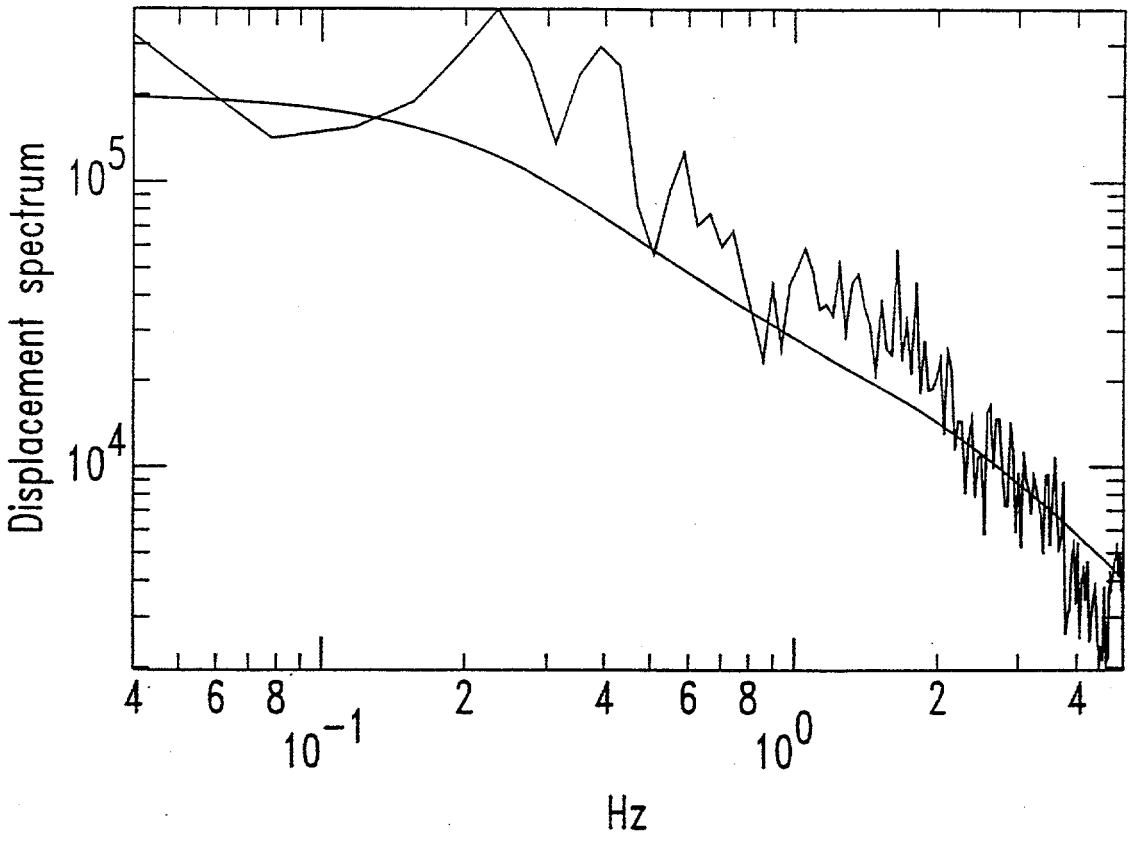

Figure 33. Comparison of Atkinson and Boore (1995) model to magnitude 5.6 West Texas earthquake (see Table 9 and text).

3.8 SOURCE PARAMETERS AND SOURCE SCALING

As apparent in the previous section, the proper source spectral model and the number of parameters required to model the seismic source is still a matter of debate. However, as a first attempt, the NSN data have been modeled using a single corner frequency model. This section of the report presents the source parameter and source scaling results of that modeling. It should be kept in mind that the results are dependent on the particular source model used.

One of the nice features of the single corner frequency model is that it provides a way of estimating the stress drop from the corner frequency and the seismic moment (Brune, 1970):

$$\Delta\sigma = 7/16\ (2\pi/2.34v)^3\ M_0\ f_c^3\ , \qquad (19)$$

where $\Delta\sigma$ is the stress drop. These stress drops are widely used in seismic hazard analysis. For example, prior to Atkinson and Boore (1995), the most widely accepted estimator of the spectral amplitudes of CEUS earthquakes has been the single corner frequency Brune (1970) model with a stress drop of 100 bars.

The source parameters determined from the joint fits for both P and S waves and for $\alpha = 0$ and $\alpha = 0.5$ are shown in Figures 34-37. For $\alpha = 0$, most stress drops range between 1 and 10 bars. Stress drops increase somewhat with increased α and, as with the t* measurements, the scatter in the results increases somewhat with the larger α value. For $\alpha = 0.5$, stress drops fall between 1 and 100 bars. There does not appear to be any systematic increase of stress drop with seismic moment for this data set.

This report covers a range in seismic moments from relatively small earthquakes, down to approximately 10^{20} dyne-cm, to a relatively large earthquake, approximately 10^{24} dyne-cm. For the small earthquakes, previous studies of CEUS earthquakes have typically found relatively small stress drops, with most stress drops ranging from less than 1 bar up to a few tens of bars for earthquakes in the 10^{15} to 10^{22} dyne-cm range (e.g. Boatwright, 1994; Cranswick et al., 1985; Feng and Ebel, 1995; Glassmoyer and Borcherdt, 1990; Shin and Herrmann, 1987; Xie et al., 1991). The results of this study are in good agreement with these other studies of small earthquakes.

Studies of larger earthquakes, however, from roughly 10^{23} to 10^{26} dyne-cm, have typically found stress drops on the order of 100 bars (e.g. Somerville et al., 1987; Toro and McGuire, 1987; Boore and Atkinson, 1987; Nabelek and Suarez, 1989; Johnston, 1994). Combining the results from the larger earthquakes with the results from the smaller earthquakes suggests that stress drop increases with moment for CEUS earthquakes.

In this report we do not find a systematic increase of stress drop with moment. We also obtain a relatively low stress drop for the largest earthquake studied, considerably less than the 100 bars that might be expected. This may indicate that the West Texas earthquake had an unusually low stress drop for a large CEUS earthquake, although this conclusion is speculative.

Another complication in examining the results is the tradeoff between the corner frequency and t* in the spectral fits. Since stress drop varies as the corner frequency cubed (equation 19), it would not take much of an increase in the corner frequency to increase the stress drop. It is possible that increasing the t* values slightly would result in corner frequencies that imply a significantly higher stress drop

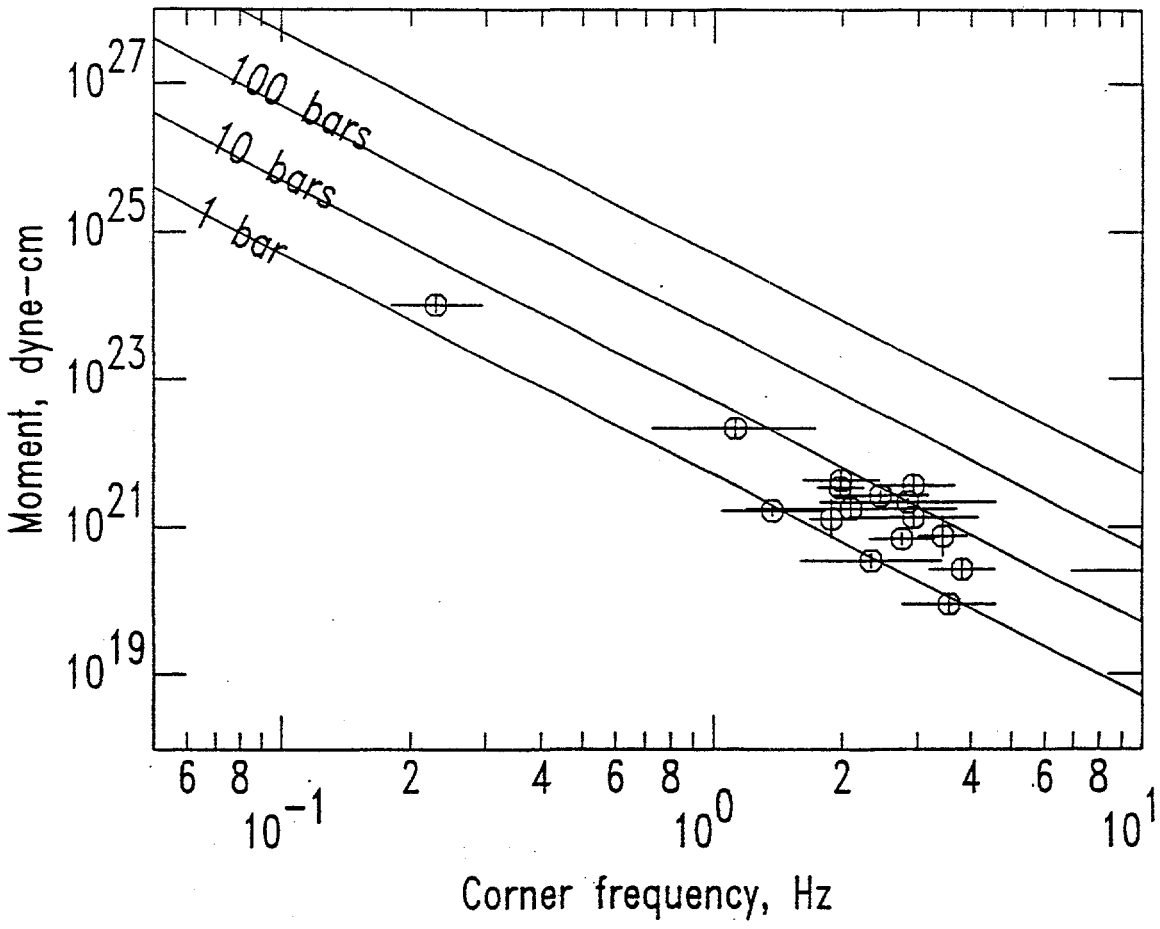

Figure 34. Source parameters determined from joint fits to Lg and Sn spectra. α = **0.0**. Error bars are two standard deviations of the mean.

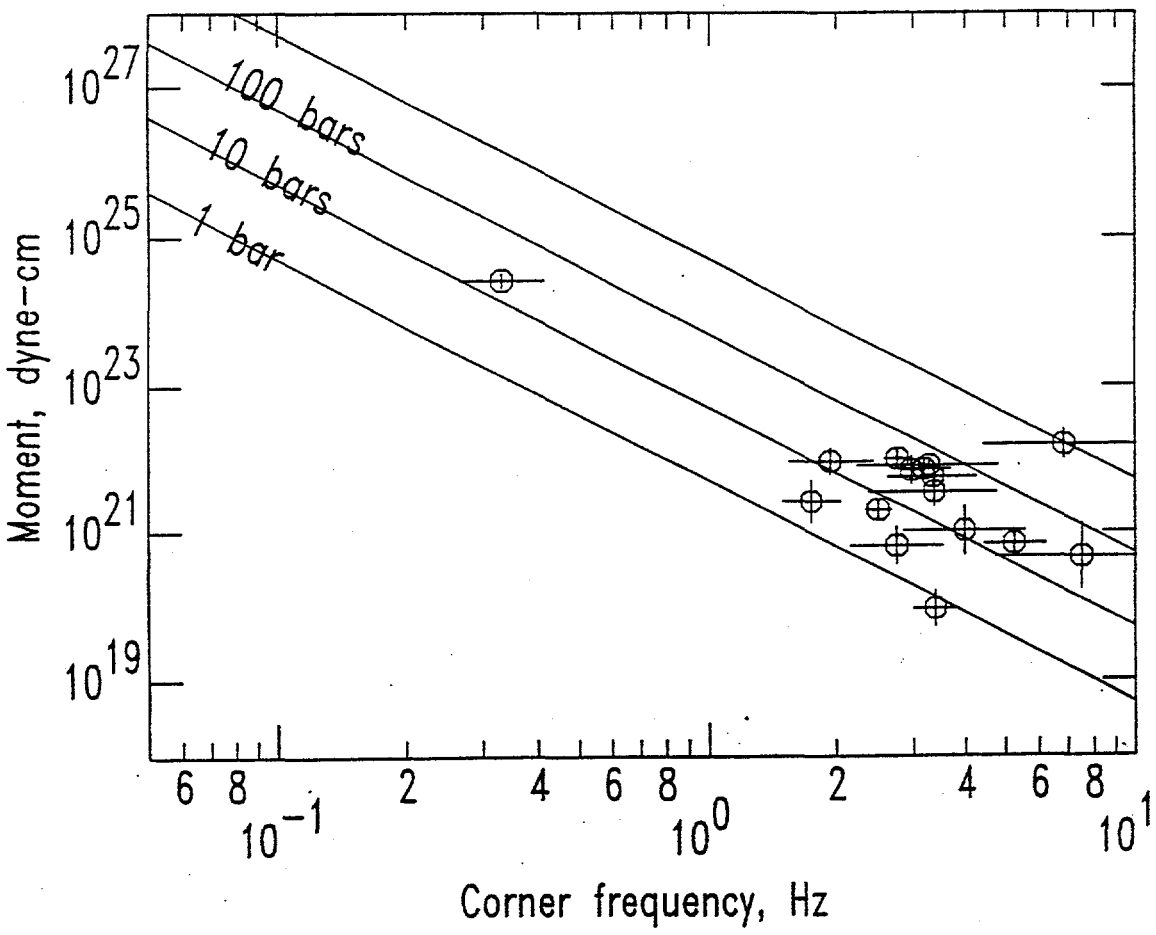

Figure 35. Source parameters determined from joint fits to Lg and Sn spectra. $\alpha = 0.5$. Error bars are two standard deviations of the mean.

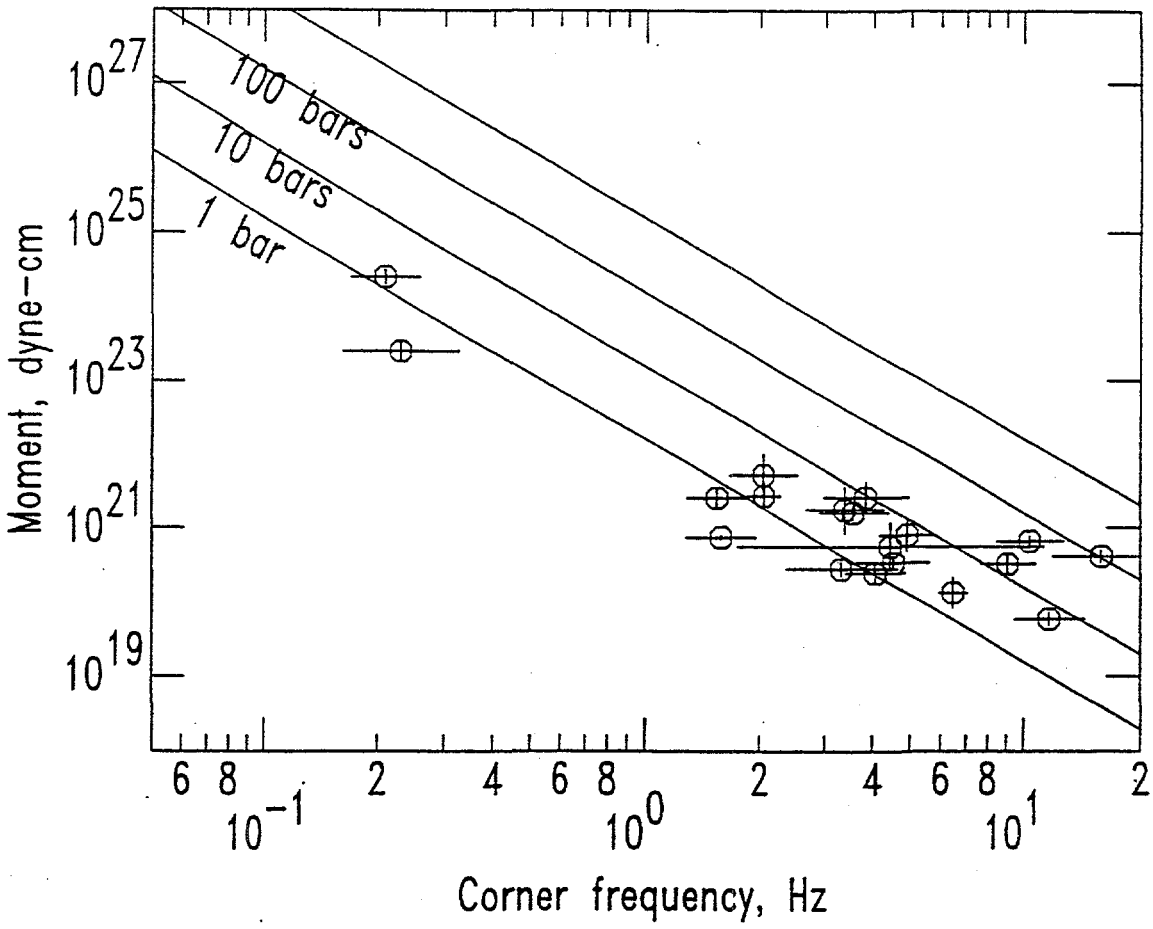

Figure 36. Source parameters determined from joint fits to Pg and Pn spectra. α = **0.0**. Error bars are two standard deviations of the mean.

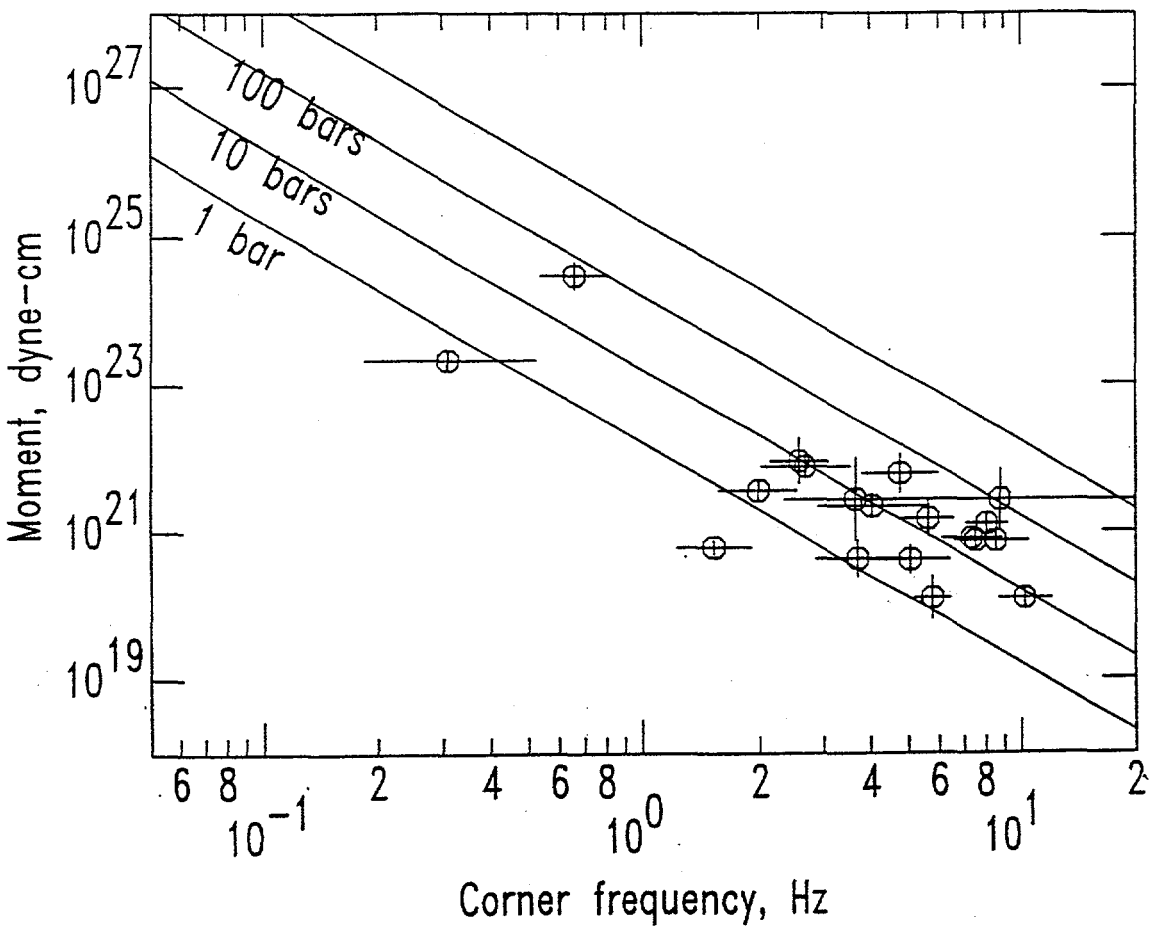

Figure 37. Source parameters determined from joint fits to Pg and Pn spectra. $\alpha = 0.5$. Error bars are two standard deviations of the mean.

3.9 SITE RESPONSE

Finally, this section presents some preliminary results of efforts to estimate the site response at the NSN stations. The site response is estimated from the misfit— the difference between the fits to the spectra and the spectra themselves. If the path and source effects are properly modeled in the fits, then the misfit will be equal to the site response. Of course, this is not always the case, and the misfit contains some source and path effects as well. However, by averaging at a particular site a number of misfits having different sources and azimuths, the source and path effects will tend to cancel out, leaving only the site response.

Figure 38 shows the estimated site response at station WMOK for the four regional phases. There is excellent agreement between the site responses of the Sn and Lg phases. There is less agreement between the Pn and Pg phases, although other stations that have been examined do show agreement between Pn and Pg. In general, the maxima and minima of the averaged misfits are less than a factor of two from unity. This relatively small variation may indicate that there is significant variation in site effect with back azimuth and incidence angle which is being averaged out when the site response is estimated by averaging the misfits.

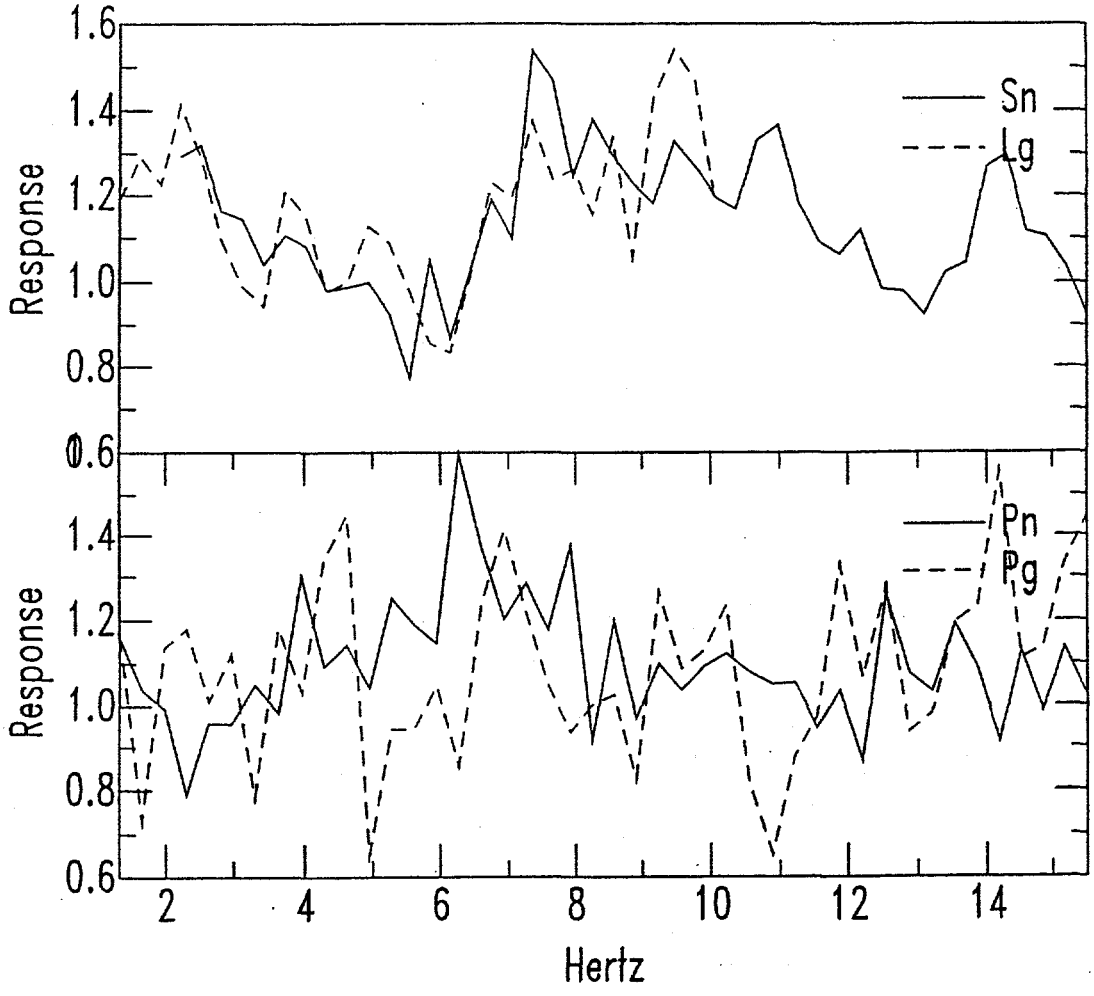

Figure 38. Site responses for four regional phases at WMOK. The site response was estimated by averaging the misfits to the joint spectral fits at the station.

4. DATA SUMMARY BY EVENT

4.1 INTRODUCTION

The data set in Table 10 was collected and processed between August, 1994 and February, 1997. The data set itself dates from January, 1992 through January, 1997. The data for 1993 and 1994 were obtained from the USGS in Golden, Colorado with some of the processing and data reduction already accomplished.

The data for 1994, 1995, 1996, and January, 1997 were obtained from the Automatic Data Request Manager (AutoDRM) of the USGS over the Internet. Likely events to have produced data were determined by daily examinations of the QED catalog of the USGS. Requests for data were subsequently sent via e-mail to the AutoDRM; requests were made for any events east of 105 W. Longitude in the United States or southeastern Canada.

Once data were retrieved from the AutoDRM, the seismograms were examined visually for the appearance of a seismic signal. If a signal was detected, a Fast Fourier Transform was computed for the *Lg* or *Sg* phase and, in some cases, for other phases such as *Sn*, *Pn*, and *Pg*. A noise FFT was also computed from the seismogram for the time interval just before the signal window. If the signal FFT appeared to be significantly larger than the noise FFT over any appreciable frequency range, the signal FFT was saved along with the original seismogram. Thus, for every station listed in the Table for a particular earthquake, the data set consists of at least one seismogram and one FFT, usually, although not always, corresponding to the *Lg* phase. The range over which the signal FFT exceeded the noise FFT is saved in the header of the signal FFT files.

Data from 478 recordings of 237 earthquakes were collected and processed in this manner. This data set includes data from 25 USNSN stations in the central and eastern United States.

Table 10. Data summary by earthquake.

Time (UTC)	Lat. (N)	Lon. (W)	Mag.	Stations
1992 08/26 05:41	37.360	89.680	3.2	CCM
1992 09/27 17:02	28.172	88.438	3.8	MIAR
1992 10/06 15:38	43.324	71.578	3.4	RSNY
1992 11/17 03:58	45.764	74.862	4.0	HRV
1992 12/17 07:18	34.744	97.581	3.5	ALQ, CCM, GOL, MIAR, WMOK
1992 12/27 10:12	37.5	89.63	3.2	CCM, MIAR
1993 01/01 05:08	35.877	82.090	3.0	CEH
1993 01/08 13:01	35.830	90.030	3.5	CCM, MIAR, WMOK
1993 01/14 17:06	36.595	98.275	3.1	MIAR, WMOK
1993 01/21 19:46	36.222	89.617	3.0	CCM, MIAR
1993 02/06 02:09	36.660	89.730	3.5	CCM, MIAR
1993 02/20 13:08	42.830	101.46	3.1	GOL, MIAR, WMOK
1993 03/02 00:29	36.670	89.490	3.0	CCM, MIAR
1993 03/16 07:38	35.670	90.550	3.0	CCM
1993 03/31 20:23	36.790	89.420	3.3	CCM
1993 04/28 22:40	36.190	89.440	3.5	GOGA, MIAR, WMOK
1993 05/06 01:23	46.300	75.500	3.5	RSNY
1993 06/05 12:45	45.674	96.293	4.1	GOGA, MIAR, RSSD, WMOK
1993 07/16 10:54	31.779	88.326	3.7	GOGA, MIAR, MYNC

1993 07/30 22:30	45.260	74.110	3.9	CBM, HRV
1993 08/27 00:08	38.090	90.360	3.3	MIAR
1993 08/30 05:15	46.450	75.060	3.8	CBM
1993 09/23 06:45	46.06	74.600	3.9	BINY, CBM, LBNH
1993 10/16 06:30	41.741	81.134	3.4	BINY, YSNY
1993 11/16 09:31	45.182	73.495	3.8	BINY, CBM, HRV, LBNH, LSCT, MCWV, YSNY
1993 11/30 03:07	35.900	103.10	3.6	ALQ, GOL, LTX, WMOK
1994 01/16 00:42	40.327	76.007	4.0	LBNH, LSCT, MCWV, YSNY
1994 01/16 01:49	40.330	76.037	4.6	CEH, GOGA, LBNH, LSCT, MCWV, MIAR, MYNC, YSNY
1994 02/05 14:55	37.370	89.180	4.2	GOGA, LTX, MIAR, MYNC, WMOK
1994 03/12 10:43	42.782	77.876	3.5	LBNH, LSCT, MCWV, YSNY
1994 08/06 19:54	35.067	76.751	3.6	BINY, CEH, MCWV, YSNY
1994 09/02 21:00	NA	NA	NA	LBNH
1994 09/02 21:23	42.800	84.543	3.4	BINY, MCWV
1994 09/16 04:22	45.300	68.200	3.6	BINY, LBNH
1994 09/16 04:36	45.300	68.200	NA	LBNH
1994 09/16 04:53	NA	NA	NA	CEH
1994 09/16 07:01a	45.300	68.200	NA	LBNH
1994 09/16 07:01b	45.300	68.200	NA	BINY, LBNH
1994 09/16 07:28	45.300	68.200	NA	LBNH
1994 09/16 07:40	45.300	68.200	NA	BINY, LBNH
1994 09/16 07:44	45.300	68.200	NA	BINY, LBNH
1994 09/25 00:53	47.77	69.96	4.3	BINY, HRV, LBNH, MCWV
1994 09/26 14:23	37.00	88.90	3.6	MIAR, OXF, WMOK
1994 09/27 19:09	37.99	81.55	3.3	CEH, MCWV
1994 09/27 19:46	NA	NA	NA	MCWV
1994 10/02 11:27	42.36	72.26	3.6	BINY, HRV, LBNH
1994 10/03 21:19	NA	NA	NA	WMOK
1994 10/03 21:28	NA	NA	NA	LBNH
1994 10/14 12:43	37.97	81.62	3.5	MCWV
1994 10/15 21:44	NA	NA	NA	OXF
1994 11/18 11:21	43.821	70.951	2.6	LBNH
1994 11/20 19:33	44.37	70.59	2.9	BINY, CBM, HRV, LBNH
1994 11/20 23:32	NA	NA	NA	OXF
1994 12/25 19:06	39.290	104.79	4.0	CBKS, RSSD
1994 12/25 19:06b	NA	NA	NA	WMOK
1994 01/18 15:41	NA	NA	NA	RSSD
1995 01/18 15:51	34.51	97.49	4.0	CBKS, JFWS, MIAR, OXF, RSSD, WMOK
1995 01/22 08:24	37.05	80.789	2.7	CEH
1995 02/11 05:54	40.50	94.98	3.1	JFWS, MIAR, RSSD, WMOK
1995 02/12 16:44	44.27	70.25	2.8	LBNH, RSNY
1995 02/15 15:53	45.90	75.04	3.4	BINY, HRV, LBNH, LSCT, RSNY
1995 02/15 15:59	NA	NA	NA	WMOK
1995 02/17 01:13	44.17	70.24	2.7	LBNH

1995 02/19 12:57	39.09	83.62	3.5	BINY, JFWS, RSNY, SSPA, YSNY
1995 03/02 05:33	44.23	74.43	2.9	BINY, LBNH, LSCT, RSNY, YSNY
1995 03/11 08:15	36.98	83.16	3.8	BINY, CBKS, CEH, JFWS, LSCT, MIAR, RSNY, SSPA, WMOK
1995 03/11 09:50	37.00	83.19	3.3	MIAR, RSNY, SSPA, YSNY
1995 03/18 22:03	NA	NA	NA	RSSD
1995 03/18 22:06	35.425	84.922	3.3	OXF
1995 03/18 22:15	NA	NA	NA	LTX
1995 03/19 18:36	34.70	104.06	3.4	ALQ, GOL, WMOK
1995 03/19 18:53	NA	NA	NA	LTX
1995 03/23 11:10	36.90	99.60	2.8	CBKS, WMOK
1995 04/05 05:31	35.20	99.03	3.0	CBKS, GOL, LTX, WMOK
1995 04/05 05:31 aftershock	see above	see above	NA	WMOK
1995 04/14 00:32 West Texas	30.2	103.3	M_b=5.6	BINY, BMN, CBKS, CMB, FFC, GOL, ISA, JFWS, LSCT, RSNY, SAO, SSPA, TUC, WDC, WMOK, WVOR
Aftershocks of West Texas earthquake: 04/14 02:13 to 04/17 09:45	see above	see above	varies	46 LTX, 5 WMOK, 1 CBKS, 1 TUC, 1 RSSD
1995 04/14 00:34	NA	NA	NA	RSSD
1995 04/14 01:46	NA	NA	NA	RSSD
1995 04/14 09:04	NA	NA	NA	RSSD
1995 04/14 12:35	NA	NA	NA	RSSD
1995 04/14 13:30	NA	NA	NA	JFWS
1995 04/14 15:06	NA	NA	NA	RSSD
1995 04/17 13:45	32.9	80.0	3.9	BINY, CEH, LSCT
1995 04/17 16:27	NA	NA	NA	RSNY
1995 04/27 00:42	36.7	89.6	2.7	OXF
1995 05/03 22:17	32.7	82.1	NA	GOGA
1995 05/03 22:19	NA	NA	NA	WMOK
1995 05/08 22:26	NA	NA	NA	BLA
1995 05/08 22:34	37.6	81.2	NA	BLA, CEH
1995 05/22 20:11	NA	NA	NA	WMOK
1995 05/24 15:42	38.1	81.6	NA	CEH, GOGA, LSCT, SSPA
1995 05/24 15:46	NA	NA	NA	BLA
1995 05/24 15:48	NA	NA	NA	OXF
1995 05/25 14:08	NA	NA	NA	JFWS
1995 05/25 14:22	43.0	78.8	3.1	BINY, RSNY
1995 05/25 14:36	NA	NA	NA	WMOK
1995 05/27 19:39	NA	NA	NA	RSNY
1995 05/27 19:51	36.1	89.5	3.8	BLA, CEH, JFWS, MIAR, RSNY, RSSD, WMOK
1995 05/28 15:28	33.2	87.8	3.4	BLA, MIAR, OXF
1995 05/31 16:13	37.9	81.8	NA	BLA

1995 06/01 01:06	30.3	103.3	3.5	CBKS, WMOK
1995 06/01 04:49	34.4	96.7	3.0	CBKS, MIAR, WMOK
1995 06/01 20:02	NA	NA	NA	WMOK
1995 06/05 15:17	43.0	76.4	NA	BINY
1995 06/06 21:27	36.1	89.5	3.6	MIAR
1995 06/08 22:03	NA	NA	NA	WMOK
1995 06/08 22:21	43.2	104.2	NA	RSSD
1995 06/08 22:34	NA	NA	NA	WMOK
1995 06/14 17:01	NA	NA	NA	EYMN
1995 06/14 17:02	NA	NA	NA	BLA
1995 06/16 12:13	44.3	71.9	3.8	BINY, HRV, LBNH, LSCT, RSNY
1995 06/16 14:13	NA	NA	NA	BLA
1995 06/16 14:31	NA	NA	NA	OXF
1995 06/16 18:35	37.1	81.9	NA	BLA, CEH
1995 06/26 00:36	36.7	81.4	3.5	BINY, BLA, CEH, MIAR
1995 06/29 09:27	36.5	89.8	3.1	MIAR, OXF
1995 06/29 20:07	36.6	89.8	3.0	OXF
1995 07/03 03:04	44.0	99.5	2.8	CBKS, RSSD
1995 07/04 03:59	36.2	104.8	3.8	ALQ, CBKS, GOL, MIAR, RSSD, WMOK
1995 07/05 14:16	35.4	84.2	3.7	OXF
1995 07/10 16:30	NA	NA	NA	WMOK
1995 08/17 23:18	36.1	89.4	3.1	CCM, MIAR, OXF
1995 08/20 16:15	45.4	73.2	2.8	BINY, LBNH, RSNY
1995 08/23 21:27	37.9	81.5	NA	CEH, RSNY
1995 09/12 03:59	45.6	74.4	3.4	HRV, LBNH, LSCT, YSNY
1995 09/21 00:31	36.9	98.8	4.1	ALQ, CBKS, CCM, EYMN, GOL, HKT, LTX, RSSD, WMOK, YSNY
1995 09/21 23:03	45.1	74.2	2.8	BINY, LBNH, LSCT, YSNY
1995 10/10 07:19	46.4	78.8	3.2	BINY, HRV, LBNH, LSCT, SSPA, YSNY
1995 10/20 15:57	45.8	96.9	3.7	EYMN, JFWS, RSSD
1995 10/26 00:37	37.0	83.2	4.0	BINY, CBKS, CCM, CEH, EYMN, GOGA, GWDE, HRV, JFWS, LBNH, LSCT, MIAR, MYNC, WMOK, YSNY
1995 11/4 19:04	37.9	81.5	3.4	CEH, LSCT, YSNY
1995 11/8 20:04	39.8	81.5	NA	MCWV, YSNY
1995 11/23 13:00	38.1	82.0	NA	CEH, MCWV
1995 12/15 10:16	36.1	83.6	2.6	CEH, GOGA, MYNC
1995 12/15 15:49	38.1	81.6	3.3	CEH, MCWV, YSNY
1995 12/31 00:37	38.7	104.9	2.8	CBKS, GOL
1996 01/08 22:15	38.0	81.7	3.6	CEH, GOGA, MCWV, YSNY
1996 02/06 15:10	42.5	97.5	3.6	CBKS
1996 02/06 16:08	43.9	103.5	3.7	CBKS, GOL, WMOK
1996 02/14 18:29	38.0	81.6	3.9	CCM, LSCT, MCWV, SSPA, YSNY
1996 03/14 10:42	46.0	74.4	4.1	HRV, LSCT, SSPA

1996 03/22 20:22	41.8	71.2	3.5	HRV, LBNH, LSCT
1996 03/25 06:43	35.6	102.6	3.5	CBKS, WMOK, ALQ
1996 04/09 02:48	43.0	104.0	3.7	CBKS, RSSD
1996 04/19 08:50	37.0	82.9	4.1	CBKS, CEH, EYMN, GOGA, HRV, JFWS, LBNH, LSCT, MCWV, MIAR, RSSD
1996 04/20 01:43	49.2	80.9	3.0	EYMN
1996 04/22 10:44	41.7	71.1	2.5	LBNH, LSCT
1996 05/03 07:47	43.1	104.1	3.1	RSSD
1996 07/23 01:19	44.5	74.1	2.6	BINY, LBNH, LSCT, YSNY
1996 07/25 22:29	37.3	98.5	2.2	CBKS, WMOK
1996 08/01 05:44	37.4	104.2	3.8	CBKS, EYMN, MIAR, RSSD, WMOK
1996 08/16 04:56	49.2	82.9	3.7	EYMN, LBNH, LSCT, YSNY
1996 08/21 07:54	44.2	71.4	3.8	BINY, LSCT, SSPA, YSNY
1996 09/18 02:16	33.7	82.1	2.8	MYNC, GOGA
1996 09/21 01:24	35.7	84.0	2.0	MYNC, GOGA
1996 10/13 11:11	35.9	90.0	2.8	MIAR, MYNC
1996 10/28 06:59	40.3	76.1	2.6	BINY, MCWV
1996 11/01 03:09	37.3	104.2	3.2	CBKS, RSSD, WMOK
1996 11/01 03:09	37.3	104.2	3.2	CBKS, RSSD, WMOK
1996 11/29 05:41	36.0	90.0	4.3	BLA, GOGA, JFWS, MIAR, MYNC, WMOK
1996 12/16 01:58	39.5	87.4	3.1	JFWS, MYNC
1996 12/19 16:29	35.1	97.6	2.5	WMOK
1997 01/09 03:07	33.2	92.6	2.8	MIAR

Notes: Locations and magnitudes are from the "QED" or "PDE" catalogs of the U.S. Geological Survey, Golden, Colorado; "NA" indicates that the event or magnitude was not found in the earthquake catalog.

REFERENCES

Aki, K. (1967). Scaling law of seismic spectrum, *J. Geophys. Res.*, **72**, 1217-1231.

Aki, K. and P. G. Richards (1980). Quantitative seismology, Volume 1, W. H. Freeman and Company, San Francisco, 557 p.

Anderson, J. G. and S. E. Hough (1984). A model for the shape of the Fourier amplitude spectrum of acceleration at high frequencies, *Bull. Seism. Soc. Am.*, **74**, 1969-1993.

Atkinson, G. M. and R. F. Mereu (1992). The shape of ground motion attenuation curves in southeastern Canada, *Bull. Seism. Soc. Am.*, **82**, 2014-2031.

Atkinson, G. M. (1993). Earthquake source spectra in eastern North America, *Bull. Seism. Soc. Am.*, **83**, 1778-1798.

Atkinson, G. M. and D. M. Boore (1995). Ground motion relations for Eastern North America, *Bull. Seism. Soc. Am.*, **85**, 17-30.

Bent, A. L. (1992). A re-examination of the 1925 Charlevoix, Quebec, earthquake, *Bull. Seism. Soc. Am.*, **82**, 2097-2113.

Boatwright, J. (1978). Detailed spectral analysis of two small New York State earthquakes, *Bull. Seism. Soc. Am.*, **68**, 1117-1131.

Boatwright, J. (1994). Regional propagation characteristics and source parameters of earthquakes in northeastern North America, *Bull. Seism. Soc. Am.*, **84**, 1-15.

Boatwright, J. and G. L. Choy (1992). Acceleration source spectra anticipated for large earthquakes in northeastern North America, *Bull. Seism. Soc. Am.*, **82**, 660-682.

Bollinger, G. A. (1979). Attenuation of the *Lg* phase and the determination of m_b in the southeastern United States, *Bull. Seism. Soc. Am.*, **69**, 45-63.

Boore, D. M. (1983). Stochastic simulation of high-frequency ground motions based on seismological models of the radiated spectra, *Bull Seism. Soc. Am.*, **73**, 1865-1894.

Boore, D. M. and G. M. Atkinson (1987). Stochastic prediction of ground motion and spectral response parameters at hard-rock sites in eastern North America, *Bull. Seism. Soc. Am.*, **77**, 440-467.

Boore, D. M. and G. M. Atkinson (1989). Spectral scaling of the 1985 and 1988 Nahanni, Northwest Territories, earthquakes, *Bull. Seism. Soc. Am.*, **79**, 1736-1761.

Boore, D. M. and G. M. Atkinson (1992). Source spectra for the 1988 Saguenay, Quebec, earthquakes, *Bull. Seism. Soc. Am.*, **82**, 683-719.

Bouchon, M. (1982). The complete synthesis of seismic crustal phases at regional distances, *J. Geophys. Res.*, 87, 1735-1741.

Brune, J. N. (1970). Tectonic stress and the spectra of seismic shear waves from earthquakes, *J. Geophys. Res.*, **75**, 4997-5009. (Correction *J. Geophys. Res.*, **76**, 5002, 1971.)

Buland, R. (1992). United States National Seismograph Network, *IRIS Newsletter*, Summer, 4-6.

Caceci, M. S. and W. P. Cacheris (1984). Fitting curves to data, *Byte magazine*, May, 340-360.

Campillo, M., M. Bouchon, and B. Massinon (1984). Theoretical study of the excitation, spectral characteristics, and geometrical attenuation of regional seismic phases, *Bull. Seism. Soc. Am.*, **74**, 79-90.

Campillo, M. (1990). Propagation and attenuation characteristics of the crustal phase, *Lg*, *Pure Appl. Geophys.*, **132**, 1-19.

Chael, E. P. (1987). Spectral scaling of earthquakes in the Miramichi region of New Brunswick, *Bull. Seism. Soc. Am.*, **77**, 347-365.

Chavéz, D. E. and K. F. Priestley (1986). Measurement of frequency dependent *Lg* attenuation in the Great Basin, *Geophys. Res. Lett.*, **13**, 551-554.

Choy, G. L. and J. Boatwright (1988). Teleseismic and near-field analysis of the Nahanni earthquakes in the Northwest Territories, Canada, *Bull. Seism. Soc. Am.*, **78**, 1627-1652.

Choy, G. L., J. Boatwright, J. W. Dewey, and S. A. Sipkin (1983). A teleseismic analysis of the New Brunswick earthquake of January 9, 1982, *J. Geophys. Res.*, **88**, 2199-2212. (Source parameters taken from: *The Earthquakes of Stable Continental Regions, Volume 1: Assessment of Large Earthquake Potential*, 1994, TR- 102261, V1, J. F. Schneider, ed., Electric Power Research Institute, Palo Alto, California.)

Chun, K.-Y., R. J. Kokoski, and G. F. West (1989a). Source spectral characteristics of Miramichi earthquakes: Results from 115 P wave observations, *Bull. Seism. Soc. Am.*, **79**, 15-30.

Chun, K.-Y., R. J. Kokoski, and G. F. West (1989b). High-frequency Pn attenuation in the Canadian shield, *Bull. Seism. Soc. Am.*, **79**, 1039-1053.

Chun, K.-Y., G. F. West, R. J. Kokoski, and C. Simon (1987). A novel technique for measuring *Lg* attenuation—Results from eastern Canada between 1 and 10 Hz, *Bull. Seism. Soc. Am.*, **77**, 398-419.

Dwyer, J. J., R. B. Herrmann, and O. W. Nuttli (1983). Spatial attenuation of the *Lg* wave in the central United States, *Bull. Seism. Soc. Am.*, **77**, 781-796.

Ebel, J. E., P. G. Somerville, J. D. McIver (1986). A study of the source parameters of some large earthquakes of northeastern North America, *J. Geophys. Res.*, **91**, 8231-8246. (Source parameters taken from: *The Earthquakes of Stable Continental Regions, Volume 1: Assessment of Large EarthquakePotential*, 1994, TR-102261-V1, J. F. Schneider, ed., Electric Power Research Institute, Palo Alto, California.)

Evernden, J. F. (1967). Magnitude determination at regional and near-regional distances in the United States, *Bull. Seism. Soc. Am.*, **57**, 591-639.

Feng, Q. and J. E. Ebel (1996). Determination of rupture duration and stress drop for earthquakes in New England, *Seism. Res. Lett.*, **67**, Number 1, 38-52.

Fletcher, J. B. (1995). Source parameters and crustal Q for four earthquakes in South Carolina, *Seism. Res. Lett.*, **66**, Number 4, 44-58.

Fowler, C. M. R. (1992). *The Solid Earth*, Cambridge University Press.

Glassmoyer, G. and R. D. Borcherdt (1990). Source parameters and effects of bandwidth and local geology on high-frequency ground motions observed for aftershocks of northeastern Ohio earthquake of 31 January 1986, *Bull. Seism. Soc. Am.*, **80**, 889-912.

Gupta, I. N. and K. L. McLaughlin (1987). Attenuation of ground motion in the eastern United States, *Bull. Seism. Soc. Am.*, **77**, 366-383.

Haddon, R. A. W. (1995). Modeling of source rupture characteristics for the Saguenay earthquake of November 1988, *Bull. Seism. Soc. Am.*, **85**, 525-551.

Hanks, T. and R. McGuire (1981). The character of high-frequency strong ground motion, *Bull. Seism. Soc. Am.*, **71**, 2071-2095.

Hasegawa, H. S. (1983). Lg spectra of local earthquakes recorded by the eastern Canada telemetered network and spectral scaling, *Bull. Seism. Soc. Am.*, **73**, 1041-1061.

Hasegawa, H. S. (1985). Attenuation of *Lg* waves in the Canadian Shield, *Bull. Seism. Soc. Am.*, **75**, 1569-1582.

Hasegawa, H. S. and J. Adams (1990). Reanalysis of the 1963 Baffin Island earthquake (M 6.2) and its seismotectonic environment, *Seism. Res. Lett.*, **61**, 181-192. (Source parameters taken from: *The Earthquakes of Stable Continental Regions, Volume 1: Assessment of Large Earthquake Potential*, 1994, TR-102261-V1, J. F. Schneider, ed., Electric Power Research Institute, Palo Alto, California.)

Hasegawa, H. S. and R. J. Wetmiller (1980). The Charlevoix earthquake of 19 August 1978 and its seismotectonic environment, *Earthquake Notes*, **51**, 23-37. (Source parameters taken from: *The Earthquakes of Stable Continental Regions, Volume 1: Assessment of Large Earthquake Potential*, 1994, TR-102261-V1, J. F. Schneider, ed., Electric Power Research Institute, Palo Alto, California.)

Herrmann, R. B., C. A. Langston, and J. E. Zollweg (1982). The Sharpsburg, Kentucky, earthquake of 27 July 1980, *Bull. Seism. Soc. Am.*, **72**, 1219-1239. (Source parameters taken from: *The Earthquakes of Stable Continental Regions Volume 1: Assessment of Large Earthquake Potential*, 1994, TR-102261-V1, J. F. Schneider, ed., Electric Power Research Institute, Palo Alto, California.)

Hwang, H.-J., and B. J. Mitchell (1987). Shear velocities, $Q\beta$, and the frequency dependence of $Q\beta$ in stable and tectonically active regions from surface wave observations, *Geophys. J. R. Astron. Soc.*, **90**, 575-613.

Johnston, A. C. (1994). Seismotectonic interpretations and conclusions from the stable continental region seismicity database, in *The Earthquakes of Stable Continental Regions Volume 1: Assessment of Large Earthquake Potential*, J. F. Schneider, ed., 4-1 to 4-103.

Kanamori, H. and D. L. Anderson (1975). Theoretical basis for some empirical relations in seismology, *Bull. Seism. Soc. Am.*, **65**, 1073-1095.

Kennett, B. L. N. (1985). On regional S, *Bull. Seism. Soc. Am.*, **75**, 1077-1086.

Kennett, B. L. N. (1989). On the nature of regional seismic phases—I. Phase representations for Pn, Pg, Sn, Lg, *Geophys. J. Int.*, **98**, 447-459.

Knopoff, L., F. Schwab, and E. Kausel (1973). Interpretation of *Lg*, *Geophys. J. R. Astron. Soc.*, **33**, 389-404.

Lamontagne, M., H. S. Hasegawa, D. A. Forsyth, G. G. R. Buchbinder, and M. Cajka (1994). The Mont-Laurier, Quebec, earthquake of 19 October 1990 and its seismotectonic environment, *Bull. Seism. Soc. Am.*, **84**, 1605-1522.

Langston, C. A. (1982). Aspects of Pn and Pg propagation at regional distances, *Bull. Seism. Soc. Am.*, **72**, 457-472.

Liu, H.-L. and H. Kanamori (1980). Determination of source parameters of midplate earthquakes from the wave forms of body waves, *Bull. Seism. Soc. Am.*, **70**, 1989-2004. (Source parameters taken from: *The Earthquakes of Stable Continental Regions, Volume 1: Assessment of Large Earthquake Potential*, 1994, TR-102261-V1, J. F. Schneider, ed., Electric Power Research Institute, Palo Alto, California.)

Mitchell, B. J. (1980). Frequency dependence of shear wave internal friction in the continental crust of eastern North America, *J. Geophys. Res.*, **85**, 5212-5218.

Mitchell, B. J. (1981). Regional variation and frequency dependence of $Q\beta$ in the crust of the United States, *Bull. Seism. Soc. Am.*, **71**, 1531-1538.

Mitchell, B. J. (1991). Frequency dependence of Q_{Lg} and its relation to crustal anelasticity in the Basin and Range province, *Geophys. Res. Lett.*, **18**, 621-624.

Mitchell, B. J. (1995). Anelastic structure and evolution of the continental crust and upper mantle from seismic surface wave attenuation, *Rev. Geophys.*, **33**, 441-462.

Nabelek, J. (1988). The January 9, 1982, New Brunswick, Canada earthquake: in Toksoz, M. N. and K. Kadinsky-Cade, *A study of New England seismicity with emphasis on Massachusetts and New Hampshire*: Final report covering the period 1976-1985, NUREG/CR-5080, U.S. Nuclear Regulatory Commission, Washington D. C., p. 60-103. (Source parameters taken from: *The Earthquakes of Stable Continental Regions, Volume 1: Assessment of Large Earthquake Potential*, 1994, TR-102261-V1, J. F. Schneider, ed., Electric Power Research Institute, Palo Alto, California.)

Nabelek, J. and G. Suarez (1989). The 1983 Goodnow earthquake in the central Adirondacks, New York: Rupture of a simple, circular crack, *Bull. Seism. Soc. Am.*, **79**, 1762-1778.Nuttli, O. W. (1981). Similarities and differences between western and eastern United States earthquakes, and their consequences for earthquake engineering, in *Earthquakes and Earthquake Engineering: The Eastern United States*, vol. 1, J. E. Beavers, ed., 25- 51.

Nabelek, J. and G. Suarez (1989). The 1983 Goodnow earthquake in the central Adirondacks, New York: Rupture of a simple, circular crack, *Bull. Seism. Soc. Am.*, **79**, 1762-1777.

Nelder, J. A. and R. Mead (1965). A simplex method for function minimization, *Computer Journal*, **7**, 308.

Nuttli, O. W. (1973). Seismic wave attenuation and magnitude relations for eastern North America, *J. Geophys. Res.*, **78**, 876-885.

Nuttli, O. W. (1981). Similarities and differences between western and eastern United States earthquakes, and their consequences for earthquake engineering, in *Earthquakes and Earthquake Engineering: The Eastern United States*, vol. 1, J. E. Beavers, ed., 25-51.

Nuttli, O. W. (1983a). Seismic wave attenuation and magnitude relations for eastern North America, *J. Geophys. Res.*, **78**, 876-885.

Nuttli, O. W. (1983b). Average seismic source-parameter relations for mid-plate earthquakes, *Bull. Seism. Soc. Am.*, **73**, 519-535.

Nuttli, O. W., W. Stauder, and C. Kisslinger (1969). Travel-time tables for earthquakes in the central United States, *Earthquake Notes*, **40**, 19-28.

Oliver, J. and M. Ewing (1957). Higher modes of continental Rayleigh waves, *Bull. Seism. Soc. Am.*, **47**, 187-204.

Oliver, J. and M. Ewing (1958). Normal modes of continental Rayleigh waves, *Bull. Seism. Soc. Am.*, **48**, 33-49.

Olsen, K. H., L. W. Braile, and J. N. Stewart (1983). Modeling short-period crustal phases (*Pg - Lg*) for long-range refraction profiles, *Phys. Earth Planet. Int.*, **31**, 334-347.

Ou, G.-B. and R. B. Herrmann (1990). Statistical model for ground motion produced by earthquakes at local and regional distances, *Bull. Seism. Soc. Am.*, **70**, 1397-1417. (Source parameters taken from: *The Earthquakes of Stable Continental Regions, Volume 1: Assessment of Large Earthquake Potential*, 1994, TR-102261-V1, J. F. Schneider, ed., Electric Power Research Institute, Palo Alto, California.)

Pechmann, J. C., W. R. Walter, S. J. Nava, and W. J. Arabasz (1995). The February 3, 1995, M_L 5.1 seismic event in the Trona mining district of southwestern Wyoming, *Seism. Res. Lett.*, **66**, 25-33.

Press, F. and M. Ewing (1952). Two slow surface waves across North America, *Bull. Seism. Soc. Am.*, **42**, 219-228.

Pulli, J. J. (1984). Attenuation of coda waves in New England, *Bull. Seism. Soc. Am.*, **74**, 1149-1166.

Romney, C., B. G. Brooks, R. H. Mansfield, D. S. Carder, J. N. Jordan, and D. W. Gordon (1962). Travel times and amplitudes of principal body phases recorded from GNOME, *Bull. Seism. Soc. Am.*, **52**, 1057-1074.

Schneider, J. F., ed. (1994). *The Earthquakes of Stable Continental Regions, Volume 1: Assessment of Large Earthquake Potential*, TR-102261-V1, Electric Power Research Institute, Palo Alto, California

Shi, J., W.-Y. Kim, and P. G. Richards (1995). Variability of attenuation in the northeastern United States from *Lg* Waves, *Seism. Res. Lett.*, **67**, 75.

Shin, T.-C. and R. B. Herrmann (1987). Lg attenuation and source studies using 1982 Miramichi data, *Bull. Seism. Soc. Am.*, **77**, 384-397.

Singh, S. and R. B. Herrmann (1983). Regionalization of crustal coda *Q* in the continental United States, *J. Geophys. Res.*, **88**, 527-538.

Somerville, P. (1986). *Source-scaling relations of eastern North American earthquakes*: EPRI NP-4790 Final Report, Electric Power Research Institute, Palo Alto, California, 152 pp. (Source parameters taken from: *The Earthquakes of Stable Continental Regions, Volume 1: Assessment of Large Earthquake Potential*, 1994, TR-102261-V1, J. F. Schneider, ed., Electric Power Research Institute, Palo Alto, California.)

Somerville, P. G., J. P. McLaren, L. V. LeFevre, R. W. Burger, and D. V.Helmberger (1987). Comparison of source scaling relations of eastern and western North American earthquakes, *Bull. Seism. Soc. Am.*, **77**, 322-346.

Somerville, P. G., J. P. McLaren, C. K. Saikia, and D. V. Helmberger (1990). The 25 November 1988 Saguenay, Quebec, earthquake: source parameters and the attenuation of strong ground motion, *Bull. Seism. Soc. Am.*, **80**, 1118-1143.

Street, R. L. (1976). Scaling northeastern United States/ southeastern Canada earthquakes by their *Lg* waves, *Bull. Seism. Soc. Am.*, **66**, 1525-1537.

Street, R. L. and F. T. Turcotte (1977). A study of northeastern North American spectral moments, magnitudes, and intensities, *Bull. Seism. Soc. Am.*, **67**, 599-614.

Street, R. L., R. B. Herrmann, and O. W. Nuttli (1975). Spectral characteristics of the Lg wave generated by central United States earthquakes, *Geophys. J. R. Ast. Soc.*, **41**, 51-63.

Sutton, G. H., W. Mitronovas, and P. W. Pomeroy (1967). Short-period seismic energy radiation patterns from underground nuclear explosions and small-magnitude earthquakes, *Bull. Seism. Soc. Am.*, **57**, 249-268.

Taylor, K. B., R. B. Herrmann, M. W. Hamburger, G. L. Pavlis, A. Johnston, C. Langer, and C. Lam (1989). The southeastern Illinois earthquake of 10 June 1987, *Seism. Res. Lett.*, **60**, 101-110. (Source parameters taken from: *The Earthquakes of Stable Continental Regions, Volume 1: Assessment of Large Earthquake Potential,* 1994, TR-102261-V1, J. F. Schneider, ed., Electric Power Research Institute, Palo Alto, California.)

Toro, G. R. and R. K. McGuire (1987). An investigation into earthquake ground motion characteristics in eastern North America, *Bull. Seism. Soc. Am.*, **77**, 468-489.

Walter, W. R., K. M. Mayeda, and H. J. Patton (1995). Phase and spectral ratio discrimination between NTS earthquakes and explosions. Part I: Empiricial Observations, *Bull. Seism. Soc. Am.*, **85**, 1050-1067.

Wetmiller, R. J., R. B. Horner, H. S. Hasegawa, R. G. North, M. Lamontagne, D. H. Weichert, and S. G. Evans (1988). An analysis of the 1985 Nahanni earthquakes, *Bull. Seism. Soc. Am.*, **78**, 590-616.

Woodgold, C. R. D. (1990). Estimation of *Q* in eastern Canada using coda waves, *Bull. Seism. Soc. Am.*, **80**, 411-429.

Xie, J. and B. J. Mitchell (1990a). Attenuation of multiphase surface waves in the Basin and Range province, part I: *Lg* and *Lg* coda, *Geophys. J. Int.*, **102**, 121-137.

Xie, J. and B. J. Mitchell (1990b). A back-projection method for imaging large-scale lateral variations of *Lg* coda *Q* with application to continental Africa, *Geophys. J. Int.*, **100**, 161-181.

Xie, J., Z. Liu, R. B. Herrmann, and E. Cranswick (1991). Source processes of three aftershocks of the 1983 Goodnow, New York, earthquake: High-resolution images of small, symmetric ruptures, *Bull. Seism. Soc. Am.*, **81**, 818-843.

Zhang, T. and T. Lay (1994). Analysis of short-period regional phase path effects associated with topography in Eurasia, *Bull. Seism. Soc. Am.*, **84**, 119-132.

Zhu, T., K.-Y. Chun, and G. F. West (1991). Geometrical spreading and Q of Pn waves: An investigative study in eastern Canada, *Bull. Seism. Soc. Am.*, **81**, 882-896.

NRC FORM 335 (2-89) NRCM 1102, 3201, 3202

U.S. NUCLEAR REGULATORY COMMISSION

BIBLIOGRAPHIC DATA SHEET

(See instructions on the reverse)

1. REPORT NUMBER (Assigned by NRC, Add Vol., Supp., Rev., and Addendum Numbers, if any.)

NUREG/CR-6564

2. TITLE AND SUBTITLE

Analyses of Source Spectra, Attenuation, and Site Effects from Central and Eastern United States Earthquakes

3. DATE REPORT PUBLISHED

MONTH	YEAR
February	1998

4. FIN OR GRANT NUMBER

W6380

5. AUTHOR(S)

G. Lindley

6. TYPE OF REPORT

Technical

7. PERIOD COVERED *(Inclusive Dates)*

August 1994 - August 1997

8. PERFORMING ORGANIZATION - NAME AND ADDRESS *(If NRC, provide Division, Office or Region, U.S. Nuclear Regulatory Commission, and mailing address; if contractor, provide name and mailing address.)*

Institute for Crustal Studies
University of California
Santa Barbara, CA 93106-1100

9. SPONSORING ORGANIZATION - NAME AND ADDRESS *(If NRC, type "Same as above"; if contractor, provide NRC Division, Office or Region, U.S. Nuclear Regulatory Commission, and mailing address.)*

Division of Engineering Technology
Office of Nuclear Regulatory Research
U.S. Nuclear Regulatory Commission
Washington, DC 20555-0001

10. SUPPLEMENTARY NOTES

E. Zurflueh, NRC Project Manager

11. ABSTRACT *(200 words or less)*

Results from 27 previous studies were used to analyze stress drop vs. magnitude in eastern North America. Stress drop was not constant, but increased approximately with the square root of the seismic moment from 3 bars at 10^{20} dyne-cm to 690 bars at 10^{25} dyne-cm.

Q_{Lg} as a function of frequency was analyzed in five regions of the contiguous United States. Simultaneous inversions using Fourier amplitude spectra were computed to determine attenuation, site responses, and source spectra. Unlike some previous studies, Q_{Lg} in the central and northeastern U.S. was found to be nearly identical from 2 to 10 Hz. Q_{Lg} in the southeastern U.S. is about 20% lower.

Anelastic attenuation of four regional phases, and source parameters of 27 earthquakes, including the 1995 West Texas earthquake (M_b 5.6) were also estimated. L_g attenuation is in good agreement with previous estimates for the central and eastern U.S. Assuming a single corner frequency source model, stress drops range from about 1 to 100 bars. The West Texas earthquake has lower values of a few bars to a few tens of bars.

12. KEY WORDS/DESCRIPTORS *(List words or phrases that will assist researchers in locating the report.)*

Stress Drop
Seismic moment
U.S. National Seism ograph Network

13. AVAILABILITY STATEMENT

unlimited

14. SECURITY CLASSIFICATION

(This Page) unclassified

(This Report) unclassified

15. NUMBER OF PAGES

16. PRICE